TOWARDS AN AUTOMATIC REGISTRATION FOR TERRESTRIAL LASER SCANNER DATA

Von der
Fakultät Architektur, Bauingenieurwesen und Umweltwissenschaften
der Technischen Universität Carolo-Wilhelmina
zu Braunschweig

zur Erlangung des Grades eines
Doktor - Ingenieurs (Dr.-Ing.)
genehmigte

Dissertation

von
(**M.Sc., Ismail Abd El hamid Mohamed, El khrachy**)
aus(Kairo/Ägypten)

Eingereicht am	11.12.2007
Mündliche Prüfung am	29.02.2008
Berichterstatter	Univ.-Prof. Dr.-Ing. Wolfgang Niemeier
	Univ.-Prof. Dr.-Ing. Otto Heunecke

2008

Abstract

This thesis presents terrestrial laser scanning as a tool for the documentation of the scan object such as heritage sites. For a typical laser scanning project there is usually more than one scan acquired from different setup locations around the scan object. Data registration means collecting of separated scans within one scan world coordinate system. Data registration could be achieved based on the targets method or the point cloud method.

If registration targets (sometimes called tie points) are available, data can be registered by a manner similar to that used in aerial triangulation method. These tie points such as special reflective target, black-white targets or sphere targets can be used as correspondence (points) between adjacent scans. These targets should be distributed within the laser scanner field of view to be scanned during the scanning process. After modeling the registration target, the transformation parameters can be calculated. The targets could be natural or artificial. Algorithms for fitting a sphere to point clouds to be used for data registration have been presented. According to the targets registration type, the sphere targets gave more accurate data registration results. The accuracy of the extracted sphere parameters is range dependent. By using range with the relative weight matrix which is used in combined least squares solution to calculate transformation parameters between adjacent scans, accuracies of transformation parameters are improved. Many configurations of registration target distributions have been studied. It has been shown that the poor target distribution, the low quality of data registration results.

If registration targets are not available, or difficult to be achieved, many techniques could be used to calculate transformation parameters between adjacent scans based on the point cloud itself. The iterative closest point (ICP) method is one of the most popular methods for this purpose. The ICP solution is an iterated method, a very good correspondence points determination between adjacent scans is requested with the ICP solution technique. Taking into consideration only the overlapped point clouds between source and target scan was a simple trial to improve starting of the ICP solution. Investigation on how to improve corresponding points based on surface information was the second trail in this study. Surface curvature is independent of any rigid transformation. Mean curvature is calculated for the two scans, the edges are detected based on threshold curvature values. The intersection points of the detected edges are fitted and calculated. The matched intersection points between adjacent scans are used as correspondence points for calculating an approximation transformation parameters. The ICP solution iterated using these correspondences points to get the transformation parameters.

Real tests have been carried out in order to evaluate the accuracy of the proposed methods. Many comparisons with the least square solution (as a reference solution based on targets registration method) have been done and indicate that the results are improved.

Zusammenfassung

Diese Dissertation stellt das terrestrische Laserscanning als ein Werkzeug für die Dokumentation von Objekten dar wie beispielsweise für kulturhistorische Bauten. Für ein typisches Laserscanning Projekt gibt es in der Regel mehr als einen Scan, der von den unterschiedlichen Einstellungen und Positionen bezüglich des zu scannenden Objektes abhängig ist. Im Rahmen der Datenaufnahme und Weiterverarbeitung werden die Punktwolken in einem gemeinsamen Koordinatensystem bereitgestellt. Die Verknüpfung der Punktwolken erfolgt in Abhängigkeit der korrespondierenden Punkte in den verschiedenen Scans. Eine Kategorisierung in Abhängigkeit dieser Punkte ist möglich.

Wenn es in den unterschiedlichen Aufnahmen korrespondierende Punkte (Verknüpfungspunkte) gibt, können die Aufnahmen mit ähnlichen Verfahren, wie sie in der Luftbildtriangulation angewendet werden, orientiert werden. Zielmarken mit besonderen reflektierenden Eigenschaften, schwarz-weiß Tafeln oder Ziele in Form einer Kugel können als Verknüpfungspunkte in den unterschiedlichen Aufnahmen genutzt werden. Diese Ziele müssen günstig im Aufnahmebereich des Laserscanners plaziert werden. Sind die Ziele objekte für die Verknüpfung der einzelnen Aufnahmen in ihren Parametern modelliert und berechnet, können die Transformationsparameter bestimmt werden. Algorithmen für die Berechnung der Parameter einer Kugel innerhalb einer Punktwolke sind dargestellt worden. Bei dem Vergleich der unterschiedlichen Ziele für die Verknüpfung von Punktwolken stellte sich die Kugel als das geeigneteste Medium bezüglich der Verknüpfungsgenauigkeit heraus. Die Genauigkeit der bestimmten Parameter der Kugel ist abhängig von der Entfernung der Kugel zum Messgerät. Berücksichtigt man in der Ausgleichung die Entfernung zum Ziel mit entsprechender Gewichtsmatrix, so erhöht dies die Genauigkeit der Kugel- und der Transformationsparameter. Viele verschiedene Verknüpfungsziele und deren geometrische Anordnung wurden untersucht. Es wurde gezeigt, dass eine schlechte Konfiguration der Verknüpfungsziele zu einer geringeren Genauigkeit der Verknüpfung der Puntkwolken führt.

Sollten keine Verknüpfungspunkte existieren oder nur schwer zu realisieren sein, können andere Techniken herangezogen werden, um die Verknüpfung der Punktwolken zu erreichen. Eine häufig angewandte Methode ist die Punkteinpassungsmethode (ICP - Iterative Closest Point Algorithm). Die ICP - Methode ist ein iteratives Verfahren, das sehr gute Ergebnisse erzielt. In ersten Versuchen wurde nur der Überlappungsbereich zweier Puntkwolken betrachtet, um damit eine Verbesserung der ICP - Methode zu erreichen. In weiteren Versuchen wurde versucht, eine bessere Zuweisung korrespondierender Elemente aufgrund von Oberflächenstrukturen zu erreichen. Flächenkurven sind unabhängig von Starrkörper-Transformationen wie Rotationen und Verschiebungen. Die mittleren Krümmungen für zwei Aufnahmen wurden berechnet und die Kanten mittels eines Kurvenschwellenwertes detektiert. Die Schnittpunkte der Kanten wurden in unterschiedlichen Aufnahmen herausgestellt. Die Schnittpunkte

wurden in angrenzenden Aufnahmen als Verknüpfungspunkte genutzt, um genäherte Transformationsparameter zu bestimmen. Die ICP - Methode nutzt diese genäherten Transformationsparameter, um iterativ die Genauigkeit der Transformationsparameter zu erhöhen.

Es sind Testkonfigurationen aufgestellt und durchgeführt worden, um die Genauigkeitssteigerung der vorgestellten Methode zu verifizieren. Als Grundlage diente eine Referenzlösung, die mit der Methode der kleinsten Quadrate ausgewertet wurde und somit sehr genau vorlag. Es wurde gezeigt, dass mit den aufgestellten Methoden eine Genauigkeitssteigerung in der Verknüpfung der Punktwolken erreicht wurde.

Acknowledgement

First I wish to acknowledge the financial support from *The Supreme Council of Universities in Egypt*. My thanks to the Egyptian Cultural Office in Berlin for successful supervision during the scholarship time.

My sincere thanks to my supervisor Prof. Dr.-Ing. Wolfgang Niemeier. I thank him for giving me the freedom to explore a wide variety of ideas and for having an open door and open mind whenever I needed it. I am also indebted to Prof. Dr.-Ing. Otto Heunecke, my second examiner, I want to thank him for his help. I would like also to thank prof. Bodo Schrader, my third examiner.

My thanks to all the co-workers and all the staff in the *Institut für Geodäsie und Photogrammetrie* for helping and discussing with me some of the difficult points in my thesis. Without their help, this work would never have been completed.

My special thanks to the surveying group at *Civil Engineering Department, Al-Azhar University Cairo Egypt*, for supporting and encouraging me to pursue a research career. I acknowledge providing the moral support from my roots mother and father during long stay away.

Last, I would like also to thank the most important people in my life, my wife, my son and daughter for always being there for me and supporting me unconditionally.

Table of Contents

List of Tables

List of Figures

Chapter 1

Introduction

1.1 Terrestrial Laser Scanner

Acquiring surface data with Terrestrial Laser Scanners (TLS) have been improved over recent years. The TLS is becoming advanced and cost-effective and getting ready to enter many engineering geodesy applications. It allows for fast and reliable generation of millions of 3D points for very complex structural environments.

The market offers a lot of the laser scanners with different system specifications. They are classified in different ways:

1. To make scanning from the earth (Airborne Laser Scanning).
2. Scanning from the ground (TLS).
3. Hand-held scanners.

The second type (Terrestrial Laser Scanners) will be considered in this study. Nowadays, the third generation of TLS is available on the market. Geodesists and many others are interested in laser scanning systems. TLS's are used for instance for architecture, virtual reality, heritage documentation and preservation. Now the laser scanner technology offers many advantages over the traditional surveying and photogrammetric method [Kern, 2003] to acquire surface data of an object.

In contrast to classical photogrammetric method, which needs a minimum of two images and many complicated processing steps to generate a 3D information, laser-scanning generates directly a 3D information (called point cloud) with just one single setup of the scanner. For every scanned point cloud, the laser ray is deflected with two predefined angles (vertical and horizontal) to the scan object, the slope distance to the object is measured. Each point of this cloud has the intensity of the received signal and three-dimensional coordinates with accuracies up to few millimeters.

Although the laser scanner gives very rich surface details, it does not target specific points. All the scanners are similar to the reflectorless total station but they have the advantage of a high data

acquisition rate. Because the laser scanner measures points on objects without prisms and reflectors, the distance accuracy is influenced by several parameters. The main of these parameters are :

1. Nature of the scan object (e.g. material, roughness, color),
2. Angle of incidence (angle between surface normal and laser ray)
3. Distance between scanner and scan object.

There is no universal Terrestrial Laser scanner for all applications. The decision which laser scanner is the right one depends on the application [Schulz and Ingensand, 2004]. One scanner is more suitable for indoor use and medium ranges (up to 150 m), another scanner is more suitable for outdoor use with long ranges (up to several 100 m).

1.2 Objectives of the Thesis

Most of the scanned objects have more than one scan to describe their surface with completely manner. The process of collecting all of these scans in one common coordinate system is called data registration. Registration methods of point clouds that are acquired from multiple viewpoints is the main topic of this thesis. Data registration could be done based on targets or point clouds itself. If the targets method is used, then the data registration problem simply is reduced to the calculation of a rigid body transformation, which make the similar targets in the adjacent scanworlds match as closely as possible. Registration targets could be special targets attached onto the scan object like plain retro-reflective, black-white targets as well as such targets, which have well-known geometrical 3D shapes (e.g. spheres, planes, cylinders). If the data is registered based on point clouds, the scan data must be overlapped. Correspondence (the overlapped point clouds areas) between adjacent scanworlds could be established by calculating a feature of one scanworld and then finding the same ones in the second scanworld.

There is a need to obtain an accurate 3D model for the scan object. The accuracy of the final 3D model is affected by the uncertainty of the transformation parameters. Errors computed for the transformation parameters will be propagated into the transformed scan data. The geometrical distribution of registration targets around the scanner position is a very important task. With this background, the present study aims to searching and developing for several registration approaches in order to obtain a complete 3D model with high accuracy for the scan object.

The main objectives of this study are summarized as:

1. **If registration is based on targets method:**
   (a) Explain and define different data registration techniques and algorithms.
   (b) Comparing and evaluating precision of sphere target parameters and study the impact of their fitting quality on data registration accuracy.

(c) Procedure a stochastic assessment to take into account the range between the scanner and the registration targets which are used for data registration in the adjacent scans.

(d) Define some practical rules for capturing the data. An example is the distribution of the tie-points which are used in the registration and their position according to the laser scanner position.

To achieve these objectives, the mixed least square solution was used to calculate the transformation parameters. Using this model, the coordinates of registration targets in left and right scans are considered as observations. The advantage of this approach is giving the same registration target different weights in every two adjacent scans. Sphere targets are used as artificial registration target. Spherical targets are omni directional, the main advantage of using spherical targets for data registration is their viewing from every laser standpoint.

2. **If registration is based on point cloud method:**

(a) Improving initial transformation information to be used by the ICP data registration method.

(b) Establishing some geometrical features for identifying overlapped zones between adjacent scanworlds.

A lot of features in different scans have been extracted and carefully chosen for data registration purposes. As a feature for corresponding search, the surface curvature information is used. It is invariant under rigid transformations. The curvatures of the selected part from overlapped scans is calculated and filtered. Edges of two scans are segmented based on curvature values. Edges intersection points are used to define correspondence points between adjacent scans.

1.3 Thesis Outline

The thesis is organized according to the following chapters:

- Chapter 2: Fundamentals of Terrestrial Laser Scanner. This chapter explain the basic understanding of laser light and how to build laser light. The main components of a terrestrial laser scanner are discussed. Laser scanning applications and distance measurement methods, angles deflection system are also described. Geometrical quality of laser scanners measurements are discussed in this chapter.

- Chapter 3: Data Registration Concepts. Chapter 3 deals with terrestrial laser scanner data registration methods. Types of registration targets are explained. Techniques and algorithms for fitting targets are discussed. The advantages and disadvantages of the different registration targets are also presented.

- Chapter 4: Data Registration Algorithms. Chapter 4 deals with algorithms of data registration methods. Different representations of transformation matrix are also explained. Two methods for calculation of approximation transformation parameters are discussed. The first trial to improve start correspondences points identification for the ICP solution is used with a real point cloud.

- Chapter 5: Improving Data Registration Accuracy.

  This chapter involves an investigation of several parameters, which have to be taken into account for getting precise transformation parameters. The target registration method is considered in this chapter. Many types of registration targets have been studied also. Defining the best target distribution and improving data registration accuracy have been discussed.

- Chapter 6: Correspondence Features Identification Between Point Clouds. This chapter deals with define the correspondence features between overlapped scanworlds for the point cloud registration method. Establishing some geometrical features for correspondence search between adjacent scans are also discussed.

- Chapter 7: Experimental Test. With a real scan data the algorithms are tested. The improved solution method is compared with another solution method to compare the accuracy.

- Chapter 8: Conclusions and Future Directions. This chapter summarizes the findings of the thesis and gives an outlook for the future work.

Chapter 2

Fundamentals of Terrestrial Laser Scanner

TLS collect $3D$ coordinates of a defined region of an object surface automatically and in a systematic pattern with a high data collecting rate. With TLS achieving $3D$ coordinates in real time. The point clouds of the scan object can be visualized simultaneously with the scanning process. This chapter will outline many topics about physical characteristics of laser light and components of laser scanners. Scanning systems and laser scanner types are also discussed during this chapter.

2.1 Laser Light

The word LASER is an acronym for Light Amplification by Stimulated Emission of Radiation. The explanation of these words are [Svelto, 1998]:
Light. All light is a form of electromagnetic radiation that is visible to the human eye.
Amplification: This is simply the process of making something bigger or or more powerful. When you turn up the volume on a radio, you are amplifying the sound; but with lasers, amplification makes the light brighter.
Stimulated: To stimulate means to stir to action. Laser light is created when a burst of light (electricity) excites the atoms in the laser to emit photons. These photons then stimulate the creation of additional identical photons to produce the bright laser light.
Emission: The word emission refers to something that is sent out or given off. Stimulated laser emission consists of large numbers of photons that create the intense laser light.
Radiation: The laser light is a form of energy that radiates, or moves out, from the laser source. Laser action is explained by the theories of quantum mechanics and thermodynamics. Many materials have been found to have the required characteristics to form the laser gain medium needed to power a laser, and these have led to the invention of many types of lasers with different characteristics suitable for different applications.

2.1.1 Electromagnetic Waves

In the late 1800's, physicists knew about radio waves and light, but considered them as different things. *Maxwell*, in formulating his equations explaining the two, showed that both are the same thing. They are all examples of electromagnetic radiation (EM). They differ only in frequency. The chart below shows the spectrum of EM. Light, microwaves, x-rays, as well as TV and radio transmissions are all kinds of EM waves. They are all the same kind of wavy disturbance that repeats itself over a distance called the wavelength. The behavior of EM radiation depends on its wavelength. When EM radiation

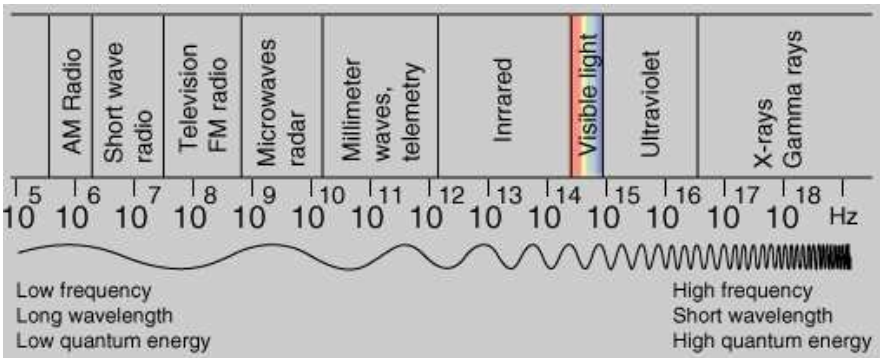

Figure 2.1: The electromagnetic spectrum [Nave, 2006].

interacts with single atoms and molecules, its behavior depends on the amount of energy per quantum it carries.

2.1.2 Laser Radiation Properties

The laser light has three major properties as follows:

1. Coherent: Electromagnetic waves have the the following equation:

$$y = A \cdot \cos(wt + f) \tag{2.1}$$

where:

y	=	Vertical displacement.
A	=	Amplitude (maximum displacement).
w	=	Angular Frequency.
f	=	Initial Phase of the wave (Describe the starting point in time of the oscillation).
$(wt + f)$	=	Angular displacement from 0°, called the phase angle.

Coherent waves are waves that maintain the relative phase between them. Figure 2.2 describes two waves that have the same phase will give a constructive case, but the others give destructive case while the phase angle is different.

2. Monochromatic: Laser light consists of essentially one wavelength, having its origin in stimulated emission from one set of atomic energy levels.

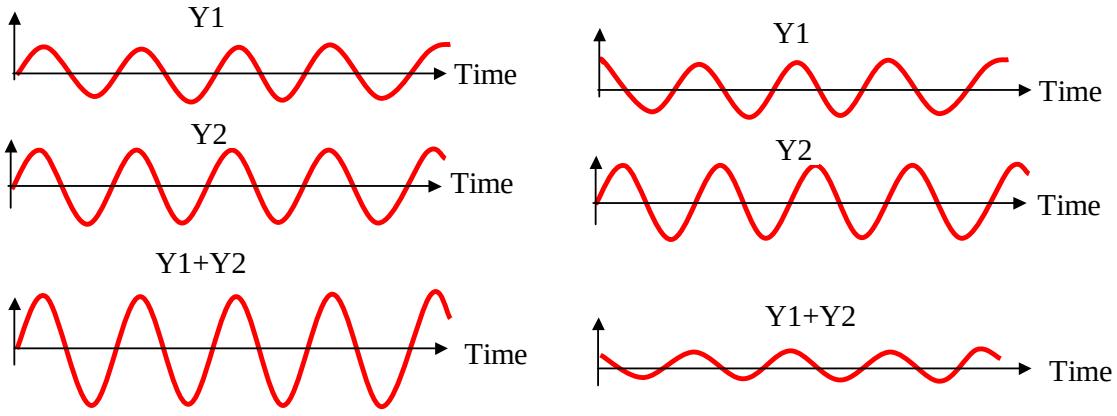

(a) Waves with same phase (b) Waves with different phase

Figure 2.2: Superposition of waves.

3. Collimated or Directionality: Because of bouncing back between mirrored ends of a laser cavity, those paths which sustain amplification must pass between the mirrors many times and be very nearly perpendicular to the mirrors.

In summary, laser radiation properties are:

- Very small divergence of the beam. The beam is almost a parallel beam and moves in one direction in space directionality.
- High degree of monochromaticity. The radiation is almost one wavelength, as can be measured by the very narrow spectral width.
- Coherence

The combination of these properties gives the laser radiation many advantages, like achieving very high power densities that are not available from other sources.

2.1.3 Creating a Laser

The main components for most lasers to operate are:

- The active medium: Collections of atoms, molecules or ions in the form of solid, liquid or gas.
- Population inversion.
- Optical feed back.

Three key elements in a laser creating are, see figure 2.3:

- Pumping process prepares amplifying medium in suitable state.

- Optical power increases on each pass through amplifying medium.
- If gain exceeds loss, the device will oscillate, generating a coherent output.

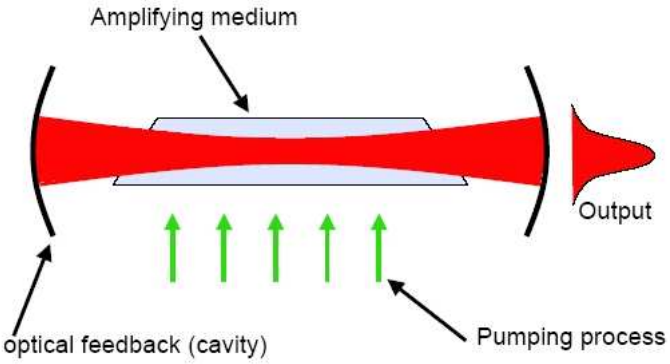

Figure 2.3: Creating a Laser [Sakeek, 2007].

Consider a collimated beam of light traveling in z-direction and passing through an atomic gas. For simplicity assume that there is only a single radiative transition, which occurs between two energy states E_1 and E_2 where $E_2 > E_1$. The incident light is monochromatic at the transition frequency.

$$f_{21} = (E_2 - E_1)/h$$

The light beam is characterized by its irradiance I.

$$I_v = c \cdot \rho(\nu)$$

Where:

I_v	=	irradiance (energy per unit area per sec).
c	=	speed of light (m/sec).
$\rho(\nu)$	=	energy density (J/m2.sec).

2.1.4 Laser Classes

According to the danger for humans the lasers are divided in device classes. The laser is classified from the manufacturer as follows:

- Class 1: Accessible laser radiation is harmless.
- Class 2: Accessible laser radiation lies only in the visible spectral region ($400Nm$ to $700Nm$). It is at brief irradiation duration (to $0.25s$) harmless also for the eye.
- Class 3A: Accessible laser radiation becomes dangerous for the eye, if the radiation cross section is made smaller by optical instruments. If this is not the case, the sent laser radiation is harmless in the visible spectral region ($400Nm$ to $700Nm$) at brief irradiation duration (to $0.25s$), in the other spectral regions also during long-term irradiation.

- Class 3B: Accessible laser radiation is dangerous for the eye and in special cases also for the skin.
- Class 4: Accessible laser radiation is very dangerous for the eye and for the skin. Also vaguely strewn radiation can be dangerous. Laser radiation can cause fire or danger of explosion.

2.2 Laser Scanning Applications

High resolution tripod-mounted laser scanners are used for many engineering and civil applications, because the laser scanner technology offers many advantages compared to the traditional surveying and photogrammetric methods. It is fast and cost-effective, it is well suited for many civil engineering applications that could be summarized as follows [Schulz, 2007], [Jaselskis, 2003] and [Dutescu, 2006]:

- **Reverse Engineering:** Reverse Engineering (RE) is the art of taking 3D surface data from a component and creating a CAD model that can be used in the digital design process or, in some cases, utilized directly for creating CNC tool paths. This process requires comprehensive, high density, high accuracy data. The more comprehensive and accurate the scan data is, the less manipulation that is required by the operator to reproduce the surface geometry.
- **Mechanical Engineering:** Laser scanning is ideal for mechanical applications because the software solutions available convert point data into CAD primitives quickly and accurately.
- **Construction Design:** Construction design is one of the largest areas for 3D modeling development. Applications include roadway, bridge, and building design and rehabilitation. Designing construction projects using 3D modeling has been found to have many benefits for example:
  1. Coordination issues can be minimized with virtual design and construction.
  2. 3D modeling provides efficient generation of multiple views.
  3. The 3D modeling process can generate automated bills of material.
  4. The data generated through laser scanning and modeling can be efficiently integrated into analysis software like CAD-Programs.
- **Transportation Related Applications:** Laser scanning for highway design can provide many benefits, such as the ability to survey during heavy traffic times without positioning surveyors in the roadway and without closing the road. Laser scanning can be used for creating as built drawings of bridges to assist in modifications. This technology also has the potential to perform storm simulations to evaluate the flooding and ponding effects of current and proposed drainage structures.
- **Surveys:** When accessibility and safety issues prevent a traditional survey, laser scanning provides an excellent replacement. Laser scanning can be used to perform accurate and efficient as built surveys and before and after surveys. Inaccessible locations, complex arrangements, and hazardous locations can all be easily modeled.

- **Historical Modeling:** Laser scanning provides new options to model historical sites and large ornate structures.
- **Accident Investigation:** Laser scanned data are very useful in forensics, as well as in general investigation and documentation. For example, in the area of accident investigation. At the accident place, it could develop 3D models related to accidents and accident scenes.
- **Planning, Logistics, and Management:** Existing buildings in an area can be laser scanned, and then what if scenarios related to installing new buildings can be performed using 3D modeling. A 3D hologram could show where everything is located, allowing the designer and builder to walk through walls and see the studs and other components. Many applications also show promise in other areas of logistics and management. 3D modeling could be used to measure and verify quantities of work to be performed. Laser scanning could also be useful in improving quality control (e.g., measuring the location of anchor bolts and evaluating cut/fill requirements).
- **Industrial Environments:** In industrial applications, the time needed for surveying is an important factor, because long down times in production should be avoided. It is therefore an ideal environment for using the laser scanner. Beside generating CAD models of the environment for as built documentation or simulation purposes, it is also the base for robot navigation especially in the area of robot vehicles.
- **Structural deformation monitoring:** Acquire measurements in a uniform sampling pattern. This operation is different to that of surveying instruments, which are considered pointable[1] and thus allow measurements of the same point at different epochs in time. Since scanners are non point able, the same point can not be re measured and therefore compared from one epoch to the next for possible deformation. To circumvent the problem, scanner data can be reduced to a surface representation (e.g., a finite element mesh), the nodes which constitute the "virtual" points compared for deformation.

2.3 Digitizing Objects with Laser Scanning Systems

Laser scanners are spherical measurement systems that measure the area of interest with a very high frequency. The output from the scanner for each point are one oblique distance ρ and two orthogonal angles θ and α, together with the additionally registered intensity of the returning signal distance. These spherical coordinates fully describe the three dimensional position of each point at the scan object in a local coordinate system relative to the scanner stand point. The geometric relation between these measurements and three-dimensional information of the scanned points could be calculated from equation 2.2.

$$\begin{bmatrix} x \\ y \\ z \end{bmatrix} = \rho_i \begin{bmatrix} \sin\theta_i \sin\alpha_i \\ \cos\theta_i \sin\alpha_i \\ \cos\alpha_i \end{bmatrix} \tag{2.2}$$

where :

[1] TLS can not measures the coordinates of a point, it scans a selected surface.

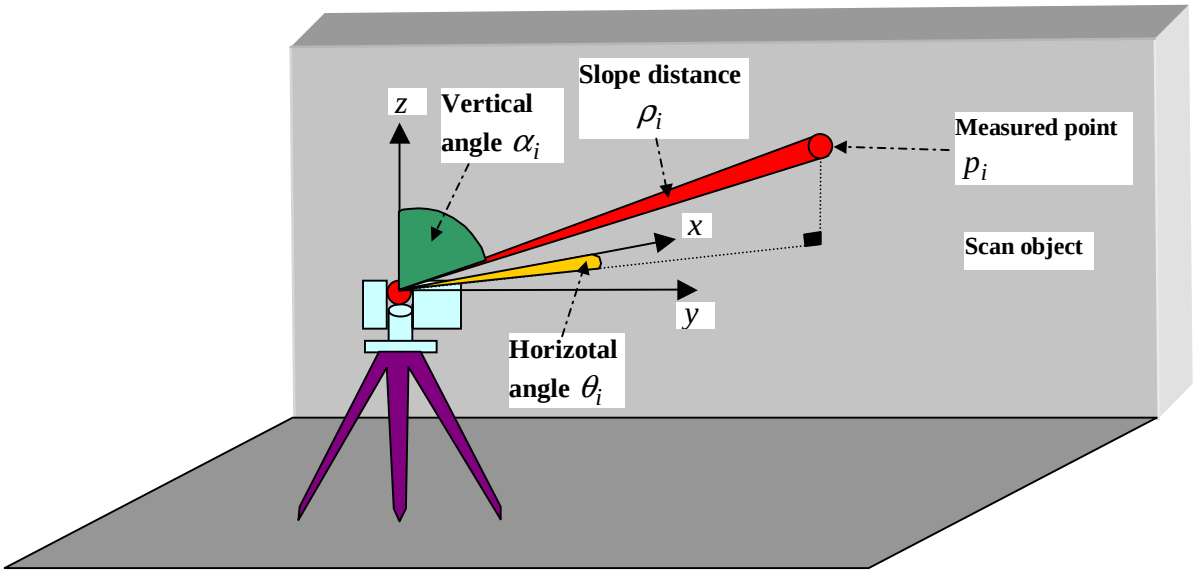

Figure 2.4: Polar measuring system with a laser scanner system.

x, y, z	=	point cloud coordinate.
ρ_i	=	slope distance between laser scanner instrument and object.
θ_i	=	horizontal angle at scanner head.
α_i	=	vertical angle at scanner head.

2.4 Components of Scanning Systems

Laser scanning is a fast method of collecting 3D data for object modeling or mapping. Laser scanner can also be used in virtual reality applications. Any laser scanning system includes:

1. a laser scanner positioned on a tripod see figure 2.4.
2. laptop PC with a scanning software (for old scanning systems). For the newest scanning system like IMAGER 5006, with a PDA and blue tooth antenna it is possible to control and transport scanning data.
3. Power Supply.
4. Standard accessories like reflective targets.

2.5 Laser Ranging Measurement Systems

There are many different ways to use a laser for measuring the distance of an object point to a laser scanner stand point. All of them take advantage of three basic attributes of laser light: unobscured light travels in straight lines; the velocity of light when traveling in space is known; the light produced by a

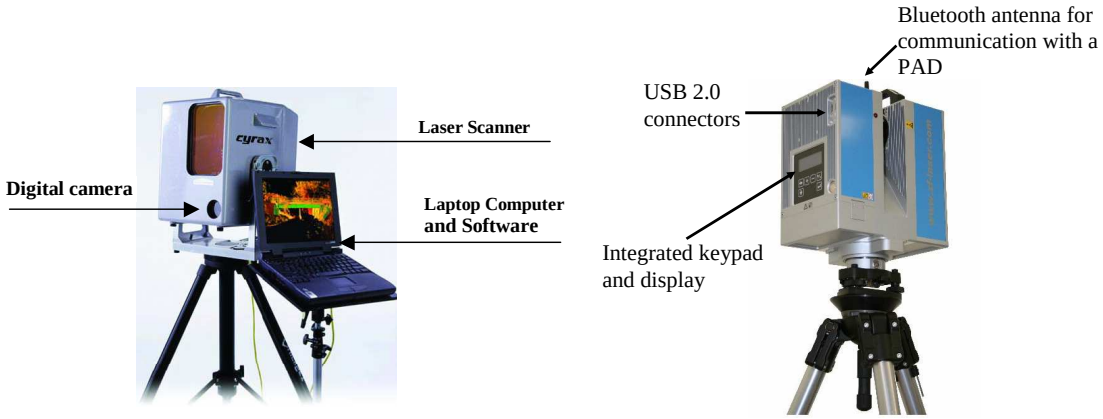

(a) Cyrax 2500 (b) IMAGER 5006

Figure 2.5: Scanner components.

laser is typically only a single wavelength light and is thus easy to detect. There are three traditional approaches in measuring distances with laser scanning systems (range-finding):

1. Time of flight ranging method.
   - Direct time of flight.
   - Indirect time of flight.
2. Triangulation ranging method.
3. Interferometry ranging method.

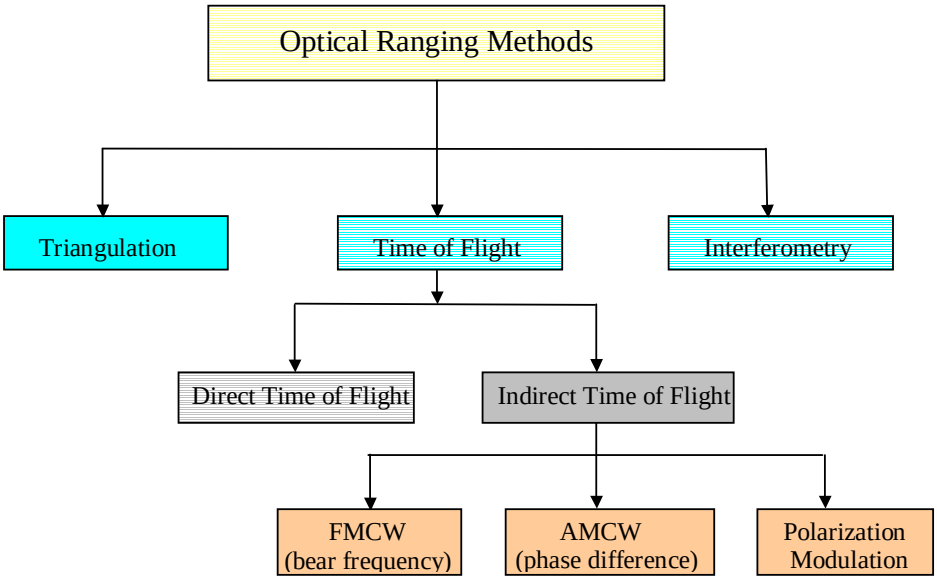

Figure 2.6: Techniques for ranging methods in terrestrial laser scanners [Schulz, 2007].

Since the interferometry ranging method is not used in terrestrial laser scanners, in the following sections the first two ranging methods will be discuss in detail.

2.5.1 Direct Time of Flight Ranging Method

The time of flight 3D laser scanner is an active scanner that uses laser light to probe the subject. At the heart of this type of scanner is a time of flight laser range finder. The laser range finder measures the distance of a surface by timing the round trip time of a pulse of light. These laser ranging systems are used to measure the distance (or range) between the source (where the ranging system is located) and some object, which will be called the target. In practice, the active light source and the receiver are located very close to each other. This facilitates a compact setup and avoids shadowing effects. The basic principle of a time of flight (TOF) ranging system is shown in figure 2.7. A source emits a

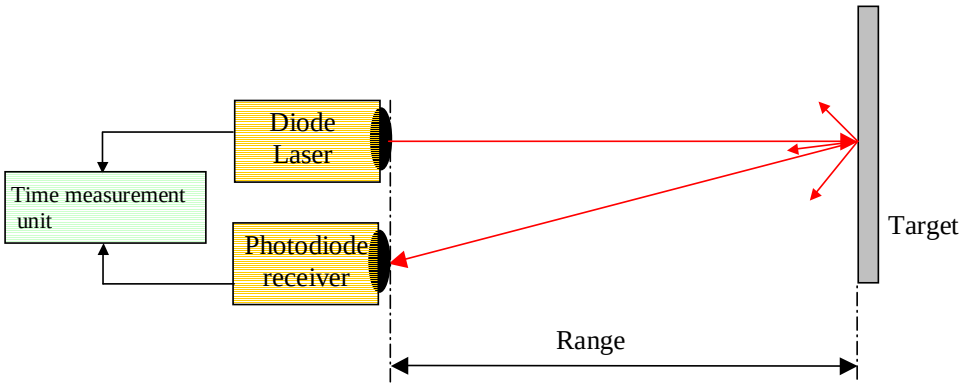

Figure 2.7: Principle of time-of-flight ranging.

light pulse and starts a high accuracy *nanosecond stop watch*. The light pulse travels to the target and back. Reception of the light pulse by the detector mechanism stops the stop watch. A clock measures the time elapsed between the beginning of the pulse and the leading edge of the return pulse.

When operating in some environments, it is possible for some of the outgoing laser energy to be reflected by dust or fog, while the remainder of the energy travels until it reaches a solid surface and returns to the detector. In this case, the receiver will see multiple return pulses. Pulsed light operation is the most obvious method because the time of flight is measured directly. The advantage of using pulsed light is the possibility of transmitting a high amount of energy in a very short time. Thus a high short-term optical signal-to-noise ratio is attained while maintaining a low mean value of optical power. This is an important factor for eye safety, which is the limiting criterion for many measurement applications [Lange et al., 1999]. Furthermore, it reduces the demand on a very high sensitivity and signal-to-noise ratio of the detector, thus enabling long distance measurements. It is, however, difficult to produce very short light pulses with fast rise and fall times. Such pulses are necessary to assure an accurate detection of the incoming light pulse, independent of the detection level .

$$2Range = c \cdot \Delta t = c \cdot (t_R - t_E) \tag{2.3}$$

Where:

$Range$	=	distance between instrument and target.
Δt	=	difference in time.
t_E	=	time of departure of pulse
t_R	=	time of arrival of pulse
c	=	speed of light.

The laser most often used for laser ranging is a Q-switched laser with a short pulse. The shorter the pulse, the more accurate the range measurement. The laser should have a high value of peak power, to increase the received power. Usually a digital circuit, such as a time interval counter is used to measure Δt. Precision ranging requires that this time is to be measured relative to a specific point on the pulse, e.g., the "leading edge". The leading edge of a pulse is the rising or buildup side of the pulse. This is called "leading-edge detection" and is shown in Figure 2.8. In reality, pulses with

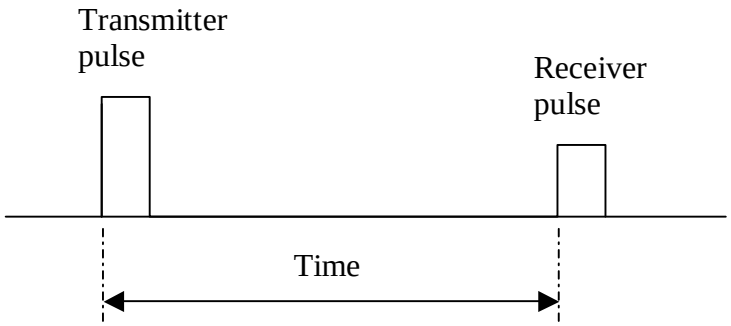

Figure 2.8: Pulse range measurement by leading-edge detection.

instantaneous rise times as shown in Figure 2.8 do not occur. Consequently, the "leading edge" for detection has to be defined more precisely. This is done by measuring time from a point on the leading edge where the signal voltage has reached a predetermined value. As discussed in this section, if one wants a resolution range of 1 mm then a time delay could be calculated as following:

$$Range = c \cdot \frac{\Delta t}{2} = 1 \ \ mm = 3 \cdot 10^{11} \cdot \frac{\Delta t}{2}$$

$$\Delta t = \frac{2}{3 \cdot 10^{11}} \ \ sec = 6.67 \ \ picoseconds$$

This means to get 1 mm resolution, 6.67 picoseconds should be measured. The accuracy of a pulsed ranging system is determined by three major factors:

1. Ability to select the same relative position on the transmitted and received pulse to measure the time interval. This is limited by noise, time jitter, signal strength and sensitivity of the threshold detector, and shortness and reproducibility of the transmitter pulse.

2. The accuracy with which fixed time delays in the system are known.

3. The accuracy of the time interval measurement instrumentation.

The advantage of this method is that long ranges are possible (a few hundred meter range), thus allowing large object to be scanned. The main disadvantage of time of flight ranging method is a slow

data rate, while the pulsed system rate is slow to generate the pulses. The range uncertainty for a single pulse is approximately given by the following equation [Beraldin, 2004]:

$$\sigma_{Range} \approx \frac{c}{2}\frac{T_r}{\sqrt{SNR}} \tag{2.4}$$

Where:

σ_{Range}	=	uncertainty in range estimation pulse system
T_r	=	Pulse rise time
SNR	=	signal-to-noise ratio

In analog and digital communications, signal-to-noise ratio, often written SNR or S/N, is a measure of a signal strength relative to background noise. For example, if a round trip of 1 microsecond is measured then the corresponds range about 150 m. Assuming a SNR=100 and $Tr = 1$ nanosecond, the range uncertainty is close to 1.5 cm. Different efforts have been made to calibrate and test accuracies of TLS, for example [Schulz, 2007], [Lichti et al., 2000a], [Johansson, 2004] and [Boehler et al., 2003].

2.5.2 Indirect Time of Flight Ranging Method (Phase difference method)

Continuous wave (CW) lasers are also used in optical ranging systems. For CW modulation generally the phase difference between sent and received signal is measured, see Figure 2.9. The transmitted

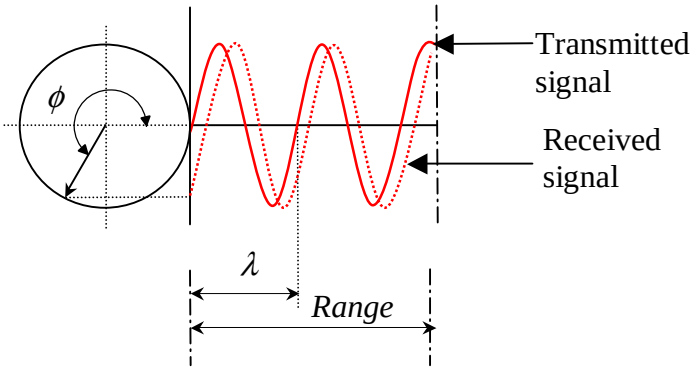

Figure 2.9: Phase comparison measurement in CW.

laser light is intensity modulated (Amplitude Modulated Continuous Wave, AMCW), with the laser light reflected by an object being received by a photo diode. The time of flight of the laser light from the sensor to the object and back results directly in a phase difference between transmitted and received laser light. That phase difference is proportional to range (object distance) and laser modulation frequency. The amplitude of the received, diffusely reflected laser light is proportional to surface reflectivity and distance of the object, see equation 2.5.

$$2 \cdot Range = N \cdot \lambda + \Delta\lambda \tag{2.5}$$

Where:

N = number of full wavelengths
λ = wavelength
$\Delta\lambda$ = rest of wavelength.

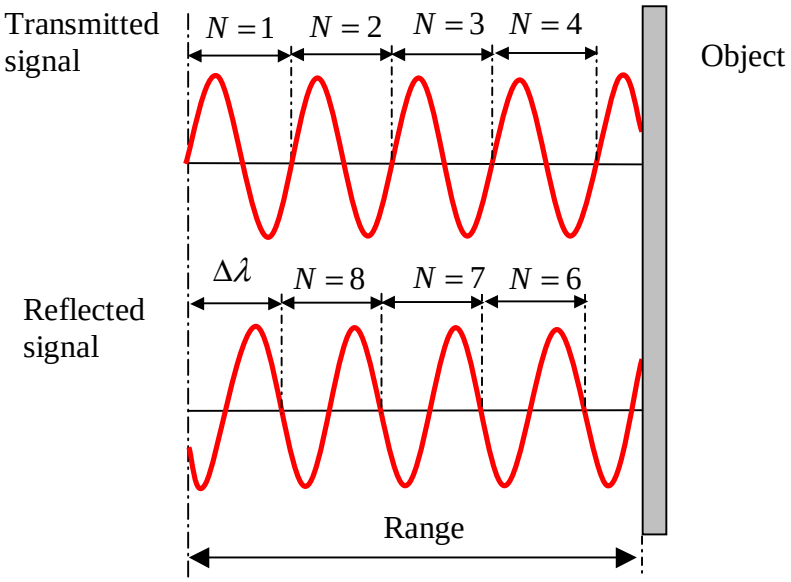

Figure 2.10: Phase difference techniques measuring.

To get the range between source and target, the values N and $\Delta\lambda$ should be defined. There is a relation between rest of wavelength $\Delta\lambda$ and rest of phase angle $\Delta\phi$

$$\Delta\lambda = \frac{\Delta\phi}{2\pi} \cdot \lambda \tag{2.6}$$

Where:

$\Delta\phi$ = rest of phase difference angle

The range distance will be:

$$Range = \frac{N \cdot \lambda}{2} + \frac{\Delta\phi}{4\pi} \cdot \lambda \tag{2.7}$$

As shown in equation 2.7, it is not possible to get the range between source and target from a simple AMCW ranging method. This is known as the ambiguity interval and can be in the order of several meters. The equation of maximum unambiguous range is given by equation 2.8 or equation 2.9.

$$Range_{max.} = \frac{c}{2 \cdot f} \tag{2.8}$$

$$Range_{max.} = \frac{\lambda}{2} \tag{2.9}$$

If the range is unambiguous (less than $Range_{max.}$), the range can be determined from the following equation:

$$Range = \frac{\Delta\phi}{4\pi} \cdot \lambda \tag{2.10}$$

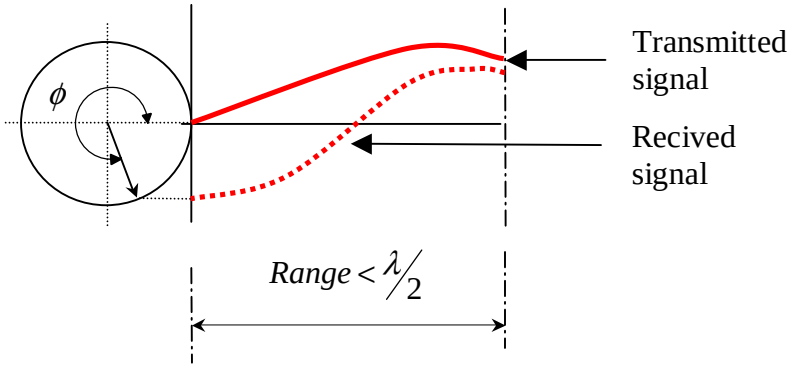

Figure 2.11: Phased difference case of $Range < \frac{\lambda}{2}$.

To get around the inconvenience of a range ambiguity interval, one can use multiple frequency waveforms, see Figure 2.12. The lower-frequency tones are used to prevent an ambiguous range measurement. The higher-frequency tones are used for more accuracy. For example, assuming a two-tone AM system (low frequency of 10 MHz and high frequency of 150 MHz), the range uncertainty is about 0.5 cm (using the high frequency) and the ambiguity is 15 m (using the low frequency) [Beraldin, 2004]. Another example, if the values 15, 150, 1500 and 15000 kHz frequencies are used in ranging system, the range could be calculated by collecting the distance from different used frequencies as shown in table 2.1.

Table 2.1: Ranging by using different frequences [Schlemmer, 1996].

Measuring steps	Frequency (kHz)	Max. Range=$\lambda/2$ (m)	phase angle (Rad.)	rest distance (m)
Range from phase f_1	15	10000	0.662	6220
Range from phase f_2	150	1000	0.216	216
Range from phase f_3	1500	100	0.156	15.6
Range from phase f_4	15000	10	0.573	5.73
Final distance				**6215.73 m**

For example, the Z+F laser scanning instrument uses the phase difference method to determine the object range [Fröhlich et al., 2000]. The range is calculated by a combination of two modulation frequencies. There are 23 MHz and 2.875 MHz to provide improved accuracy, see Figure 2.12. So the range ambiguity by using the low frequency is:

$$Range_{max.} = \frac{c}{2 \cdot f} = \frac{3 \cdot 10^8}{2 \cdot 2.875 \cdot 10^6} = 52.174 \ m$$

For instance, with the frequencies 2.875 and 23 MHz and a phase resolution of $\Delta\phi = 0.01$ degree (not too difficult with standard electronics), the resolution in range can be calculated as follows:

$$\Delta Range_1 = \frac{\lambda_1}{4\pi} \cdot \Delta\phi_1 = \frac{c}{4\pi \cdot f_1} \cdot \Delta\phi = \frac{3 \cdot 10^{11}}{4\pi \cdot 2.875 \cdot 10^6} \cdot \frac{0.01 \cdot \pi}{180} = 1.45 \ mm$$

$$\Delta Range_2 = \frac{\lambda_2}{4\pi} \cdot \Delta\phi_2 = \frac{c}{4\pi \cdot f_2} \cdot \Delta\phi = \frac{3 \cdot 10^{11}}{4\pi \cdot 23 \cdot 10^6} \cdot \frac{0.01 \cdot \pi}{180} = 0.18 \ mm$$

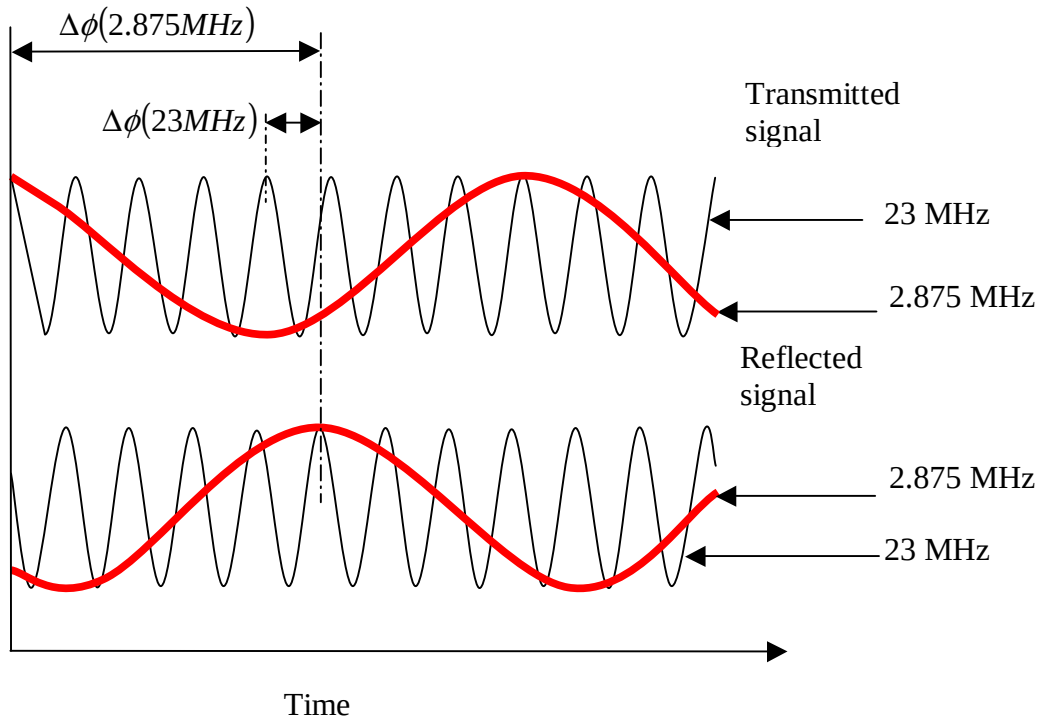

Figure 2.12: The combination of two modulation frequencies for Z+F laser scanning system.

So the factors that affecting accuracy of the phase difference ranging method could be concluded as follows:

1. Frequency of the tone or modulation.
2. Accuracy of the phase-measurement loop, depends on signal strength, noise, and so on.
3. Stability of the modulation oscillator.
4. Number of cycles (or measurements) that can be averaged together for a range measurement.
5. Turbulence in the air during scanning process.
6. Variations in the index of refraction of the air.

2.5.3 Triangulation Method

The triangulation 3D laser scanner is also an active scanner that uses laser light to probe the environment. Sending a laser beam at a defined incrementally changed angle from one end of a mechanical base onto the object. A CCD[3] camera at the other end of this base, which detects the laser spot on the object. This means the range between object and laser scanner within limited range (some meters) is based on optical triangulation. The 3D position of the reflecting surface element can be derived from the resulting triangle. The length of one side of the triangle, the distance between the camera and the

[3]A charge-coupled device (CCD) containing grids of pixels are used in digital cameras, optical scanners and video cameras as light-sensing devices.

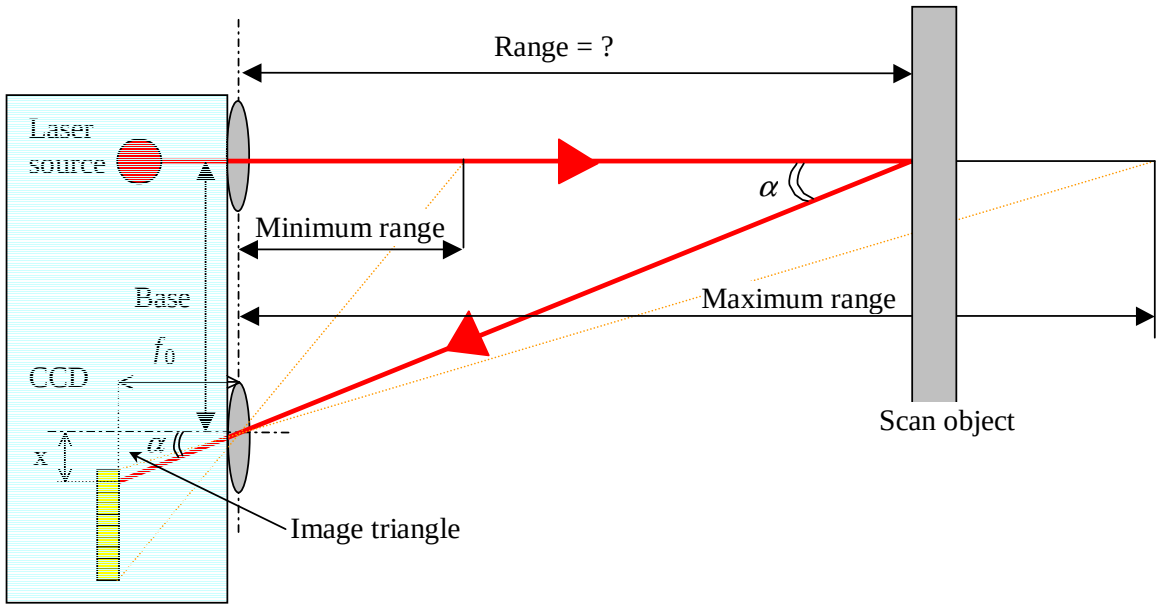

Figure 2.13: Triangulation measuring technique [Kern, 2003].

laser emitter is known see Figure 2.13. The angle of the laser emitter corner is also known. The angle of the camera corner can be determined by looking at the location of the laser dot in the camera's field of view. These three pieces of information fully determine the shape and size of the triangle and give the location of the laser dot corner of the triangle. In most cases a laser stripe, instead of a single laser dot, is swept across the object to speed up the acquisition process. From Figure 2.13 the range could be calculated from the following equation.

$$Range = \frac{f_0}{x} \cdot Base = \frac{Base}{\tan \alpha} \tag{2.11}$$

Where:

$Range$	=	distance between instrument and object.
f_0	=	effective distance between the position detector and the CCD lens.
$Base$	=	mechanical base distance.
x	=	distance from image triangle.
α	=	the deflection angle of the laser beam.

The triangulation range detecting method is exactly the opposite for the advantage and disadvantage of TOF method. They have a limited range of some meters, but their accuracy is relatively high. The scanning systems which are based on optical triangulation ranging method are the most accurate, allowing measurement uncertainty lower than on tenth of millimeter. The range uncertainty is approximately given by the following equation [Beraldin, 2004]:

$$\sigma_{Range} \approx \frac{Range^2}{f_0 \cdot Base} \cdot \sigma_x \tag{2.12}$$

Where:

σ_x = standard deviation of the error in the measurement distance x.

The range uncertainty is therefore inversely proportional to both the Base distance $Base$ and the effective focal length f_0, but directly proportional to the square of the distance $Range^2$.

The main disadvantage of triangulation ranging methods is f_o and $Base$ cannot be made as large as desired. The baseline is limited mainly by the mechanical structure of the optical set-up (stability of the whole system decreases as base distance increases), and also the value of the deflection angle of the laser beam α should be limited according to the quality of triangulation solution.

2.6 Direction Determining Systems

In laser-scanners the direction of the laser ray is controlled by high-resolution angular encoders attached to rotating mirrors, oscillating or rotating polygon-mirrors. The deflection technology is related to the angular working range and allows a categorization into profilers, camera-view type and panoramic scanners, which rotate 360 degrees around the vertical axis.

In today's theodolites, the reading out of the horizontal and vertical circles is usually done electronically. The readout is done by a rotary encoder, which can be absolute, e.g. using gray codes, or incremental, using equidistant light and dark radial bands. In the latter case the circles spin rapidly, reducing angle measurement to electronic measurement of time differences. For the scanners, sweeping the laser beam is measured electro-optically by encoders with respect to a horizontal and a vertical direction.

2.6.1 Incremental Encoding

The determination of the angle is carried out by a coarse measurement and a fine measurement. The coarse measurement counts the number of passing transparent and opaque strips. Therefore, the output signal of the photo diode is triggered and the number of pulses, i.e. transitions between positive and negative states are counted. Due to the pattern consisting of up to 20, 000 elements, the rotation angle has a resolution up to 0.02 gon.

2.6.2 Binary Encoding

With the binary encoding method, a light source passes through the encoded glass circle, which is marked with the number of the graduation in a binary code. Each corresponding digit of the binary code is represented by a transparent or an opaque element, (for more details see [Schlemmer, 1996]). Figure 2.14 illustrate the binary encoding method for angle measuring.

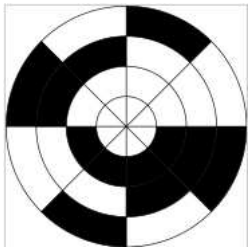

Figure 2.14: Rotary encoder for angle-measuring devices marked in 3-bit binary.

2.7 Mechanical Design of Laser Scanners

TLS instruments could be classified based on many mechanical design and scanning methods. TLS classified based on many characteristics. In this section the different methods which are used to control laser light to detect and scan object will be discuss.

2.7.1 Field of View

The scanner systems on the market today can be divided into two different types.

- Camera scanner:
  Field of view of vertical 40 degree and horizontal 40 degree. Examples are laser scanner Cyrax 2500.
- Panorama-Scanner:
  The field of view is only limited by the base of the instrument (incl. the tripod). This type is designed for indoor purposes, esp. the digitization of rooms, facilities, etc. Examples are Imager 5003 (Zöller and Fröhlich) or Calidus (Calidus Precision).

2.7.2 Sweeping Techniques

A major issue that needs to be addressed is how to move the laser beam around the designated area. Rotational mirrors provide a solution to this problem. They offer the advantage of moving the laser beam around the scene very quickly. Rotating motors could be also another solution, or by using the two tools. In the next two following subsections the two sweeping methods will be discussed.

2.7.3 Angular Deflection by Using Two Oscillating Mirrors

Laser scanner only detects the distance of one point in its direction of view. Thus, the scanner scans its entire field of view one point at a time by changing laser source direction of view to scan different points. The view direction of the laser can be changed by either rotating the laser source itself, or by using a system of rotating mirrors. The latter method is commonly used because mirrors are much lighter and can thus be rotated much faster and with greater accuracy. Typical time of flight

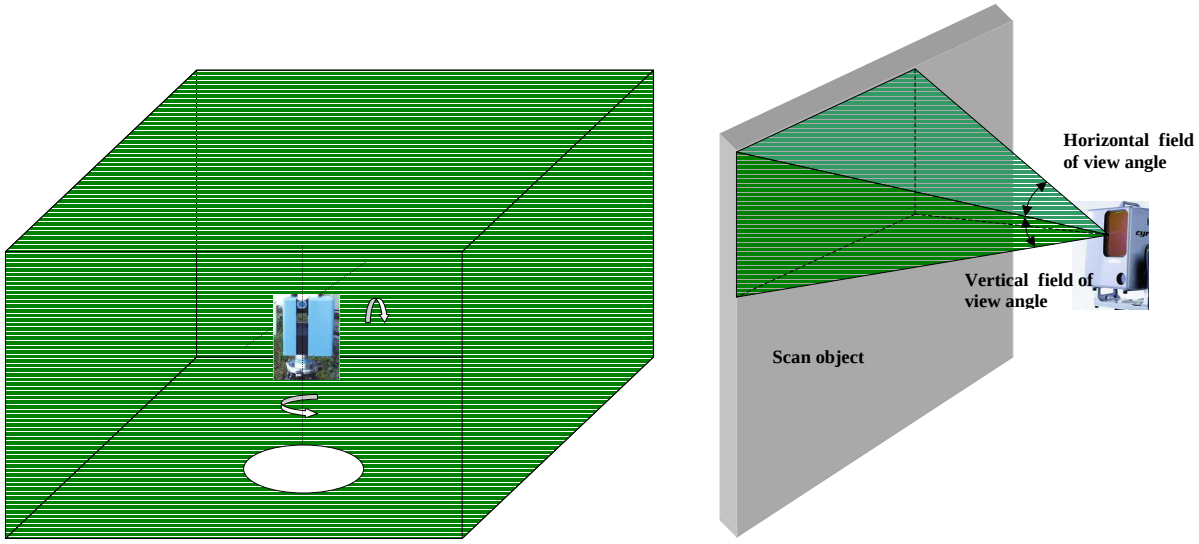

(a) Panorama scanner (b) Camera scanner

Figure 2.15: Scanner types according to field of view.

3D laser scanners can measure the distance of 10,000 points every second. The scan mirrors are rectangular mirror of light weight. They are to be used for high speed two-axis laser scanning system. The dimensions of each mirror have been calculated to allow for scanning of a laser beam with no beam spill over at the extremes of scan. The mirrors have high reflectivity of 99.7% or above and so may be safe at high powers. For a 3D scanning two plane mirrors are to be used. Meaningful it is

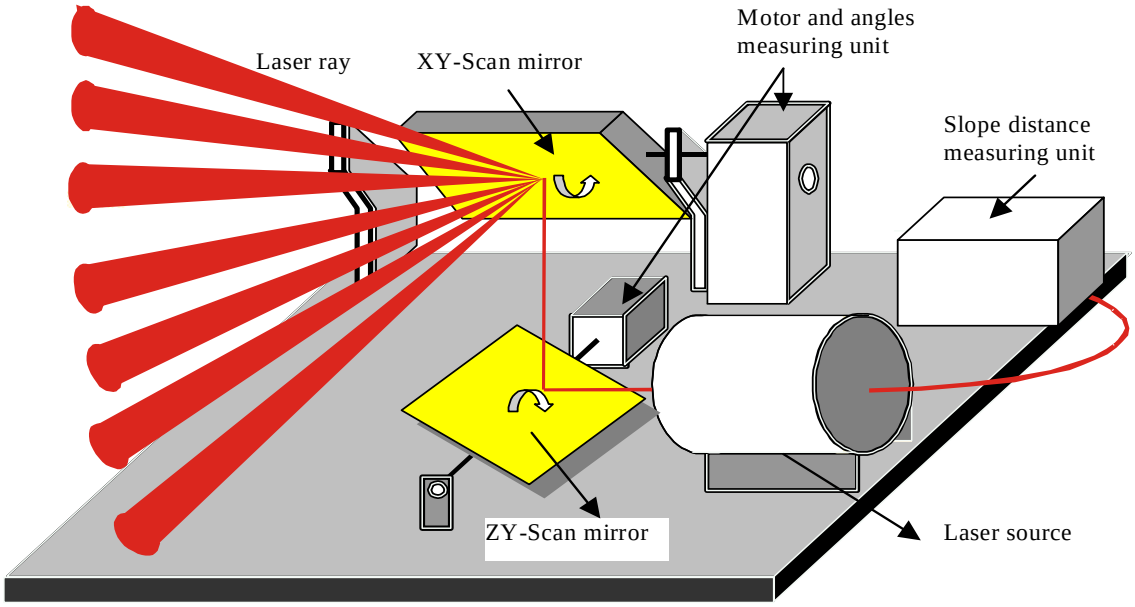

Figure 2.16: Mirror scanning technique [Schlemmer, 1996].

to be arranged the rotation axles of both mirrors in the right angle, in order to receive as large a scanning field as possible. In Figure 2.16 a sensing system which is based on two plane mirrors lying one above the other is outlined. The first mirror can be turned over perpendicularly to the laser light

Figure 2.17: Cyrax 2500.

concerning the y axis. The reflected light cannot leave so the $x-z$-level and on the second mirror is diverted. Depending upon skew angle the point of impact moves on this second mirror along the x axis. The second mirror rotates around the x axis with the angle. By the moving point of impact the light reflected by the first mirror does not always break perpendicularly to the rotation axis on the second mirror. The laser beam is diverted in such a way from the x-z-level. A scanning into arbitrary directions in space is possible. The minimum increment of the encoder unit which cause the mirror to oscillate from one point to the next one define the sample minimum interval or minimum scanning resolution. The disadvantage of angular deflection by using mirrors is the limitation field of view as the case in Cyrax 2500 and HDS 3000 laser scanning system (see table 2.3 for more details about characteristic of some Leica Geosystems laser scanners which are available on the market).

2.7.4 Angular Deflection by Using Only One Rotating Mirror

With this scanning system, the vertical angle is measured by using a mirror that rotates around the horizontal axis (to measure vertical angles α_i). To measure horizontal angles θ_i, the laser beam is deflected by the rotation of the scanner around its vertical axis. The rotation of the mirror around the horizontal axis is faster than the rotation of scanner around its vertical axis. By sweeping the laser scanner itself around the z axis, several scanning profiles are generated one after the other to get a 3D model of the target object, see Figure 2.18. According to this sweeping technique the scanning system is considered a panorama scanner, e.g. laser scanners of Zoller+Fröhlich.

2.8 Geometrical Quality of Laser Scanner Measurements

The quality of a $3D$ model of an object derived from laser scanning is influenced by a number of factors which can be grouped as follows:

1. Non-Instrumental Errors: Errors caused by the laser system (resolution and spot size, scan range and scan angle), and characteristics of scan object (e.g. color, surface nature and scan point resolution).

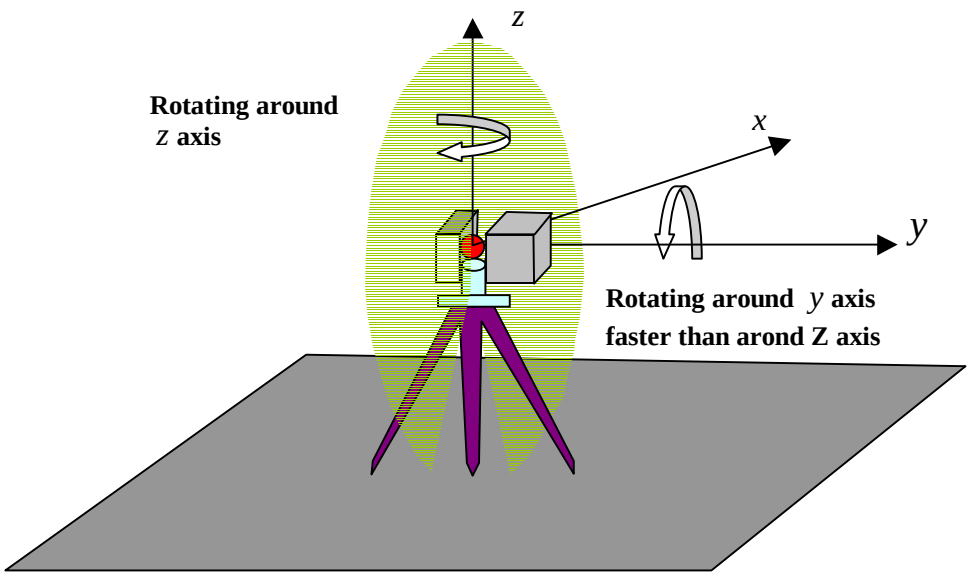

Figure 2.18: Sweeping by using one motor and one rotating mirror technique.

2. Instrumental Errors: Errors due to the mechanical realization of laser scanner components.

3. Errors created during data processing: The sources of these errors could be interpolation errors, filtering errors, errors caused by improper break line detection, segmentation and smoothing of the data.

In the following section the non-instrumental errors will discuss in detail.

2.9 Non-Instrumental Errors

Since laser scanner measure points on objects without prisms or reflectors, the distance accuracy is influenced by several parameters [Schulz, 2007] and [Lichti et al., 2000a]. The main parameters are:

1. Effect of resolution and spot size.

2. The angle of incidence and the distance.

3. Surface properties (e.g. material, roughness, color).

4. The present atmosphere (temperature, air pressure).

All the above sources of errors are classified under the systematic errors for the terrestrial laser scanner system.

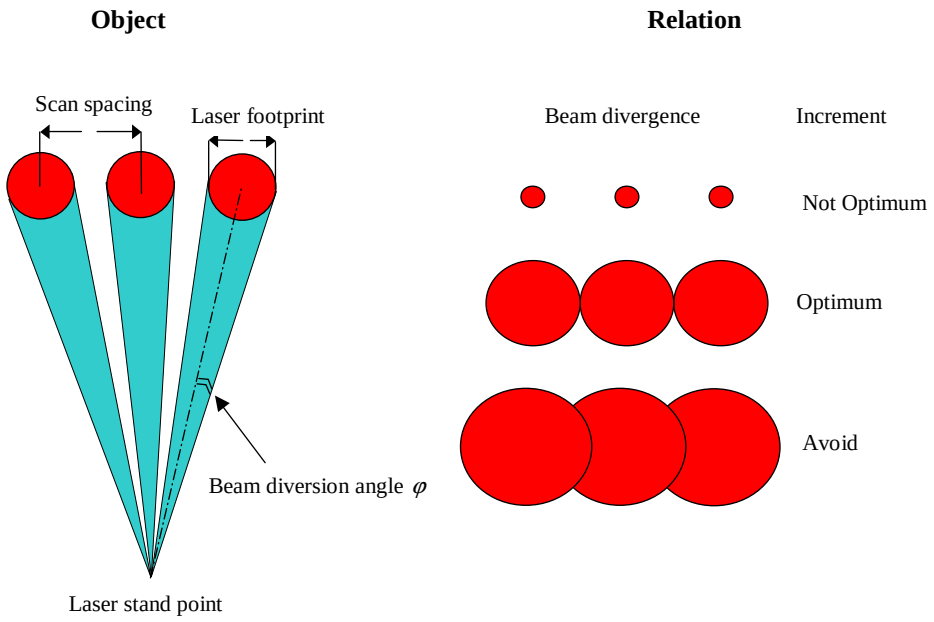

Figure 2.19: 3D surface information by using laser scanners is sensitive to laser beam divergence. Because it affect directly the object resolution. The laser spot is depending on the beam divergence also which takes a direct influence on the goodness of the distance measurement [Schlemmer, 1996].

2.9.1 Effect of Resolution and Spot Size

Beam characteristics, such as size, light distribution and divergence, depend on the design of the laser cavity and the output optics. The beam size refers to the diameter of the beam at the point of exit from the laser cavity. Beam diversion allows to calculate the radius of a laser spot. The transmitter and receiver are both optical systems for laser scanning system. The transmitting optical system acts as an antenna to reduce the divergence angle of the transmitted beam and to aim the beam at the target. The geometrical factors that affect the relation between transmitted power and received power will be discussed. The transmitter geometry of the radiation pattern is shown in Figure 2.20. In this Figure,

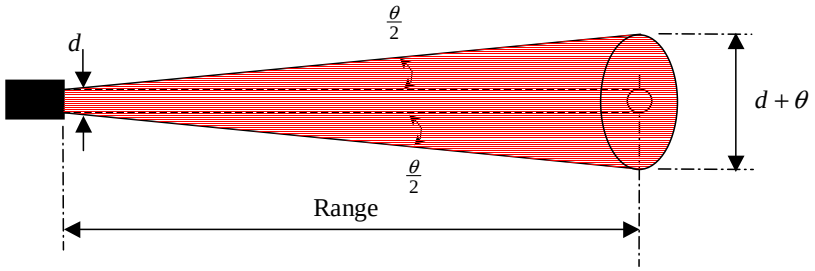

Figure 2.20: Laser transmitter target geometry.

the beam is shown leaving the transmitter antenna with an aperture diameter d, and divergence angle θ (radians). At the target plane, a distance *Range* from the transmitter, the illuminated area from

the transmitter is:

$$Area = \pi \frac{(\theta + d)^2}{4} \tag{2.13}$$

The power density φ_r within this area (assumed for simplicity to be uniform) is equal to the transmitter power φ_t divided by this illuminated area, and reduced by the atmosphere transmission:

$$\varphi_r = 4 \cdot \frac{\varphi_t}{\pi(\theta + d)^2} \cdot T \tag{2.14}$$

The value of T varies from 0 to 1, depending on the amount of absorption and scattering of light by the atmospheric condition. For a beam propagating in space, T will have a value of 1. Equation 2.14 will be used to describe the power density at the target in two target cases non cooperative and cooperative targets. Non cooperative target generally is regarded as a diffusely reflecting object (such as a rock, tree, building, or tank). The term non cooperative is used because the target has not been prepared in advance to enhance the reflected return of the transmitted beam. This means that the reflectivity, r, at the laser wavelength of different targets can vary from less than 1% to almost 100%. When the reflectivity is not known and cannot be estimated, a value of 20 % or 0.2 (absolute number) is generally used.

The laser scanner has an accuracy problem to define edges of the scan object, the reason for that is the mixed pixel phenomenon. This phenomenon occurs when the footprint of the laser falls on the edge between two surfaces which are located at different distances. The fact that the range is measured by integrating over the entire projected footprint may produce phantom objects due to mixed measurements that are inaccurate. Figure 2.21 is a diagram which illustrates this phenomenon at the signal level of an AMACW ranging laser scanner system. The transmitted signal of an AMACW could be split into two or more signals of differing phase ϕ_1 and ϕ_2. The recorded range in this case will be somewhere in between. Edge effects could be avoided by using small beam divergences.

2.9.2 Angle of Incidence Effects

The angle of incidence between the emitted light beam and the scanned surface also introduces inaccuracies. The area of the laser footprint increase proportional with the angle of incidence. As the area of the footprint increases, the precision of the range measurement degrades. This is because of reduced energy being reflected back along the collimated beam of light onto the detector.

2.9.3 Scan Object Nature (Surfaces/Materials) Effect

The proportion of the pulse reflected depends on the properties of the surface material and wavelength of the laser. The amount of light that is returned from a target's surface is characterized by the reflection coefficient r. For a diffusely reflecting target, the maximum value of r is 100 %. For mirror-like or retroreflecting targets, the (theoretical) value of reflectivity can exceed 100 % by far. The reflection coefficient is, of course, also depending on the wavelength.

- Diffuse reflection: The signal is reflected omni-directionally according to Lambert's cosine law.

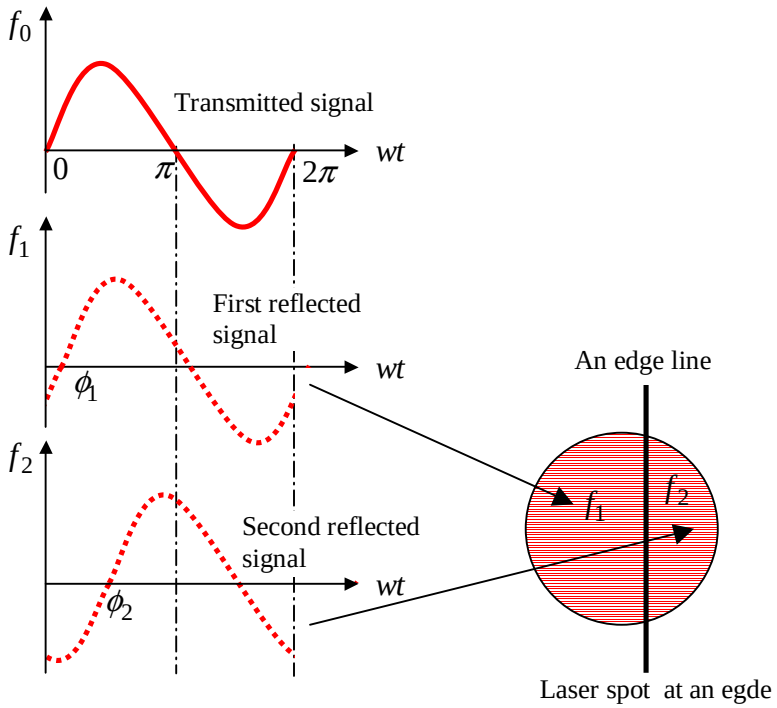

Figure 2.21: Edge accuracy with Laser scanners.

- Mirror-like reflection: The angle of the reflected beam with respect to the targets surface is equal to the angle of incidence. Incident beam and reflected beam lie in the same plane.
- Retro reflection: The retro reflected beam is returned in the same direction from which the incident beam came. This property is maintained over a wide range of directions of the incident beam.

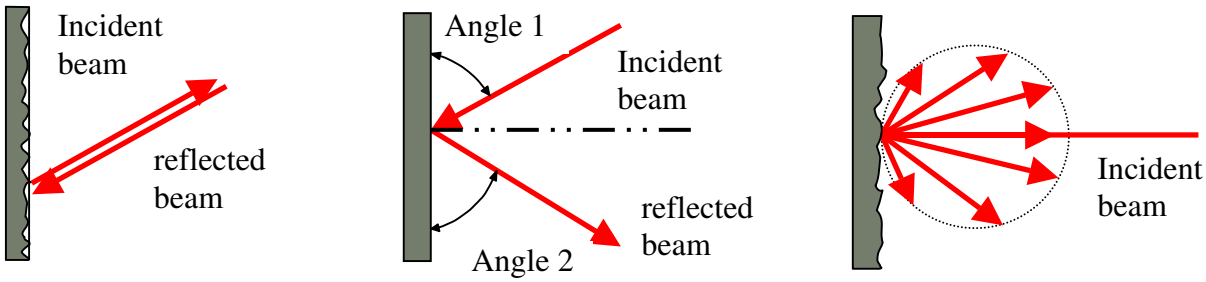

Figure 2.22: Reflection and diffuse reflection.

2.9.4 Atmospheric Refraction Correction

All electromagnetic waves travel through a vacuum at constant speed. When these waves travel through a transmitting material, however, their speed is reduced. The index of refraction of a material is the

Table 2.2: Diffusely reflecting surfaces/materials [Riegl, 2006].

Material	**Reflectivity**
White paper	up to 100%
Dimension lumber (pine, clean, dry)	94%
Snow	80-90%
Beer	foam 88%
White masonry	85%
Limestone, clay	up to 75%
Newspaper with print	69%
Tissue paper, two ply	60%
Deciduous trees typ.	60%
Coniferous trees typ.	30%
Carbonate sand (dry)	57%
Carbonate sand (wet)	41%
Beach sands, bare areas in dessert typ.	50%
Rough wood pallet (clean)	25%
Concrete, smooth	24%
Asphalt with pebbles	17%
Lava	8%
Black neoprene	5%
Black rubber tire wall	2%

ratio of the speed of light in a vacuum to its speed in that material and is given by Equation 2.15.

$$n = \frac{c}{\nu} \tag{2.15}$$

where :

$$\begin{aligned} n &= \text{Index of refraction} \\ \nu &= \text{Speed of light inside material.} \end{aligned}$$

The frequency of a light wave does not change when it enters a material, but its wavelength is reduced (Figure 2.23). The index of refraction is also the ratio of wavelength in vacuum to the wavelength in the material (Equation 9). The index of refraction is also the ratio of wavelength in vacuum to the wavelength in the material (Equation 2.16).

$$n = \frac{\lambda_0}{\lambda_i} \tag{2.16}$$

where :

$$\begin{aligned} \lambda_0 &= \text{Wavelength in vacuum.} \\ \lambda_i &= \text{Wavelength in material.} \end{aligned}$$

Laser scanning instruments are using light to ranging distances between objects and laser stand point. Refraction is directly related with the speed of light as it travels through various materials. Light travels faster through vacuum. When light travels through any material, for example air, it slows

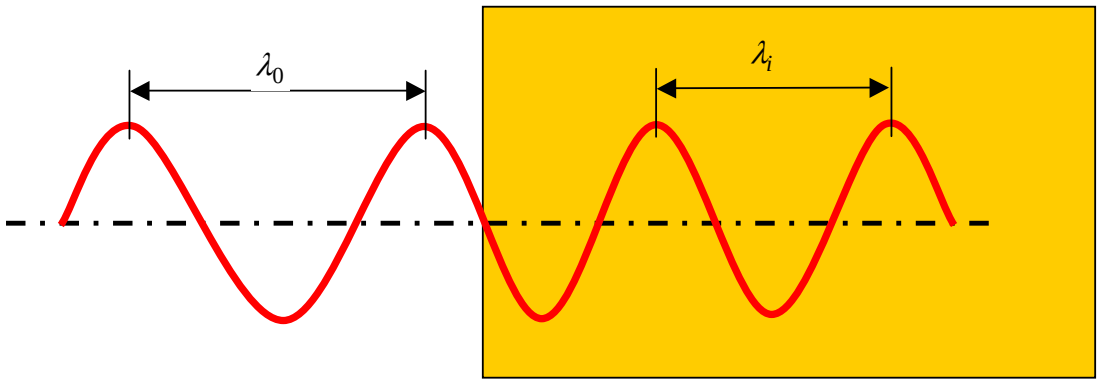

Figure 2.23: Wavelength reduction in material.

down in atmospheric pressure. An important measure is the index of refraction to correct distances with EDM instruments. General, slope distances must be corrected for the actual refractive index of air along the measured line. Measurements of atmospheric conditions at several points along the optical path must be performed with well calibrated thermometers and barometers in order to achieve the 1 *ppm* accuracy. Calculation procedure for atmospheric refraction correction [Rüeger, 1996]:

1. Calculate the refractive index of air under standard conditions, n_{Gr}.

$$(n_{Gr} - 1)10^6 = 287.604 + 3\frac{1.6288}{\lambda^2} + 5\frac{0.0136}{\lambda^4} \tag{2.17}$$

where :

n_{Gr} = refractive index of air under standard conditions
λ = wavelength of carrier beam in μm.

2. Calculate the index of refraction of air at the time of observation, n_L:

$$(n_L - 1) = 987 \cdot 10^{-6} \cdot \frac{n_{Gr} - 1}{1 + \alpha \cdot t} \cdot p - \frac{4.1 \cdot 10^{-8}}{1 + \alpha \cdot t} \cdot e \tag{2.18}$$

where :

n_L = index of refraction of air at the time of observation
t = observed temperature in C°
p = atmospheric pressure in $mmHg$
e = vapor pressure

3. Calculate the reference index of refraction for the instrument, n_0

$$n_0 = \frac{c_0}{\lambda_m f_m} \tag{2.19}$$

where :

λ_m = modulation wavelength
f_m = modulation frequency
c_0 = velocity of light in a vacuum (299,792.458 km/sec at dray air 0° C, 1013.25 hPa and 0.03% CO_2) [Schlemmer, 1996].

4. Finally compute the correction factor for measured slope distances:

$$Corr_n = s' \ \frac{n_0 - n_L}{n_L} \tag{2.20}$$

where :

$Corr_n$ = correction factor for measured slope distances
s' = measured slope distances

The average measuring range for most laser scanning systems lies between 5m to 150m, for example using laser scanner at 40 C°, the correction value is 50 ppm [Kern, 2003]. It means for a distance of 100 m range an atmospheric correction of 5 mm needs to be added.

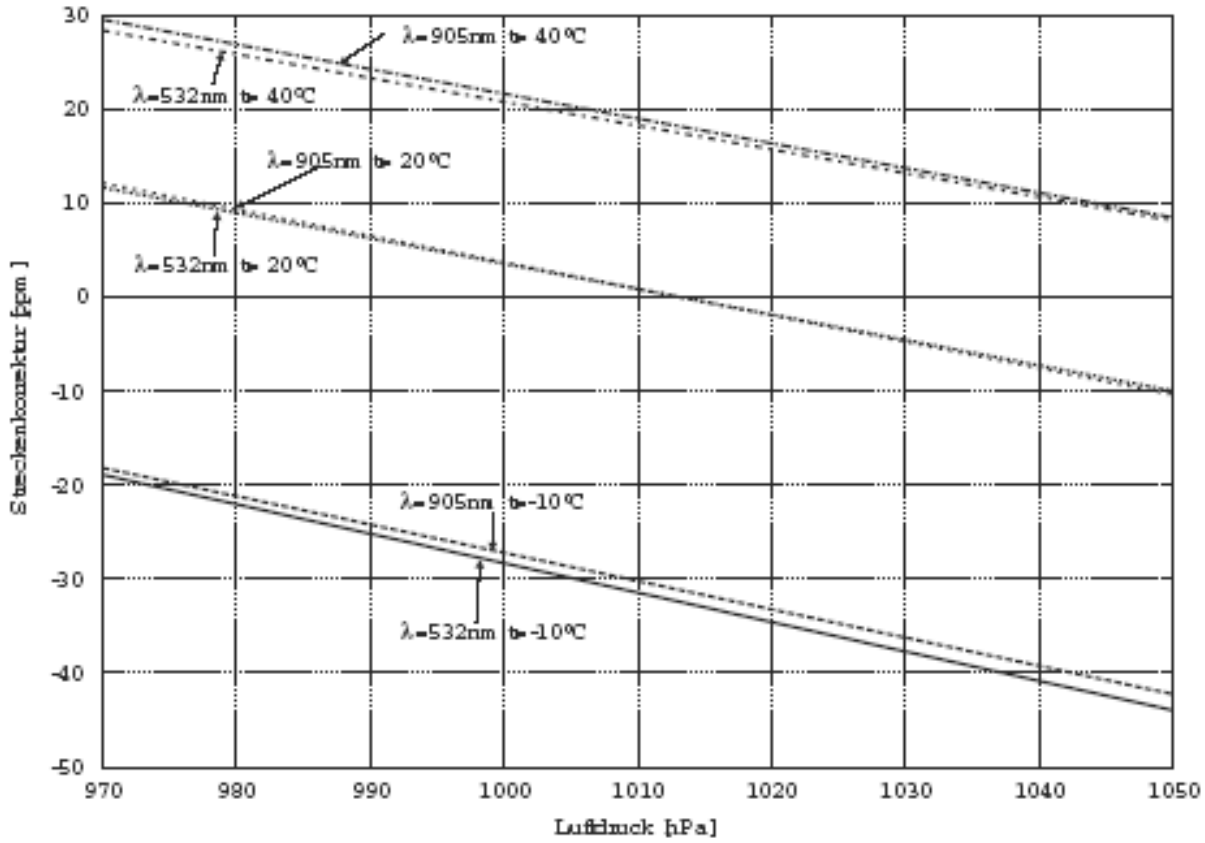

Figure 2.24: Atmospheric correction for lasers (λ =532 nm and 905 nm) slope distance measuring [Kern, 2003].

2.10 Instrumental Errors

Instrumental errors depend on errors in the measuring devices used. The measuring techniques of a laser scanner is similar to the theodolite system. The possible errors from this type for laser scanner are:

1. The eccentricity of the vertical axis and eccentricity of the scan center.
2. Wobble of vertical axis. The variation in the axis during rotation.
3. Errors of collimation axis.

Figure 2.25 shows the vertical and horizontal axes for laser system Imager 5003. For more details about instrumental errors and calibration of a terrestrial laser scanner see [Schulz, 2007] and [Rietdorf, 2004].

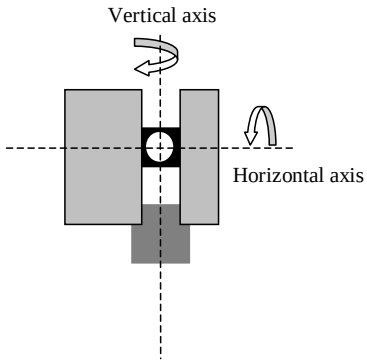

Figure 2.25: Axes of rotation for laser system Imager 5003.

2.11 Used Laser Scanning Systems During Scanning Tests

The market offers a lot of the laser scanners with different system specifications. Two scanning systems are used during the thesis field work, Cyrax 2500 (Figure 2.26) scanning system and Imager 5003 from z+f company (Figure 2.27). The technical specifications of Cyrax 2500 and HDS 3000 scanning systems are listed in table 2.3 [Geosystems, 2005].

(a) Cyrax 2500.

(b) HDS 3000.

Figure 2.26: Cyrax 2500 and HDS 3000 laser scanner.

Figure 2.27: Laser system Imager 5003.

Table 2.3: Characteristic of some scanning systems.

Product	Cyrax 2500	HDS 3000	Imager 5003
Laser wavelength (in nm)	532	532	
Laser power (in W, mW)	1 mW, avg.	1 mW, avg.	CW 23 mW red
FDA Laser classification	2	3R	3R
Beam Diameter	6 mm at 50 m	6 mm at 50 m	ca. 3 mm 1 m
Measurement Technique	Pulsed laser; TOF	Pulsed laser; TOF	phase shift
Data acquisition rate (pps)	1000	Dependant on scan conditions	125,000
Distance accuracy	4mm at 50 m	4mm at 50 m	6mm at 25 m
Angular accuracy	12 seconds	12 seconds	0.020 gon
Minimum range (m)	1.5	1	1
Maximum Range (m)	100	300 m at 90%; 134 m at 18%	53.5 m
Field of view (vertical angle)	40°	270°	310°
Field of view (horizontal angle)	40°	360°	360°
Minimum vertical scan increment	0.25 mm to 50 m	1.25 mm to 50 m	
Minimum horizontal scan increment	0.25 mm to 50 m	1.25 mm to 50 m	

Chapter 3

Data Registration Concepts

3.1 Introduction

Any terrestrial laser scanner project can be divided into three major steps, data processing, data registration, data modeling and visualization. Both the terms registration or matching are used to describe the same process. Data registration is considered an important step to get the whole 3D model in one scanworld coordinate system for the scanned object while one scan is not enough to describe an object geometrically. Unlike total stations, the terrestrial laser scanner is not optically oriented toward a known point. Each scanworld has its local coordinate system.

3.2 Data Registration Methods

Data registration can be described mathematically by a rigid body transformation. Depending on economical, manufacturer, technical or practical reasons, (TLS's) data could be registered based on one of three concepts or a combination of them. Figure 3.1 is a sketch to give a general overview for different terrestrial laser scanner data registration concepts.

3.2.1 Data Registration Using Targets

This method is the most one which is used for data registration. The targets should be well distributed through the field of view for the adjacent scanworlds. The targets should be also scanned during scanning process. The final 3D model for the scanned object could be registered as follows:

For registration to a predefined coordinate system:

- In this case, the coordinates of the registration targets should be also available from another measuring tool for example a total station (the targets are called ground control points). Fix the coordinates from the total station coordinate system and transform the local coordinates of each

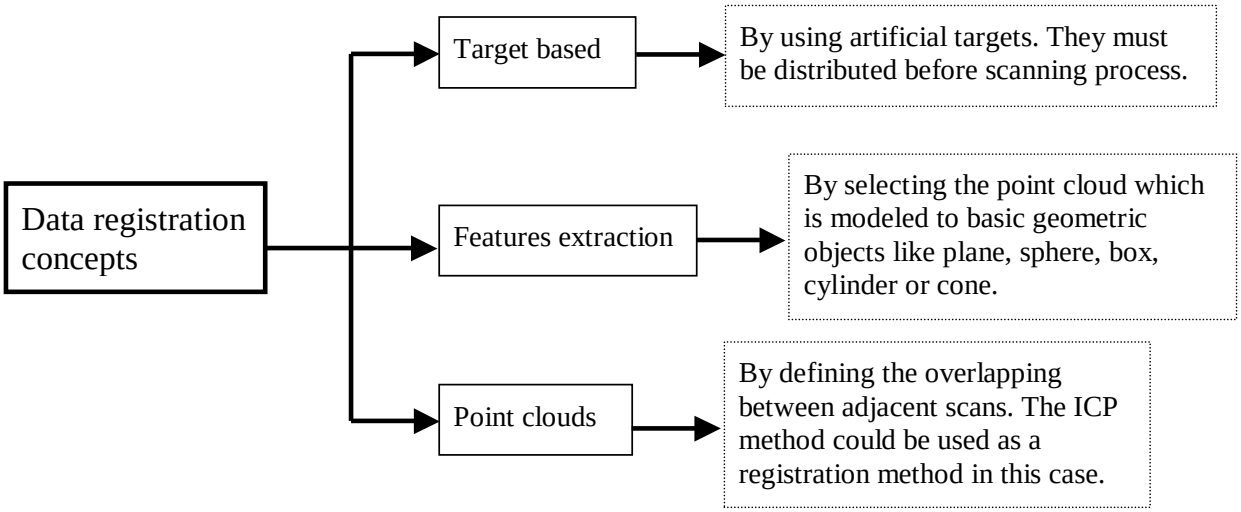

Figure 3.1: Different concepts for laser scanner data registration.

scanworld into it. The disadvantage of this method is using an extra instrument (total station) which will raise the cost of the projects.

For registration to a local coordinate system:

- Fix the coordinate system of the targets in the first scanworld (home scan) then transform all the neighboring scanworlds (floating scans) into the first one.

Registering to a local coordinate system is preferable in some applications in which using ground control points are difficult to be achieved. The target acquisition accuracy from the most scanning systems can be determined with a fitting accuracy better than 1-2 mm. The advantage of the targets based on the registration method is their increasing accuracy of the final 3D Model for the scanned object. The main drawback of this method is the time required for targets setting before the scanning step. Also, the targets should be rescanned with a very fine scanning process to get accurate target parameters. Leica scanning systems are able to rescan the reflective targets.

3.2.2 Data Registration Based on Point Clouds

Data registration based on point clouds without using artificial or natural targets is possible to be achieved. With this data registration technique, all the adjacent scans must be overlapped during the scanning step. Many techniques could be used to calculate transformation parameters between adjacent scans. These techniques depending on establishing a set of corresponding points from two data sets which could be used to collect or register data to one scan world coordinate. The advantages of data registration based on point clouds could be summarized as follow:

- No more time and cost as artificial or natural targets are not required.
- No more special scanning processes for targets identification.

3.3 Types of Registration Targets

There are two types of targets which are used for the registration process, artificial and non artificial targets. Figure 3.2 gives an overview of the type of targets together with the advantages and disadvantages of using each type.

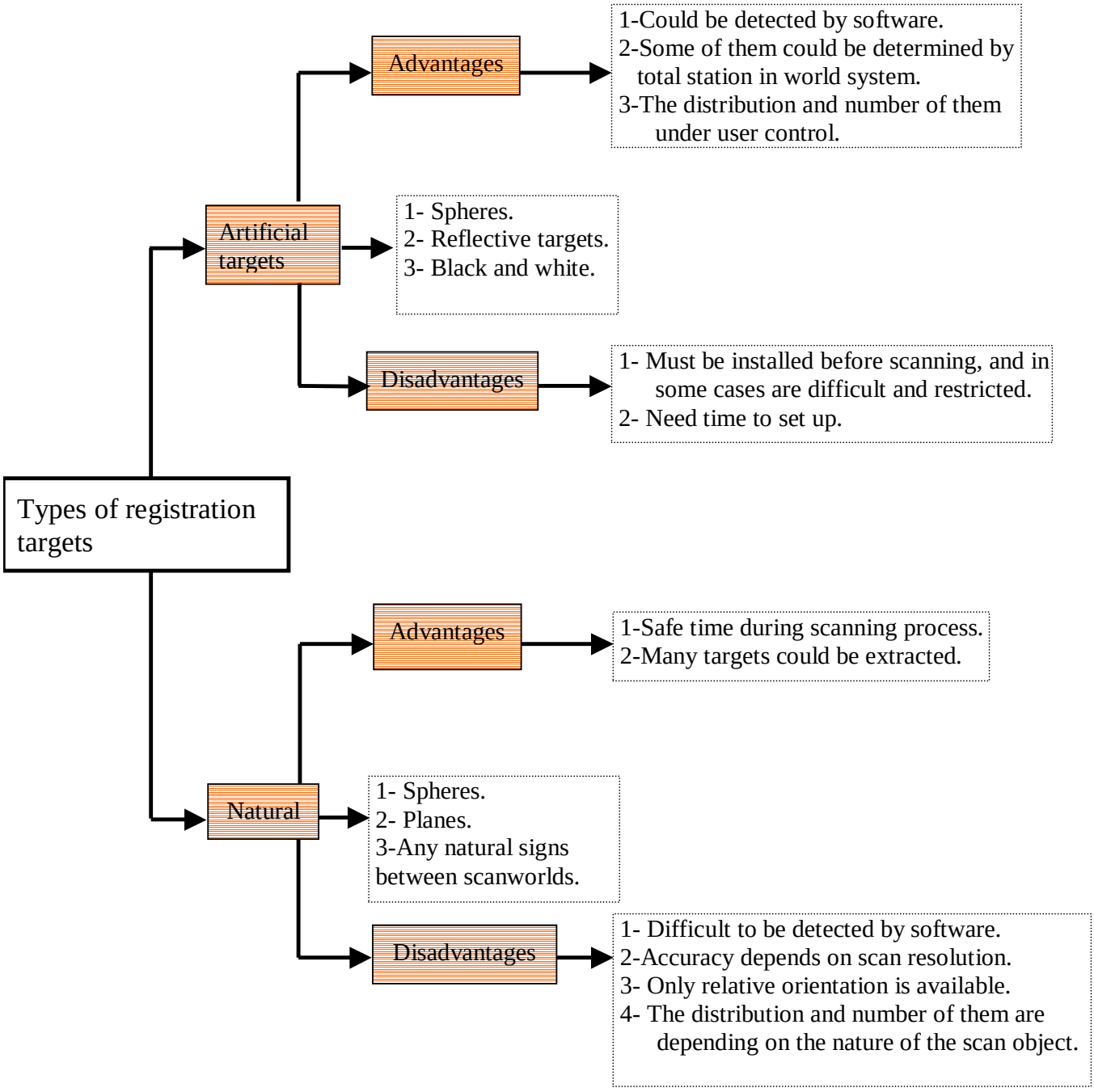

Figure 3.2: Different registration targets for laser scanner data registration.

3.3.1 Artificial Targets

The laser scanner companies introduced special ideal accessories for registration purposes like artificial registration targets. Figure 3.3 represents the artificial registration targets which are produced by the company *Leica Geosystems*. Three types are introduced: cyra's planer target, cyra's tilt and turn target and cyra's twin-target pole. They allow for accurate geo-referencing of scanworlds to known control points and accurate registration of multiple scanworlds to each other. Cyra's targets could be surveyed by traditional surveying instruments. They are easy to be placed on any kind of surface. Furthermore, they could be left in place as useful reference points. Each target needs to be acquired after the initial scanning and given an identification number for each target. Theoretically at least three targets should be used in every scanworld for the data registration process. Cyra's planar targets allow an

(a) Cyra planar targets (b) Cyra tilt and turn targets (c) Cyra Twin-Target pole

Figure 3.3: *Cyra's* registration targets.

automatic identification and extraction by *Cyclone* software thanks to carefully designed differences in reflectivity between the target center and the main target surface, plus tight manufacturing tolerances. The advantages of this kind of the linkage of point of view, are the possibility of combination with any reflectiveness total station measurements and the possibility of detecting the targets automatically in the point clouds. Figure 3.4 shows the acquired targets from the point clouds by using Cyclone software for data registration purpose.

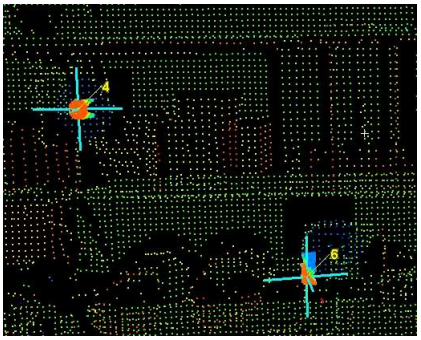

Figure 3.4: Acquiring registration targets by using Cyclone software.

Zoller+Fröhlich produced a black and white plane registration target, figure 3.5 shows the acquired target from the point clouds by using *Z+F LaserControl* Software for data registration purpose [Zoller+Fröhlich, 2005].

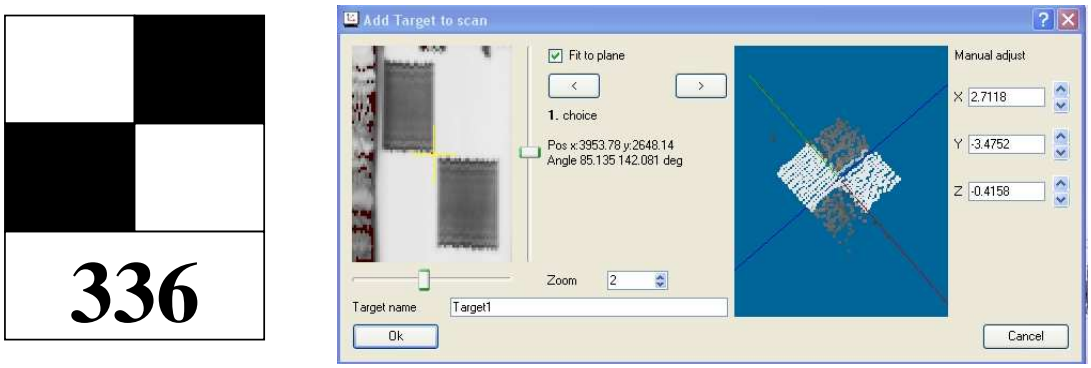

(a) Black and white plane target (b) Acquiring black and white target by using *Z+F LaserControl*

Figure 3.5: Black and white plane registration target from Zoller+Fröhlich company.

Sphere targets could be also used as registration object, they should be situated within the scanner field of view during scanning process, and their 3D coordinates are estimated. The main advantage of the spherical targets is their viewing from any laser standpoint. In the scanning testes, polystyrene spheres with non calibrated radius $\approx 15cm$ see figure 3.6.

(a) $\Phi \approx 10$ cm (styrofoam) (b) $\Phi \approx 30$ cm (polyester)

Figure 3.6: Spheres as registration targets.

The extracted planar patches from 3D laser scanning data could be also used as natural targets [Rietdorf, 2004]. A search technique is used to find corresponding patches in two overlapping scanworld positions. Figure 3.8 shows the parameters for the same plane in two different scanworld. These parameters are the normal vector N and the distance to origin d. A search technique [Dold and Brenner, 2006] based on image information is also used to find corresponding patches in two overlapping scanworld positions.

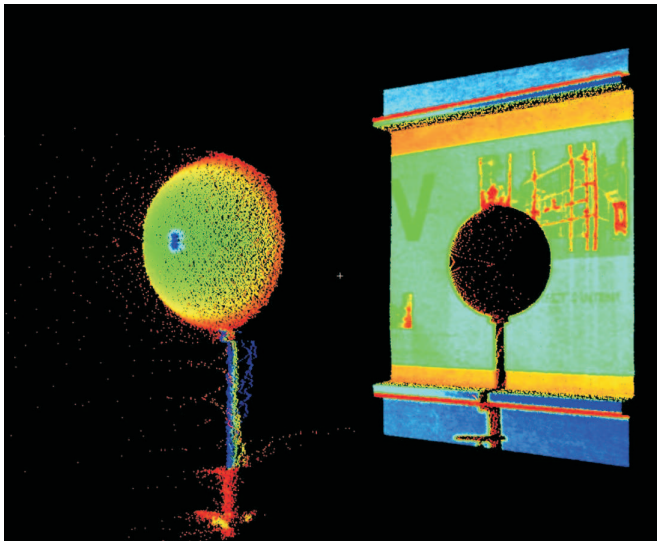

Figure 3.7: Point cloud on a sphere target. Outliers, which often occur at the boundary of the spheres caused by multi path effect should be not involved as sphere representative

.

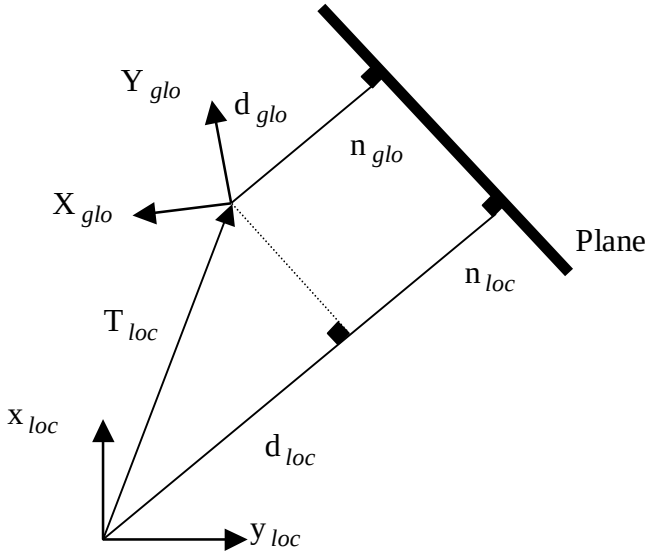

Figure 3.8: The same plane has been scanned from two different portions. By getting geometrical information (normal vector n and distance from origin d) from two scans, the two scans can be registered. [Rietdorf, 2004] for more details about method and used algorithm.

3.3.2 Sphere as an Artificial Target

Artificial sphere targets may be distributed in the adjacent scans and used as tie points during the scanning process. By using some algorithms the coordinates of tie targets will be known in the adjacent

scans. The required sphere target diameter for data registration purpose depends on the angular step width, the divergence of the laser beam and the range between the scanner and the target. The following two equations are used to determine the number of surface points that will meet surface of a sphere see figure 3.9.

$$\tan^{-1}(\frac{\theta}{2}) = \frac{r}{range} \tag{3.1}$$

$$n = \frac{\theta}{stepwidth} \tag{3.2}$$

where :

r = sphere radius.
θ = space angle at scanner head between two tangent lines for a sphere with diameter r.
n = number of surface points in one scanning direction.

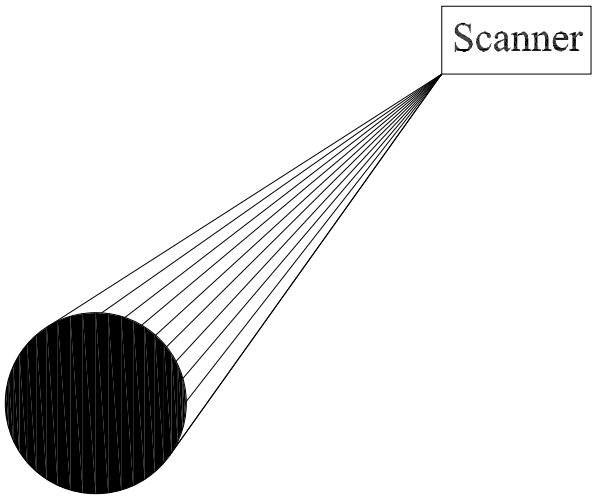

Figure 3.9: Scanning the surface of a sphere target.

For example, theoretically 36 points should be measured for parameters determination of a sphere with a diameter of 30 cm. This means that 6 horizontal and vertical scan lines have to hit the sphere, with an angular step width of 0.10°, which is used as minimum step width of some scanners, at a range of 25 m from the scanner. In practice sphere parameters are calculated only form a small part of the surface and outliers, which often occur at the boundary of the spheres caused by multi path effect as shown in Figure 3.7 should be not involved as sphere representative.

3.3.3 Fitting a Sphere to 3D Point Clouds

Assume that the given surface coordinates of a sphere are x, y and z. The unknown parameters are x_c, y_c and z_c and r are the set of data points that causes a sphere to best fit. Equation 3.3 describes the relation between the observations and unknowns of sphere parameters.

$$(x_i - x_c)^2 + (y_i - y_c)^2 + (z_i - z_c)^2 = r^2 \tag{3.3}$$

where:

r = sphere radius.
x, y, z = surface coordinate of the sphere.
x_c, y_c, z_c = sphere center coordinates.

The best sphere fitting means that minimizes the sum of squared distances from the center point to the surface coordinates of the sphere (Equation 3.4).

$$v_i = \sqrt{(x_i - x_c)^2 + (y_i - y_c)^2 + (z_i - z_c)^2} - r \tag{3.4}$$

where :

v_i = residuals.

An assumption of this algorithm is to consider that not all the surface coordinates of a sphere are coplanar. Finding the parameters of a sphere is an iterative process, therefore, approximate values for the parameters are base on [Eberly, 1999] algorithm. The energy function to be minimized is:

$$E(x_c, y_c, z_c, r) = \sum_{i=1}^{m} (L_i - r)^2 \tag{3.5}$$

Where L_i:

$$L_i = \sqrt{(x_i - x_c)^2 + (y_i - y_c)^2 + (z_i - z_c)^2} \tag{3.6}$$

Take the partial derivatives for equation 3.5 with respect to r, x_c, y_c and z_c and litting the result to zero we obtain the following:

$$\hat{r} = \frac{1}{m} \sum_{i=1}^{m} L_i \tag{3.7}$$

$$\bar{x} = \frac{1}{m} \sum_{i=1}^{m} x_i, \quad \bar{y} = \frac{1}{m} \sum_{i=1}^{m} y_i, \quad \bar{z} = \frac{1}{m} \sum_{i=1}^{m} z_i \tag{3.8}$$

$$\bar{L}_x = \frac{1}{m} \sum_{i=1}^{m} \frac{x_c - x_i}{L_i}, \quad \bar{L}_y = \frac{1}{m} \sum_{i=1}^{m} \frac{y_c - y_i}{L_i}, \quad \bar{L}_z = \frac{1}{m} \sum_{i=1}^{m} \frac{z_c - z_i}{L_i} \tag{3.9}$$

$$\hat{x}_c = \bar{x} + \bar{L}_x, \quad \hat{y}_c = \bar{y} + \bar{L}_y, \quad \hat{z}_c = \bar{z} + \bar{L}_z, \tag{3.10}$$

By using approximations for sphere parameters, the final parameters of the sphere are obtained by least squares solution. At least four surface point clouds are needed to define a sphere. The proposed algorithm has been implemented in a C++ program, in order to calculate the parameters of the sphere.

3.3.4 Advantages and Disadvantages of Artificial Targets

TLS uses high resolution scanning and a centered estimation algorithm to observe the center of the target (black and white, see figure 3.5 [Akca, 2004]). Radiometric and geometric information (shape, size, and planarity could be used to automatically find these targets in the point clouds. [Lichti et al., 2000b] reported on the problem of target reduction in case of coarse sampling resolution. The centering algorithm typically weights the samples based on the intensity attribute, which is a relative measure of the strength of the returned laser signal and is recorded as an additional observation. Therefore, it is beneficial to use targets that have a highly reflective center spot surrounded by a low reflecting, contrasting background, see Cyra's reflective plane targets figure 3.3.

3.3.5 Natural Registration Targets

It is possible to register the adjacent scanworld without artificial targets. Depending on the existence of many natural features in each scanworld. These features have well-known geometrical 3D shapes, such as cylinders, planes and spheres or any features in the point clouds, such as edges or intersection points. Their parameters are modeled from the laser scanner point clouds in a local coordinate system for every scanworld. Based on searching for pairs of identical objects in different scanworlds, the registration is performed. Figure 3.10 represents an example of using edges of arrow singes as natural targets case of using terrestrial laser scanner to document traffic intersection for accident investigation purposes.

3.3.6 Advantages and Disadvantages of Natural Registration Targets

The main advantage of using natural targets is time and cost saving. The disadvantage of using natural targets is their accuracy, while 3D information which are provided by natural targets are not highly accurate as that provided by artificial targets. The nature of the scan object may restrict the accuracy of the natural target parameters or their geometrical distribution.

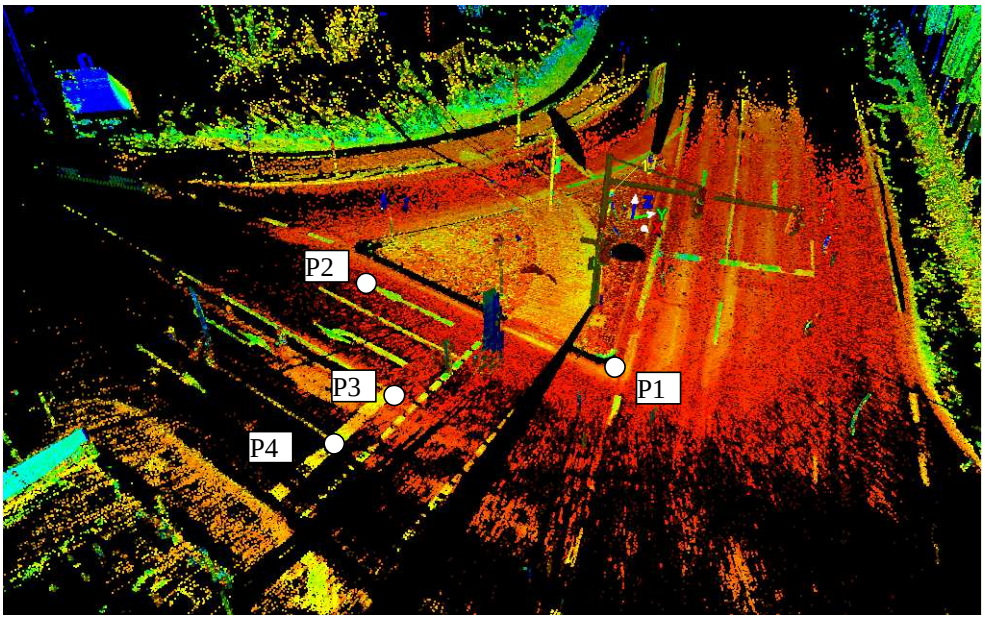

(a) An intensity image of point cloud for first scanworld

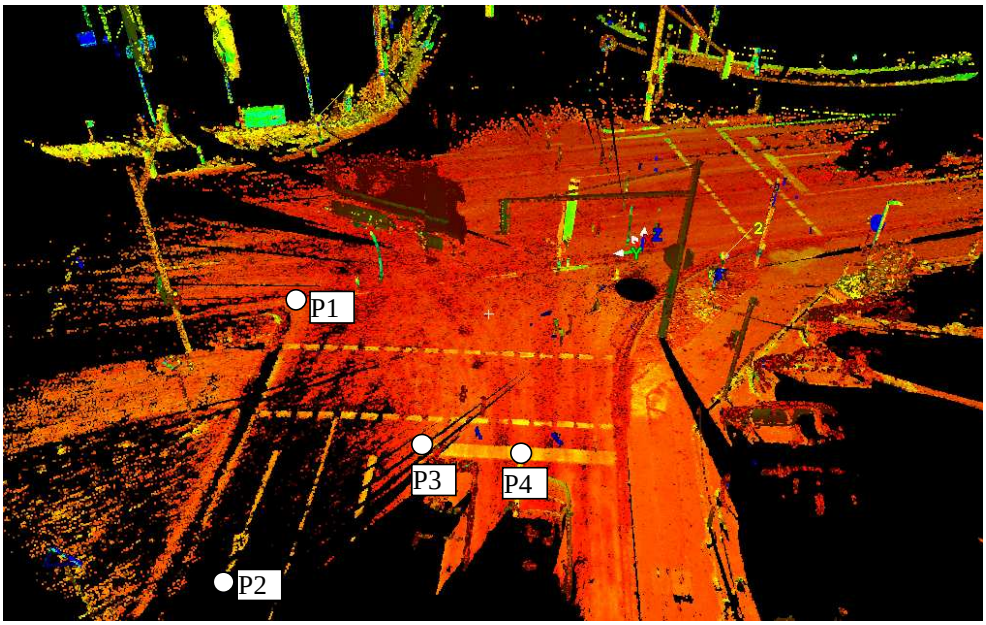

(b) An intensity image of point cloud for second scanworld

Figure 3.10: Using natural points as registration targets between adjacent scanworlds.

Chapter 4

Data Registration Algorithms

Data registration algorithms for terrestrial laser scanner data can be based on targets or point clouds as shown in figure 4.1. For all algorithms the final solution is the computation of a 3D conformal coordinate transformation between an adjacent scanworld. In the following sections the different algorithms for data registration will be discuss.

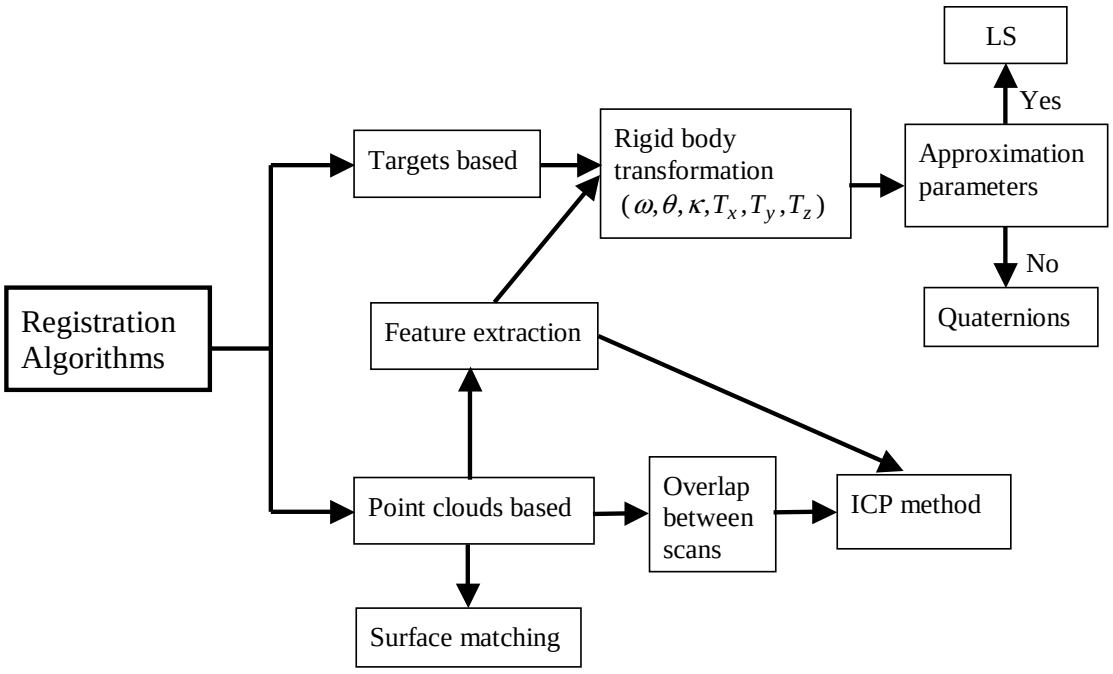

Figure 4.1: Data registration algorithms.

4.1 Algorithms for Target Registration Method

The 3D conformal transformation matrix could be represented by ω, ϕ and κ or quaternions. Both representations in the following sections will be discussed. After that the least square solution as an algorithm for target registration method will be discussed in detail.

4.1.1 Transformation Matrix with ω, ϕ and κ

A 3D conformal coordinate transformation (see [Wolf, 1974], p. 529) involves converting coordinates from one 3D system to another one. In figure 4.2 it is required to transform coordinates of points from xyz coordinate system to a XYZ coordinate system. Every scanworld has a local coordinate system (see figure 4.2). The targets coordinates are available for each scanworld. The adjacent scanworlds need to be transformed into the inner reference system of the first scanworld as shown in figure 4.2. Assuming that only two scanworlds are required to register. Further on, assume we have the coordinates

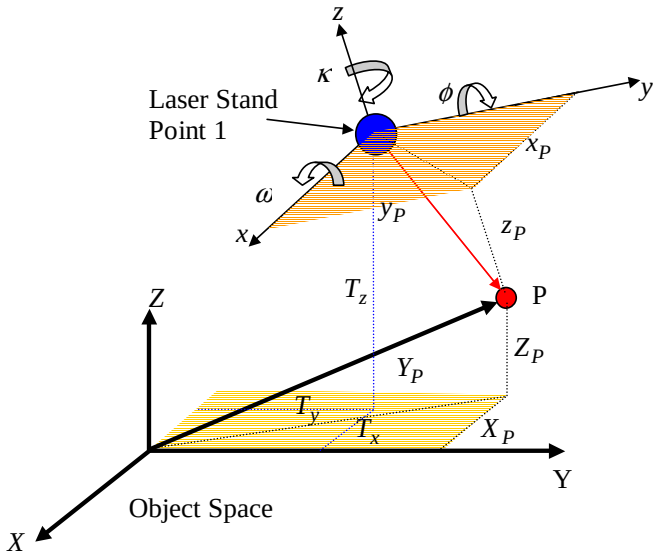

Figure 4.2: Data registered to a predefined global coordinate system.

of registration targets in the two coordinate systems as following:

$$\begin{aligned} \boldsymbol{X} &= [\ldots, X_i, Y_i, Z_i, \ldots]^{\mathrm{T}} \\ \boldsymbol{x} &= [\ldots, x_i, y_i, z_i, \ldots]^{\mathrm{T}} \end{aligned}$$

Where:

$$\begin{aligned} \boldsymbol{X} &= \text{coordinate vector for identical registration targets from the global system.} \\ \boldsymbol{x} &= \text{coordinate vector for identical registration targets from the local system.} \end{aligned}$$

The transformation relation between two systems can be described mathematically as follows:

$$\boldsymbol{X_i} = \boldsymbol{T} + S \cdot \boldsymbol{r} \cdot \boldsymbol{x_i} \tag{4.1}$$

Where:

$\boldsymbol{X_i}$	=	vector containing the 3 coordinates of a point n_i in the first scanworld coordinate system.
S	=	scale factor between two systems.
$\boldsymbol{T}$	=	translation vector.
$\boldsymbol{r}$	=	rotation matrix.
$\boldsymbol{x_i}$	=	vector containing the 3 coordinates of the same point n_i in the second coordinate system.

The scale factor is not assumed between the adjacent scanworlds [Gordon and Lichti, 2004], assuming the laser scanner instrument is calibrated before taking the measurements. The relation between the two coordinate systems using only six transformation parameters in a matrix form will be as follows.

$$\begin{bmatrix} X \\ Y \\ Z \end{bmatrix} = \begin{bmatrix} T_x \\ T_y \\ T_z \end{bmatrix} + \begin{bmatrix} r_{11} & r_{21} & r_{31} \\ r_{12} & r_{22} & r_{32} \\ r_{13} & r_{23} & r_{33} \end{bmatrix} \begin{bmatrix} x \\ y \\ z \end{bmatrix} \tag{4.2}$$

where:

$$T_x, T_y, T_z \quad = \quad \text{translation of the origin in the } x_r, y_r, z_r \text{ directions.}$$

The definitions of the elements of the rotation matrix **r** is given as follow.

$$\begin{aligned} r_{11} &= \cos\phi \cos\kappa \\ r_{12} &= \cos\omega \sin\kappa + \sin\omega \sin\phi \cos\kappa \\ r_{13} &= \sin\omega \sin\kappa - \cos\omega \sin\phi \cos\kappa \\ r_{21} &= -\cos\phi \sin\kappa \\ r_{22} &= \cos\omega \cos\kappa - \sin\omega \sin\phi \sin\kappa \\ r_{23} &= \sin\omega \cos\kappa + \cos\omega \sin\phi \sin\kappa \\ r_{31} &= \sin\phi \\ r_{32} &= -\sin\omega \cos\phi \\ r_{33} &= \cos\omega \cos\phi \end{aligned}$$

where:

$$\omega, \phi, \kappa \quad = \quad \text{rotation angles around the } x, y, z \text{ axes, respectively.}$$

4.1.2 Rotation by Using Quaternions

Equation 4.2 describes the mathematical relation between the transformed two coordinate systems. For any given rotation matrix, the rotation matrix could also be represented by quaternions [McGlone et al., 2004, p. 47]), [K.Agoston, 2005, p. 760] and [Hinsken, 1987]. Converting from (ω, ϕ, κ) rotation angles to a quaternion gives us the advantage of the absent of trigonometric term which appear in equation 4.2. So if we have three rotation angles (ω, ϕ, κ), then the rotation matrix could be represented by using quaternion as follows:

$$\boldsymbol{r} = \begin{bmatrix} q_0^2 + q_1^2 - q_2^2 - q_3^2 & 2(-q_0q_3 + q_2q_1) & 2(q_0q_2 + q_3q_1) \\ 2(q_0q_3 + q_2q_1) & q_0^2 - q_1^2 + q_2^2 - q_3^2 & 2(-q_0q_1 + q_3q_2) \\ 2(-q_0q_2 + q_1q_3) & 2(q_0q_1 + q_2q_3) & q_0^2 - q_1^2 - q_2^2 + q_3^2 \end{bmatrix} \tag{4.3}$$

The rotation matrix using quaternion has only a four-elements unit quaternion:

$$q = [q_0 \quad q_1 \quad q_2 \quad q_3]^T$$

The relation between the 4 elements takes the following form:

$$q_0^2 + q_1^2 + q_2^2 + q_3^2 = 1 \tag{4.4}$$

Quaternion operations are faster because they can be done using fewer operations.

4.1.3 Approximation Transformation Parameters Calculation First Method

Linearization of the equations need six approximate values for the six unknown parameters (the three rotations angles and the three translations) of each model to the global reference system, because the equations of the transformation are not linear, and a least squares iterative solution is applied. Many algorithms can be found in literature, to overcome this difficulty, e.g. based on quaternion orthogonal procrustes analysis [Beinat and Crosilla, 2001] and vector algebra [Dewitt, 1996].

In this work the approximation parameters have been calculated using the concept of [Dewitt, 1996]. The advantage of this method to calculate the approximation values is that it requires only three shared targets coordinates between every two adjacent scanworlds. The rotation angles are determined in seven steps as follows:

1. Select the three geometrically strongest points which have widely distributed base. A formula for the square of the altitude is given by the following equation.

$$h^2 = b^2 - \left(\frac{a^2 + b^2 - c^2}{2a} \right) \tag{4.5}$$

where :

h	=	height of the triangle.
a, b, c	=	lengths of the triangle see figure 4.3.

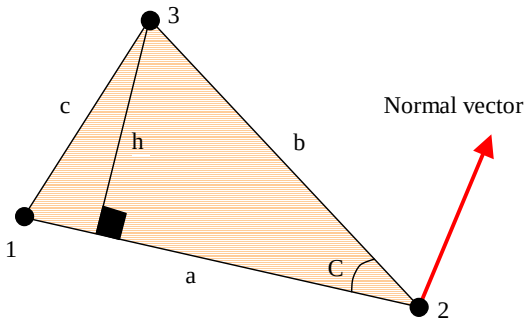

Figure 4.3: Height from longest side and normal vector to its plane [Dewitt, 1996].

2. Compute the normal vector at the strongest points in the two scanworlds. The results will be two sets of i, j, and k coefficients, one for the local scanworld and the second for the global scanworld.

3. Determine tilt and azimuth for the normal in each scanworld from equations 4.6 and 4.7.

$$tilt = \tan^{-1}\left(\frac{k}{\sqrt{i^2 + j^2}}\right) \tag{4.6}$$

$$azimuth = \tan^{-1}\left(\frac{i}{j}\right) \tag{4.7}$$

4. Perform an initial rotation of points in the two scanworlds using corresponding values of tilt and azimuth.

5. Determine swing by difference in azimuths for the common line.

6. Combine the two tilts, two azimuths, and one swing into one overall rotation matrix.

7. Form rotation matrix and compute values for ω, ϕ and κ.

The transformation equation is linear in terms of the translation vector, initial values are not required. However, it could be calculated by rearranging the transformation equation and calculate all the values of the translation vector.

4.1.4 Approximation Transformation Parameters Calculation Second Method

By using quaternion, we have only four unknowns see equation 4.3. The solution of the unknowns is found by the solution of four homogeneous linear equations $\boldsymbol{A}$ in the components of $\boldsymbol{q}$ [Sanso, 1973].

$$\boldsymbol{A} \cdot \boldsymbol{q} = \boldsymbol{\rho} \cdot \boldsymbol{q} \tag{4.8}$$

Where:

$$\begin{aligned} \boldsymbol{\rho} &= \text{eigenvalue of the symmetrical matrix } \boldsymbol{A}. \\ \boldsymbol{q} &= \text{eigenvector of the symmetrical matrix } \boldsymbol{A} \ . \end{aligned}$$

Assuming that the scale factor is not significant for the laser scanner observation. All the set of n registration targets coordinates should be referred to the geometric centers X_g and U_g where:

$$X_g = \frac{1}{n}\sum_{i=1}^{i=n} X_i \tag{4.9}$$

$$U_g = \frac{1}{n}\sum_{i=1}^{i=n} U_i \tag{4.10}$$

Vectors coordinate according to the geometric centers will take the following forms:

$$\boldsymbol{x_i} = X_i - X_g \tag{4.11}$$

$$\boldsymbol{u_i} = U_i - U_g \tag{4.12}$$

Matrix $\boldsymbol{A}$ constructed from the vectors coordinate according to the geometric centers data as described in equations 4.11 and 4.12, ($\boldsymbol{x_i} = [x_i \quad y_i \quad u_i]^T$ and $\boldsymbol{u_i} = [u_i \quad v_i \quad w_i]^T$). Matrix $\boldsymbol{A}$ takes the following form:

$$\boldsymbol{A} = \frac{1}{n}\begin{bmatrix} A_{11} & A_{12} & A_{13} & A_{14} \\ & A_{22} & A_{23} & A_{24} \\ & & A_{33} & A_{34} \\ & & & A_{44} \end{bmatrix} \tag{4.13}$$

Where:

$$\begin{aligned}
A_{11} &= -[\textstyle\sum_{i=1}^{n} u_i \cdot x_i + \sum_{i=1}^{n}(v_i \cdot y_i + w_i \cdot z_i)]. \\
A_{12} &= -[\textstyle\sum_{i=1}^{n}(v_i \cdot z_i - w_i \cdot y_i)]. \\
A_{13} &= -[\textstyle\sum_{i=1}^{n}(w_i \cdot x_i - u_i \cdot z_i)]. \\
A_{14} &= -[\textstyle\sum_{i=1}^{n}(u_i \cdot y_i - v_i \cdot x_i)]. \\
A_{22} &= [(\textstyle\sum_{i=1}^{n}(u_i \cdot x_i + v_i \cdot y_i + w_i \cdot z_i) - 2\sum_{i=1}^{n} u_i \cdot x_i]. \\
A_{23} &= -[\textstyle\sum_{i=1}^{n}(v_i \cdot x_i + u_i \cdot y_i)]. \\
A_{24} &= -[\textstyle\sum_{i=1}^{n}(w_i \cdot x_i - u_i \cdot z_i)]. \\
A_{33} &= [(\textstyle\sum_{i=1}^{n}(u_i \cdot x_i + v_i \cdot y_i + w_i \cdot z_i) - 2\sum_{i=1}^{n} v_i \cdot y_i]. \\
A_{34} &= -[\textstyle\sum_{i=1}^{n}(w_i \cdot y_i - v_i \cdot z_i)]. \\
A_{44} &= [(\textstyle\sum_{i=1}^{n}(u_i \cdot x_i + v_i \cdot y_i + w_i \cdot z_i) - 2\sum_{i=1}^{n} w_i \cdot z_i].
\end{aligned}$$

The eigenvector of the matrix $\boldsymbol{A}$ corresponding to the smallest eigenvalue is the correct solution of vector $\boldsymbol{q}$. The translation vector could be calculated by rearranging equation 4.2 by taking in consideration the geometric centers X_g and U_g of the two coordinate systems. The important advantage of this method is that no convergence problem arise and there's the ability to determine the large rotation angles between two coordinate systems.

4.1.5 Least Square Solution Based on ω, ϕ and κ Parameters

Transformation of coordinates can be either linear or non-linear. In linear solution case, the unknown's number will be twelve (nine from rotation elements matrix and three translation) after neglecting the

influence of the scale factor between the adjacent scanworlds. Therefore the number of registration targets to be measured for every adjacent scanworld should be four, but a higher number is strongly recommended to increase the numerical stability and reliability of the solution. For non-linear solution, coordinates of minimum three target points in every adjacent scanworlds is required to compute the registration parameters or the orientation to the object system. For non-linear solution, transformation parameters between the adjacent scanworlds will be calculated in two steps as follows:

1. Calculation of the approximate parameters.
2. Refine the approximate parameters by using least squares solution.

The first step is based on the approach proposed by [Dewitt, 1996] (see next section for more detail). For every registration target three equations are considered in the mathematical model as follows:

$$f_1 = T_x + (r_{11} \cdot x_i + r_{21} \cdot y_i + r_{31} \cdot z_i) - X_i \tag{4.14}$$

$$f_2 = T_y + (r_{21} \cdot x_i + r_{22} \cdot y_i + r_{32} \cdot z_i) - Y_i \tag{4.15}$$

$$f_3 = T_z + (r_{31} \cdot x_i + r_{23} \cdot y_i + r_{33} \cdot z_i) - Z_i \tag{4.16}$$

This model can be solved using the combined least squares adjustment model, which has the following mathematical model:

$$f(\hat{\boldsymbol{l}}, \hat{\boldsymbol{x}}) = \mathbf{0} \tag{4.17}$$

where:

$\hat{\boldsymbol{l}}$ = vector of adjusted observations.
$\hat{\boldsymbol{x}}$ = vector of adjusted parameters.

Equations from 4.14 to 4.16 are nonlinear equations involving 6 unknowns.
Vector of unknowns:

$$\mathbf{x_{6,1}} = [\omega, \phi, \kappa, \mathbf{T_x}, \mathbf{T_y}, \mathbf{T_z}]^{\mathrm{T}} \tag{4.18}$$

In order to solve these equations, they are linearized using Taylor series expansion for approximating a non-linear function from type $f(\hat{l}, \hat{x})$. The linearized form is:

$$\begin{array}{rcccccccccc} f(\hat{l}, \hat{x}) & = & f(l, x_0) & + & \left(\frac{\partial f(l,x)}{\partial l}\right)_0 & (\hat{l} - l) & + & \left(\frac{\partial f(\hat{l}, \boldsymbol{x})}{\partial x}\right)_0 & (x - \boldsymbol{x_0}) & = & \mathbf{0} \\ & & \underset{b,1}{\boldsymbol{w}} & + & \underset{b,n}{\boldsymbol{B}^T} & \underset{n,1}{\boldsymbol{v}} & + & \underset{b,u}{\boldsymbol{A}} & \underset{u,1}{\boldsymbol{\Delta x}} & = & \mathbf{0} \end{array} \tag{4.19}$$

Where:

$\boldsymbol{w}$ = misclosure vector.
$\boldsymbol{B}^T$ = $\frac{\partial f}{\partial l}|_{x=x^0, l=l^{obs}}$, partial derivatives with respect to observations.
$\boldsymbol{v}$ = vector of residuals.
$\boldsymbol{A}$ = $\frac{\partial f}{\partial x}|_{x=x^0, l=l^{obs}}$, partial derivatives with respect to unknowns.
$\boldsymbol{\Delta x}$ = correction vector.
b = number of conditions from type f (= $3n$ where n is number of registration targets).
n = number of observations (= $3n$ where n is number of registration targets).
u = number of unknowns (6 unknowns).

In order to clarify the coefficients of matrix $\boldsymbol{A}_{3n,6}$ suppose there is one registration target (at least three are required to get the solution), the elements of $\boldsymbol{A}$ takes the flowing form:

$$
\begin{aligned}
A_{11} &= 0 \\
A_{12} &= -\sin(\phi)\cos(\kappa)\cdot x_l + \sin(\phi)\sin(\kappa)\cdot y_l + \cos(\phi)\cdot z_l \\
A_{13} &= r_{21}\cdot x_l - r_{11}\cdot y_l \\
A_{14} &= 1 \\
A_{15} &= A_{16} = 0 \\
A_{21} &= r_{13}\cdot x_l + r_{23}\cdot y_l + r_{33}\cdot z_l \\
A_{22} &= -\sin(\omega)\cos(\phi)\cos(\kappa)\cdot x_l - \sin(\omega)\cos(\phi)\sin(\kappa)\cdot y_l + \sin(\omega)\sin(\phi)\cdot z_l \\
A_{23} &= r_{22}\cdot x_l - r_{12}\cdot y_l \\
A_{24} &= 0 \\
A_{25} &= A_{26} = 1 \\
A_{31} &= r_{12}\cdot x_l + r_{22}\cdot y_l + r_{32}\cdot z_l \\
A_{32} &= -\cos(\omega)\cos(\phi)\cos(\kappa)\cdot x_l + \cos(\omega)\cos(\phi)\sin(\kappa)\cdot y_l - \sin(\omega)\sin(\phi)\cdot z_l \\
A_{33} &= r_{23}\cdot x_l - r_{13}\cdot y_l \\
A_{34} &= A_{35} = 0 \\
A_{36} &= 1
\end{aligned}
$$

Matrix $\boldsymbol{B}_{3n,3n}$ takes the following form:

$$
\boldsymbol{B}_{3n,3n} = \begin{bmatrix} r_{11} & r_{21} & r_{31} \\ r_{12} & r_{22} & r_{32} \\ r_{13} & r_{23} & r_{33} \end{bmatrix} \tag{4.20}
$$

Variance-covariance matrix $\boldsymbol{C}_{ll}$:

$$
\underset{n,n}{\boldsymbol{C}_{ll}} = \underset{n,n}{\boldsymbol{Q}_{ll}}\,\sigma_0^2 = \begin{bmatrix} \sigma_1^2 & \sigma_{12} & \dots & \sigma_{1n} \\ \sigma_{21} & \sigma_2^2 & \dots & \sigma_{2n} \\ \vdots & \vdots & & \vdots \\ \sigma_{n1} & \sigma_{n2} & \dots & \sigma_n^2 \end{bmatrix} \tag{4.21}
$$

The weight matrix of the observations $\boldsymbol{P}$:

$$
\boldsymbol{P} = \boldsymbol{Q}_{ll}^{-1} \tag{4.22}
$$

The least square estimate Δx is based on the minimization of the function $v^{\mathrm{T}}Pv = min$, where $\boldsymbol{P}$ is the weight matrix. The advantage of the least squares solution method is to provide a set of quality parameters for unknowns which measure the goodness of the fit.

4.1.6 Least Squares Solution Based on Quaternions Parameters

The approximate transformation parameters are calculated by using quaternions. The combined least squares adjustment model is used to refine the solution. The mathematical model in this case has two

types. Equations from 4.14 to 4.16 describe the relation between unknowns and observations, equation 4.4 describes only the relations between unknowns.

$$g(\hat{x}) = \mathbf{0} \tag{4.23}$$

Vector of unknowns in this case:

$$\mathbf{x_{4,1}} = [\mathbf{q_0}, \mathbf{q_1}, \mathbf{q_2}, \mathbf{q_3}]^{\mathrm{T}} \tag{4.24}$$

Taylor series expansion for approximating a non-linear function from type $g(\hat{x})$.

$$\begin{array}{rcccc} g(\hat{x}) & = & g(\boldsymbol{x_0}) & + & \left(\frac{\partial g(\boldsymbol{x})}{\partial \boldsymbol{x}}\right)_0 \quad (\hat{x} - \boldsymbol{x_0}) \\ & & \underset{b,1}{\boldsymbol{c}} & + & \underset{b,u}{\boldsymbol{C}^T} \qquad \underset{u,1}{\boldsymbol{\Delta x}} \end{array} \tag{4.25}$$

Where:

$\boldsymbol{c}$	=	misclosure vector.
$\boldsymbol{C}^T$	=	partial derivative with respect to unknowns $\boldsymbol{x}$.
$\boldsymbol{\Delta x}$	=	correction vector.
b	=	number of conditions from type g.
u	=	number of unknown.

Matrix $\boldsymbol{C}$
partial derivative with respect to the unknown $\boldsymbol{x}$.

$$\boldsymbol{C}^T = \begin{bmatrix} \left(\frac{\partial g_1(\boldsymbol{x})}{\partial x_1}\right)_0 & \left(\frac{\partial g_1(\boldsymbol{x})}{\partial x_2}\right)_0 & \cdots & \left(\frac{\partial g_1(\boldsymbol{x})}{\partial x_u}\right)_0 \\ \left(\frac{\partial g_2(\boldsymbol{x})}{\partial x_1}\right)_0 & \left(\frac{\partial g_2(\boldsymbol{x})}{\partial x_2}\right)_0 & \cdots & \left(\frac{\partial g_2(\boldsymbol{x})}{\partial x_u}\right)_0 \\ \vdots & \vdots & & \vdots \\ \left(\frac{\partial g_b(\boldsymbol{x})}{\partial x_1}\right)_0 & \left(\frac{\partial g_b(\boldsymbol{x})}{\partial x_2}\right)_0 & \cdots & \left(\frac{\partial g_b(\boldsymbol{x})}{\partial x_u}\right)_0 \end{bmatrix} \tag{4.26}$$

The solution for this case is based on [Höpcke, 1980, S.164], which is represented in the following equations:

$$\boldsymbol{v}^T \boldsymbol{P} \boldsymbol{v} \rightarrow min. \qquad \text{objective function} \tag{4.27}$$

$$\boldsymbol{B}^T \boldsymbol{v} + \boldsymbol{A}\boldsymbol{\Delta x} + \boldsymbol{w} = \mathbf{0} \qquad \text{1. first condition} \tag{4.28}$$

$$\boldsymbol{C}^T \boldsymbol{\Delta x} + \boldsymbol{c} = \mathbf{0} \qquad \text{2. second condition} \tag{4.29}$$

$$\boldsymbol{M} = \boldsymbol{B}\boldsymbol{P}^{-1}\boldsymbol{B}^{\mathrm{T}} \tag{4.30}$$

$$\boldsymbol{N} = \boldsymbol{A}^{\mathrm{T}}\boldsymbol{M}^{-1}A \tag{4.31}$$

$$\boldsymbol{S} = \boldsymbol{C}^{\mathrm{T}}\boldsymbol{N}^{-1}C \tag{4.32}$$

$$\boldsymbol{k}_2 = \boldsymbol{S}^{-1}(\boldsymbol{C}^{\mathrm{T}}\boldsymbol{N}^{-1}\boldsymbol{A}^{\mathrm{T}}\boldsymbol{M}^{-1}\boldsymbol{w} - \boldsymbol{c} \tag{4.33}$$

$$\Delta\boldsymbol{x} = \boldsymbol{N}^{-1}\boldsymbol{C}\boldsymbol{K}_2 - \boldsymbol{N}^{-1}\boldsymbol{A}^{\mathrm{T}}\boldsymbol{M}^{-1}\boldsymbol{w} \tag{4.34}$$

$$\boldsymbol{k}_1 = \boldsymbol{M}^{-1}(\boldsymbol{A}\Delta\boldsymbol{x} + \boldsymbol{w}) \tag{4.35}$$

$$\boldsymbol{v} = \boldsymbol{Q}_{ll}\boldsymbol{B}\boldsymbol{K}_1 \tag{4.36}$$

$$\hat{\sigma}_0^2 = \frac{\boldsymbol{v}^{\mathrm{T}}\boldsymbol{P}\boldsymbol{v}}{b_f + b_u - u} \tag{4.37}$$

b_f = conditions number from equation type f.
b_g = conditions number from equation type g.
u = unknown number.

The correction vector (residual errors) from least squares solution was found equal zero. That means the approximation values from the solution method which are obtained from quaternions method were minimum parameters.

4.2 Summary

Two methods are presented for the calculation of approximation transformation parameters to be used for the least square solution. The first one takes only the best three observations. The second one (based on quaternion) takes into consideration all observations. The least square solution is applied on quaternion as unknown (q_0, q_1, q_2 and q_3). The only disadvantage is that there is no direct covariance matrix for the unknowns (ω ϕ and κ). So it is recommended to use approximation transformation parameters from the quaternion solution, after that apply the least square solution (with (ω ϕ and κ and translation vector as the unknown) to get a set of equality parameters for the unknown.

4.3 Algorithms for Point Clouds Registration Method

Data registration based on point clouds without using artificial or natural targets is possible to achieve. With this data registration technique all the adjacent scans must be overlapped during the scanning step. Many techniques could be used to calculate transformation parameters between adjacent scans. These techniques depend on establishing a set of corresponding points from two data sets, after that calculate the transformation parameters based on the corresponding points. One of the most popular methods is the Iterative Closest Point (ICP) [Besl and Meckay, 1992] and [Zhang, 1994]. Several variations and improvements on the ICP method have been presented [Masuda and Yokoya, 1995] and [Bergevin et al., 1996]. The ICP data registration technique is based on the search of pairs of nearest points in the two adjacent scans and calculate the transformation parameters between them. The advantages of this procedure are that no artificial or natural targets are required for the data registration. It save both the time and the cost during the data acquisition step.

Another data registration technique by matching different surface models by using the least square 3D surface matching [Akca and Grün, 2005]. In the next section, the ICP algorithm and improvement for this technique will be explained in detail.

4.3.1 The Iterative Closest Point (ICP) Algorithm

ICP algorithm is an iterative solution. It aims to find the optimal set of transformation parameters. After that, the rigid transformation is applied to the source scan. At each ICP iteration, correspondences are determined between target and source scans. The transformation is computed which minimizes

the evaluated errors. The iterations continue until either errors falls below some threshold value or the maximum number of iterations is exceeded. Figure 4.4 shows the different steps of the ICP algorithm based on [Besl and Meckay, 1992]. Several variations and improvements on the ICP method have been

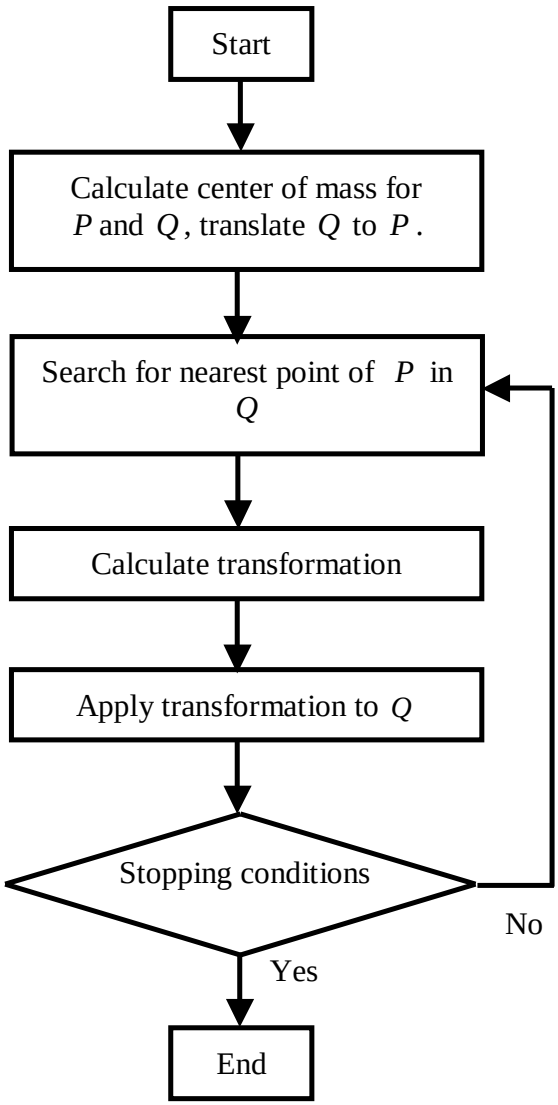

Figure 4.4: Flowchart of ICP algorithm.

presented [Masuda and Yokoya, 1995] and [Bergevin et al., 1996]. Two variants for ICP can be summarized as follows:

First: Strategies of selecting sample point

1. Using all (whole) points from two point clouds [Besl and Meckay, 1992].
2. Sub sampling from two point clouds [Turk and Levoy, 1994].
3. Random sampling and using different points in each iteration [Masuda et al., 1996].
4. Using the points with high intensity gradient around its neighbors [Weik, 1997].

Second: Finding possible corresponding points between two point clouds.

1. Point to point, e.g. Iterative Closest Point (ICP) algorithm [Besl and Meckay, 1992] and [Zhang, 1994].
2. Point to tangent plane [Chen and Medioni, 1991].
3. Point to projection [Blais and Levine, 1995].

Figure 4.5(a) shows a point to point ICP approach. An error metric d is the distance between two corresponding points. Point to plane registration is another common ICP technique. It searches the

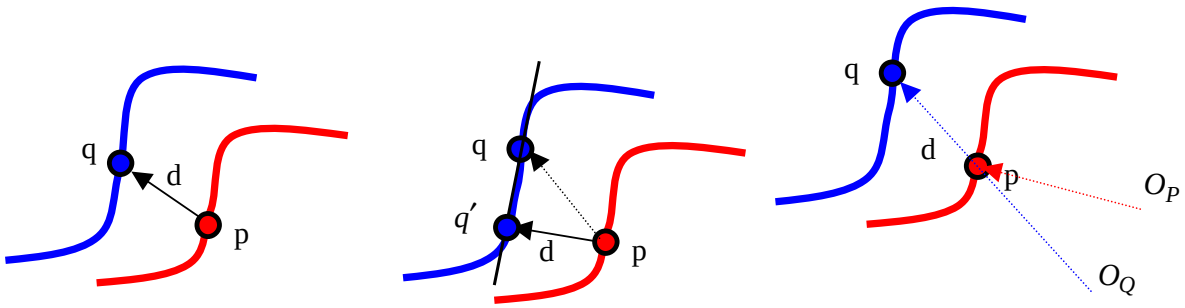

(a) Point to point (b) Point to tangent plane (c) Point to projection

Figure 4.5: Three common ICP approaches.

intersection on the destination surface from the normal vector of the source point. As shown in figure 4.5(b). The destination correspondence point $\acute{q}$ is the projection of p onto the tangent plane at q which is the intersection from the normal of p. Point to projection approach is known to be a fast registration technique. As shown in figure 4.5(c). This approach determines a point q which is the conjugate of a source point p, by forward projecting p from the point of view of the destination O_Q.

In this section the ICP algorithm will be covered in detail. Assume that there is a collection of points $(p_i; q_i)$ partially overlapping in $3D$ point clouds. The optimal rotation and translation is required to be applied to the first collection of points (i.e., the p_i) to bring them into alignment with the second (i.e., the q_i). Assume that two sets of point clouds are given as following P and Q:

$$P = \{\boldsymbol{p_1}, ...\boldsymbol{p_n}\}$$
$$Q = \{\boldsymbol{q_1}, ...\boldsymbol{q_n}\}$$

Wanted: translation and rotation that minimizes the sum of the squared error:

$$E(\boldsymbol{R}, \boldsymbol{T}) = \frac{1}{N_p} \sum_{i=1}^{N_p} \|(\boldsymbol{R} \cdot \boldsymbol{p_i} + \boldsymbol{T}) - \boldsymbol{q_i}\|^2 \tag{4.38}$$

where:

E	=	Mean square error between correspondence points (MSE).
$\boldsymbol{R}$	=	Rotation matrix.
$\boldsymbol{T}$	=	Translation vector.
N_p	=	Number of correspondence points.
$\boldsymbol{p_i}$, $\boldsymbol{q_i}$	=	corresponding points.

Assume the first scan is a reference scan (target scan) and the second one is a source scan (should be rotated and translated), ICP calculation steps could be done as follows:

1. Calculate center of mass for the target and the source scans as seen from equations 4.39 and 4.40.

$$T_x = \frac{1}{N_x} \sum_{i=1}^{N_x} p_i \tag{4.39}$$

$$S_y = \frac{1}{N_y} \sum_{i=1}^{N_y} q_i \tag{4.40}$$

   where :

T_x	=	center of mass for the target scan.
S_y	=	center of mass for the source scan.

2. Translate source scan to target scan with the value $T_x - S_y$.

3. Determine for each point in the first set the closest point in the second set.

4. Find a relative transformation between two scans based on correspondence points from step 3.

5. Transform source scan to local coordinate of target scan.

6. Calculate the mean square error (MSE) by the sum of the squared distances between the corresponding points.

7. Terminate: if the change in MSE falls below a threshold value, or the maximum number of iterations. Else, repeat from step number 3. A pseudo code description of the algorithm is given in figure 4.6.

The MSE is the average of the squared distances after transformation between corresponding points from target and source scan. It is used to evaluate the goodness of the registration process.

4.3.2 Disadvantages and Limitation of ICP Data Registration Method

The ICP method assumes that the nearest point in the source scan is the only estimate of the correct corresponding point to a point in the target scan. In case of no information about initial transformation, this assumption is not correct. Several improvements for the ICP method have been made, but several problems still remain, for example:

ICP (point set P (Source scan), point set Q (Target Scan))

Compute (Centre of mass for P and Q){}
Translate (Centre of mass for Q into P){}

while (d(T)> $E_{\max}$ || Number of iteration> for example 20) {
for each p_i in P {
s_i = nearest point(p_i ,Q)
}
transformation T = $\min_T E(T) = \min_T \sum_i \|q_i - T(p_i)\|^2$

P = Transform point set(P,T)
Number of iteration++
}

Figure 4.6: Pseudo code for ICP algorithm.

- It is not possible to get any evaluation of the precision and accuracy of the estimated relative transformation.
- It is not possible to register more than two scans at the same time.
- It needs a very good assessment for correspondence points (overlapped zone between adjacent scans) at the first iteration. In *Cyclone* software from Leica [Geosystems, 2005] the user should manually feed up the coordinates information of at least three registration target for both source and target scans.
- Geometrical representation of overlapped parts between adjacent scans are difficult to be identical, while the two scans are scanned with different laser scanning configuration (scan resolution, laser angle of incidence and distance between scanned object and laser scanner stand point). In case of using Cyrax 2500, it is possible to scan adjacent scan with almost the same resolution.
- ICP algorithm solution does not use the local surface features like curvature or gradients in order to get the minimum solution.
- The blunders and noise of the point clouds have to be completely eliminated before starting to use ICP method.

4.3.3 Simple Improvement of ICP Solution

Large objects, such as long buildings or bridges will naturally require many scans to ensure complete documentation of the structure. During data acquisition of long objects, as the case of surveying

buildings facing, the adjacent scans should be at least ≈ 30% overlapped [Bornaz et al., 2003] in order to get a registration of adjacent scans without a loss in the precision of the final scan object. With the ICP solution, the correct correspondences are not known. The correspondences are the overlap point clouds between adjacent scanworlds. To define approximately the overlap zone, the bounds coordinate of target and source scanworlds have to be computed. The bound of scanworld means calculating x_{min} and x_{max} coordinate. The Cyrax 2500 laser scanner is a view camera scanner system. It scans with a field of view of 40° horizontal and 40° vertical. The coordinate system of the Cyrax 2500 laser system is shown in figure 4.7. By applying the ICP algorithm only for the point clouds which have

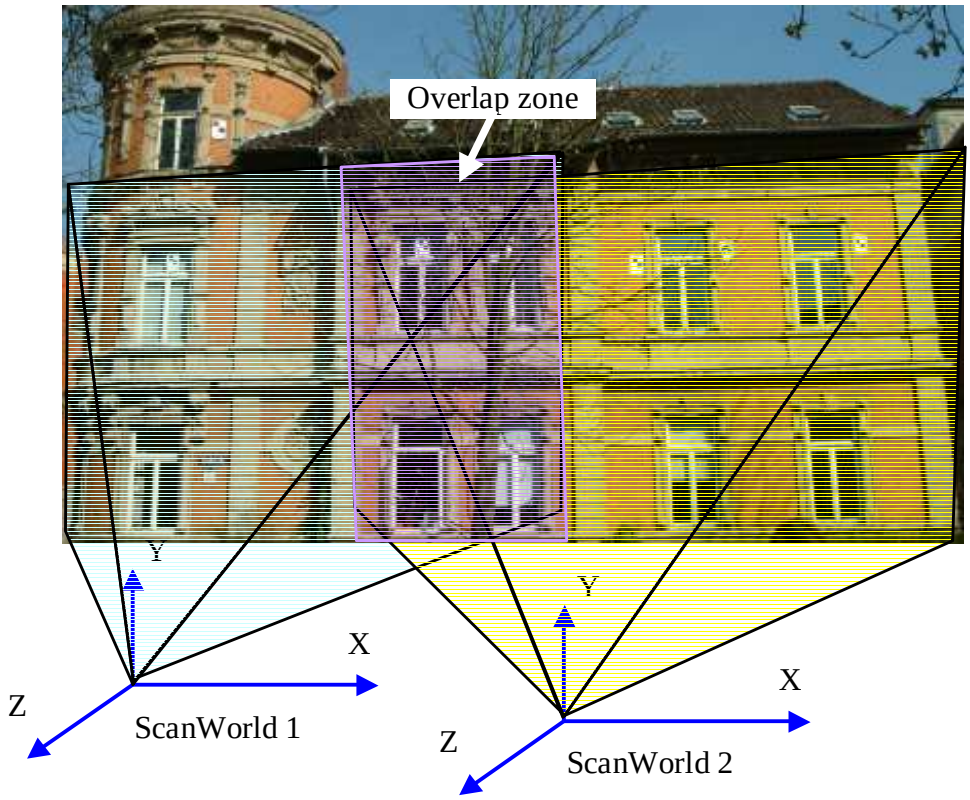

Figure 4.7: Overlap between two scanworlds based on Cyrax 2500 laser system.

x coordinate values $\geq (\frac{x_{max}-x_{min}}{2} + x_{min})$ in source scanworld with the point clouds which have x coordinate values $\leq (\frac{x_{max}-x_{min}}{3} + x_{min})$ in the target scanworld. The method summarized as follows:

- By computing the bounds coordinate of every scan data. Bounds mean calculating x_{max}, x_{min} coordinates for both source and target scans. Assuming the scanned object is a *facade* of a long building and the two scanworlds are overlapped in x coordinate direction.

- Applying ICP algorithm only for the point clouds which have x coordinate values $\geq (\frac{x_{max}-x_{min}}{2} + x_{min})$ in source scanworld with the point clouds which have x coordinate values $\leq (\frac{x_{max}-x_{min}}{3} + x_{min})$ in target scanworld.

4.3.4 Experimental Results

In order to test the registration algorithm and get the results, laser system Cyrax 2500 terrestrial laser scanner has been used to scan the west facade of the IGP *(Institut für Geodäsie und Photogrammetrie, Technische Universität Braunschweig, Germany)*, see figure 4.8. It is around 25x12 meters in size. Figure 4.9 shows the scan result of the west facade from two different scan positions. Before the

Figure 4.8: Image of IGP facade.

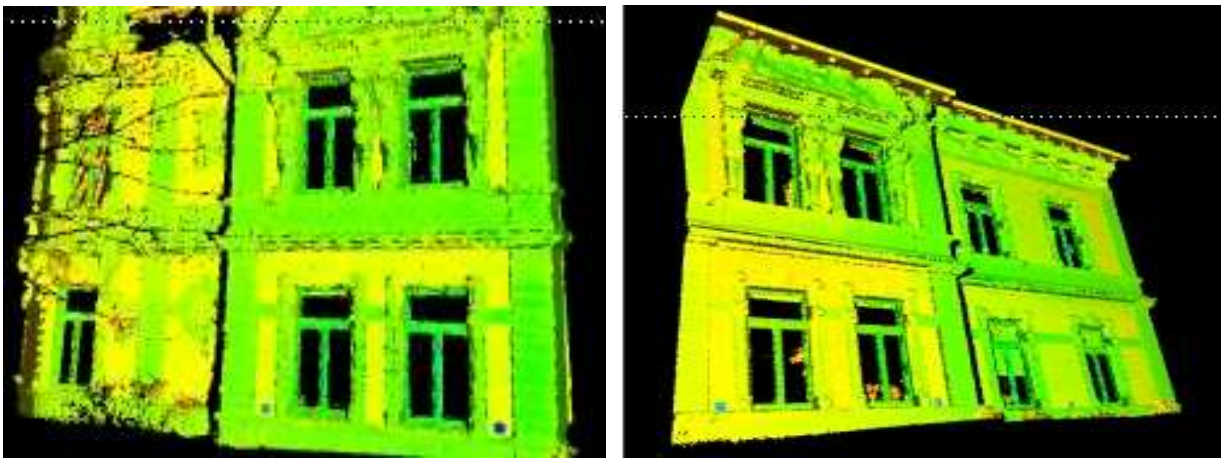

(a) Scan 1 (b) Scan 2

Figure 4.9: Scans to be registered.

scanning process special reflective targets (Cyra registration targets) are distributed and fixed on the scanned facade for data registration purpose and evaluating our results (see figure 4.10). Cyclone 5.4 (commercial software for laser scanner data processing) has been used to extract the coordinates of these targets for both scans. Calculation of registration parameters for the experiment was carried out by using a self developed C++ code based on the original ICP algorithm. *The Visualization ToolKit* (VTK) [Schroeder et al., 2002] is an open source, a freely available code is also used for visualizing

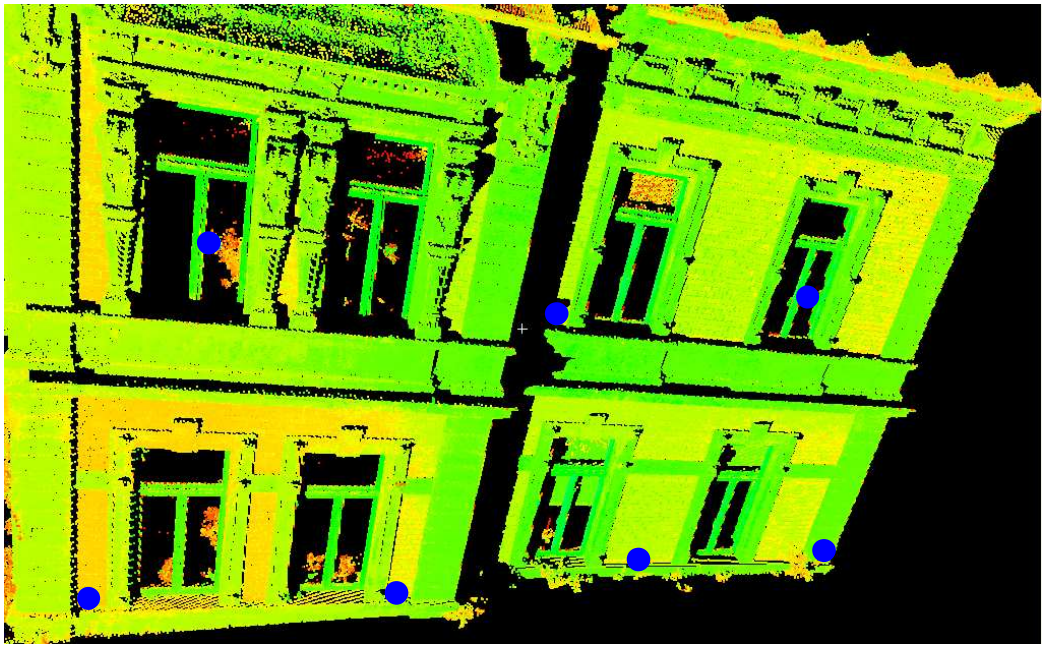

Figure 4.10: Cyra targets are used to check the results.

the point cloud. The used PC is an Intel P4 4 Ghz. The initial approximations of the transformation parameters were provided automatically according to the improvement as descried in the last section. Figure 4.11 shows a graphical display after registration of source and target scanworld based on the basic ICP solution after 50 iterations. Figure 4.12 shows a graphical display of point clouds after using the improving for ICP solution also after 50 iterations. Figure 4.13 shows the relation between

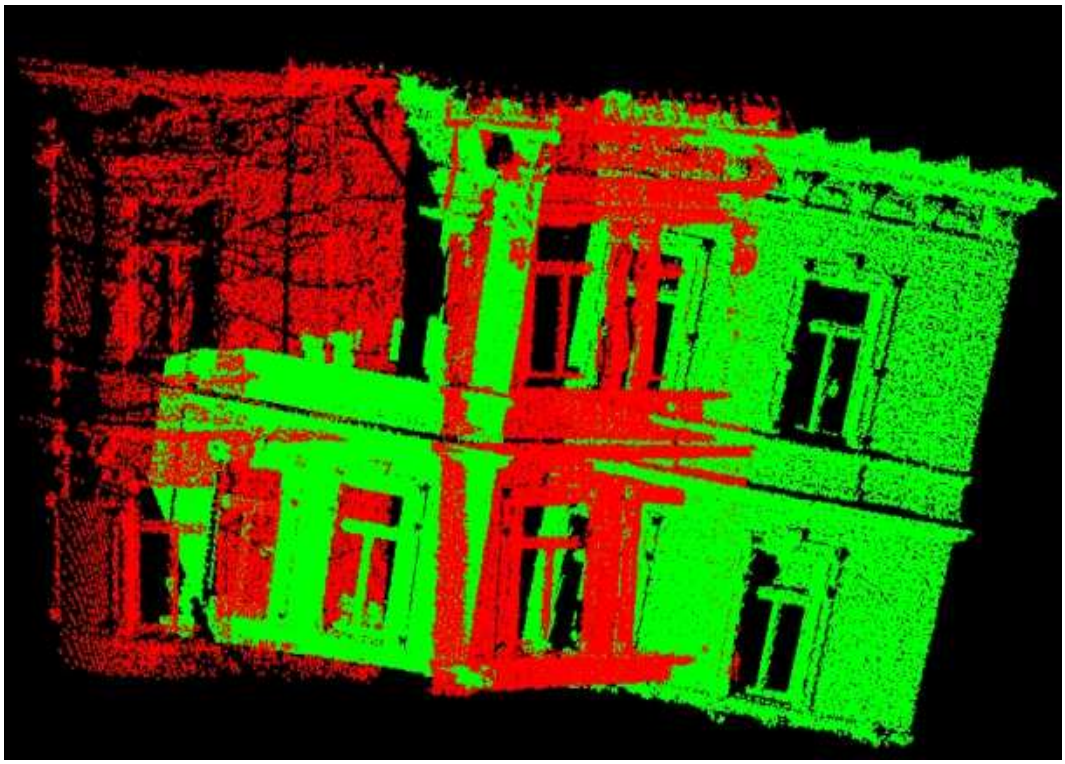

Figure 4.11: Graphical display of point clouds registration based on basic ICP technique.

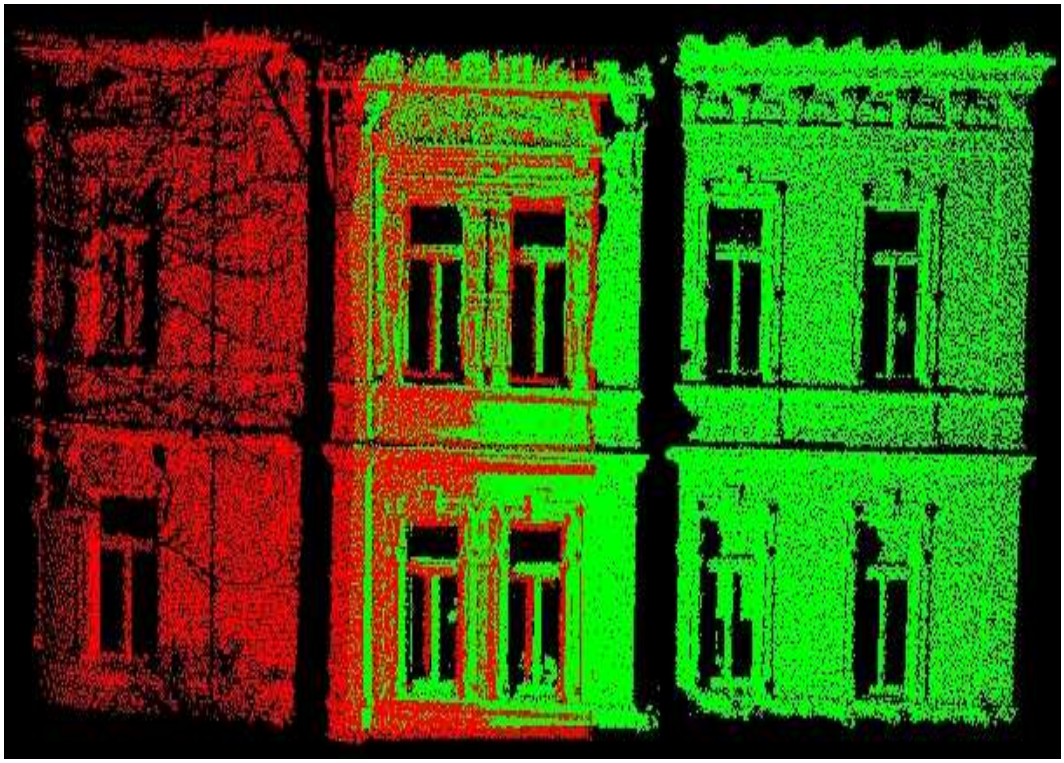

Figure 4.12: Graphical display of point clouds registration based on the improvement method.

the average distance between corresponding points and the number of iterations for two solutions. From previous work [Elkhrachy and Niemeier, 2006c] by using least square method the transformation

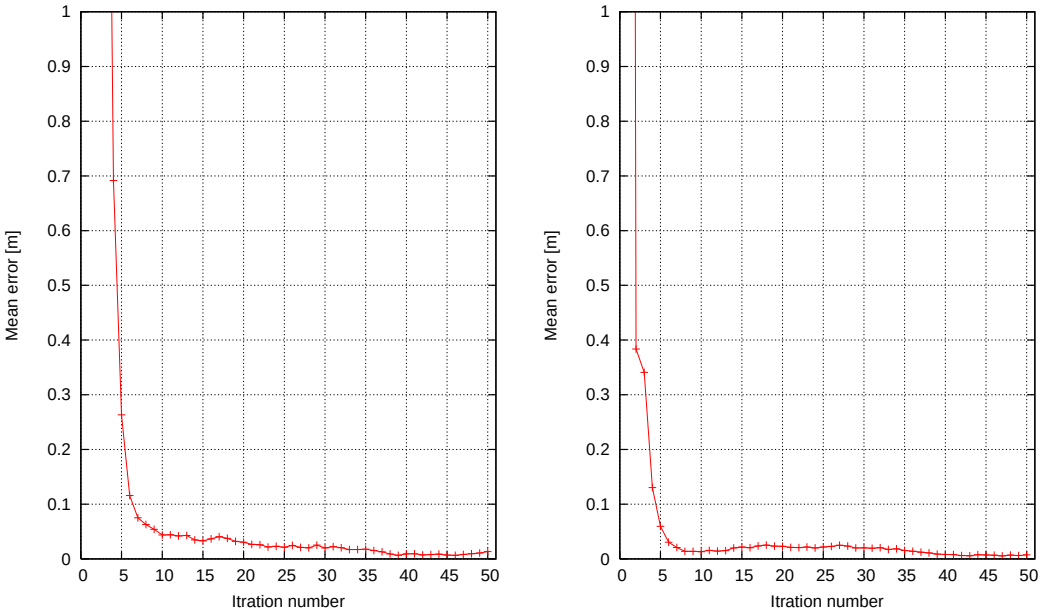

(a) Mean square error based on basic ICP.

(b) Mean square error based on improved solution.

Figure 4.13: MSE after and before ICP improvement.

parameters have been estimated based on targets registration method (Cyra targets) to evaluate the

accuracy of the current method. The registration results are compared with results based on the target method. Table 4.1 shows the coordinates of registration targets (Cyra targets) after registration and their discrepancies. Table 4.2 shows three different solutions for the transformation parameters. The

Table 4.1: Discrepancies on known correspondences (Cyra targets) after transformation based on least square solution.

Target	**Target coordinates** (m)						**Discrepancies**
	After transformation			**Scan 2(target)**			
	X	Y	Z	X	Y	Z	(m)
1	-2.2446	-3.2443	-9.7717	-2.2446	-3.2445	-9.7723	0.0006
2	0.3614	-4.2438	-12.0788	0.3623	-4.2433	-12.0782	0.0012
3	-1.5485	0.5496	-12.2920	-1.5487	0.5493	-12.2921	0.0004
4	5.3314	-6.2700	-17.2189	5.3310	-6.2694	-17.2191	0.0008
5	3.7684	-1.8572	-17.7543	3.7694	-1.8568	-17.7550	0.0012
6	2.7511	-5.5247	-14.9683	2.7505	-5.5253	-14.9679	0.0009

first is based on basic ICP method, the second is based on target based (Cyra targets) and the last one obtained from the improvement for ICP method. With the improvement for ICP method, the

Table 4.2: Transformation parameters for experimental test compared with different solutions.

Registration method	**Transformation Parameters**					
	ω °	ϕ°	κ°	T_x (m)	T_y (m)	T_z (m)
Basic ICP	28.4333	79.1583	-46.2922	21.3802	-4.7375	-14.7375
Cyra targets	10.1894	67.5948	-30.5044	17.8102	-2.6750	-7.2002
Our solution	12.7983	68.3086	-34.2369	17.7792	-3.0179	-7.4089
Differences	-2.6089	-0.7138	3.7325	0.0310	0.3429	0.2087

differences between the improved ICP method and target based method are improved as shown in table 4.2. The differences in rotation ω, ϕ and κ are -2.6089°,-0.7138° and 3.7325° respectively. All of these differences needs to be improved. Table 4.3 shows the coordinates of registration targets after registration and their relative distances (discrepancies) based on the improvement for ICP method. Discrepancies on check points (Cyra registration targets are used to evaluate the results. The minimum

Table 4.3: Discrepancies on check points (Cyra registration targets) after registration based on the improvement for ICP solution.

Target	**Target coordinates** (m)						**Discrepancies**
	After transformation			**Scan 2(target)**			
	X	Y	Z	X	Y	Z	(m)
1	-2.3255	-3.1910	-9.6352	-2.2446	-3.2445	-9.7723	0.1679
2	0.2189	-4.2804	-11.9705	0.3623	-4.2433	-12.0782	0.1831
3	-1.5915	0.5498	-12.2238	-1.5487	0.5493	-12.2921	0.0806
4	5.0562	-6.4890	-17.1624	5.3310	-6.2694	-17.2191	0.3563
5	3.5790	-2.0514	-17.7379	3.7694	-1.8568	-17.7550	0.2728
6	2.5311	-5.6551	-14.8803	2.7505	-5.5253	-14.9679	0.2695

relative distance was 0.0806 m and the maximum was 0.3563 m with 0.2015 m mean values as listed in table 4.4. From the last results, the improvement for ICP solution method produces accurate data registration results comparing with basic ICP.

Table 4.4: A statistical analysis between discrepancies on control points for three solution methods.

Registration method	Max.Diff. (m)	Min.Diff. (m)	Mean Diff. (m)
Basic ICP	5.8582	4.4660	4.8424
Improved solution	0.3563	0.0806	0.2015
Cyra targets	0.0012	0.0004	0.0009

4.4 Summary

What was presented and discussed within the previous sections was the first trial to improve start correspondence points for the ICP solution. The ICP solution does not use any local features in order to direct the solution to a minimum, it only minimizes the mean square error of the correspondence points. The accuracy of the improvement for the ICP solution was about 20 cm. In many applications this accuracy is not acceptable. So searching for accurate correspondence points (overlapped zone) between two overlapped point clouds is the key to improve the ICP solution. Therefore the objective in the following chapter is to determine the correspondence points more accurate.

Chapter 5

Improving Accuracy of Target Registration Method

5.1 Introduction

There is a need to obtain an accurate 3D model for the scan object. The accuracy of the final 3D model affected by the uncertainty of the transformation parameters and the observations precision for the scanning system. Errors computed for the transformation parameters will be propagated into the point clouds. Geometrical distribution of registration targets around the laser scanner position is also a source of registration errors and may also give an unstable solution.

An abundance of authors has addressed this problem in the recent years. With computer-based simulations, [Gordon and Lichti, 2004] have considered that the laser scanner data could be registered by calculating the origin of the scanner from three or more ground control points (GCPs) from a 3D resection solutions. They investigated the effect of the control geometry on the quality of 3D resection solutions with a narrow field of view (Cyrax 2500). But the simulation is performed under ideal conditions, which are rare to meet in the real field. For example, if the shape of the scan object is linear, like building facades, the geometric distribution of registration targets will not be ideal for the registration accuracy. In this chapter, the combined least squares as a method for data registration has been used to calculate the transformation parameters. For the purpose of analyzing the quality of the estimated transformation parameters, the standard deviations and covariances are extracted from the covariance matrix of the parameters. These values of the standard deviations are among others functions of the distribution of registration targets.

5.2 Sphere Targets and their Impact on Data Registration Accuracy

5.2.1 Problems and Objectives

Based on the target registration method, the sphere targets will be used as artificial targets between adjacent scans. The algorithms for fitting a sphere to point clouds is presented in section 3.3.2. The

centers of the fitted spheres are used as registration points between the scans. Error associated with estimating the target centers will propagate into the registration parameters. A real test has been carried out in order to evaluate the precision of sphere target parameters and the impact of their fitting quality on the data registration accuracy.

5.2.2 Experimental Test

From five standpoints, one scan has been made with a Leica HDS 3000 laser scanner, the newest high precision Leica HDS family product. This scanning system allows a larger Field of View (360° H x 270° V). Figure 5.2 shows a scan test configuration, 8 Cyra's retro-reflective targets and 12 sphere targets,

(a) Sphere target $\Phi \approx 30$ cm (polyester) (b) Sphere target $\Phi \approx 10$ cm (styrofoam) (c) Cyra plane targets Φ 6 inch diameter

Figure 5.1: Used targets.

9 with diameter of 10 cm made from styrofoam material (figure 5.2.2a) and 3 with ≈ 30 cm diameter made from polyester material (figure 5.2.2b) are placed along one side of the wall (HANNOVER MESSE) and measured with the reflector-less total station. Coordinates of corresponding target centers have been used to control the results of data registration. Figure 5.3 is an intensity images for the scan test.

5.2.3 Exporting Surface Coordinate for Sphere Target

Using Cyclone 5.2 (Leica Geosystems HDS Cyclone 5.2), point clouds data from scan number 1 to 5 were selected. Each sphere object was closely examined and unnecessary points were eliminated for the sphere fitting. Surface point clouds coordinates are manually selected and exported into ASCII file format (4 columns x, y, z, *intensity*). By using sphere-fitting algorithms, spheres parameters are determined.

Figure 5.4 shows the standard deviation of modeled sphere centers for all spheres. Their surface coordinates are exported from all five scans. The standard deviations are large when the sphere target is far away from the scanner. Results that are obtained from scan number 4 gave homogeneous and a best fitting accuracy, because the targets are nearly to be symmetrical distributed around the scanner

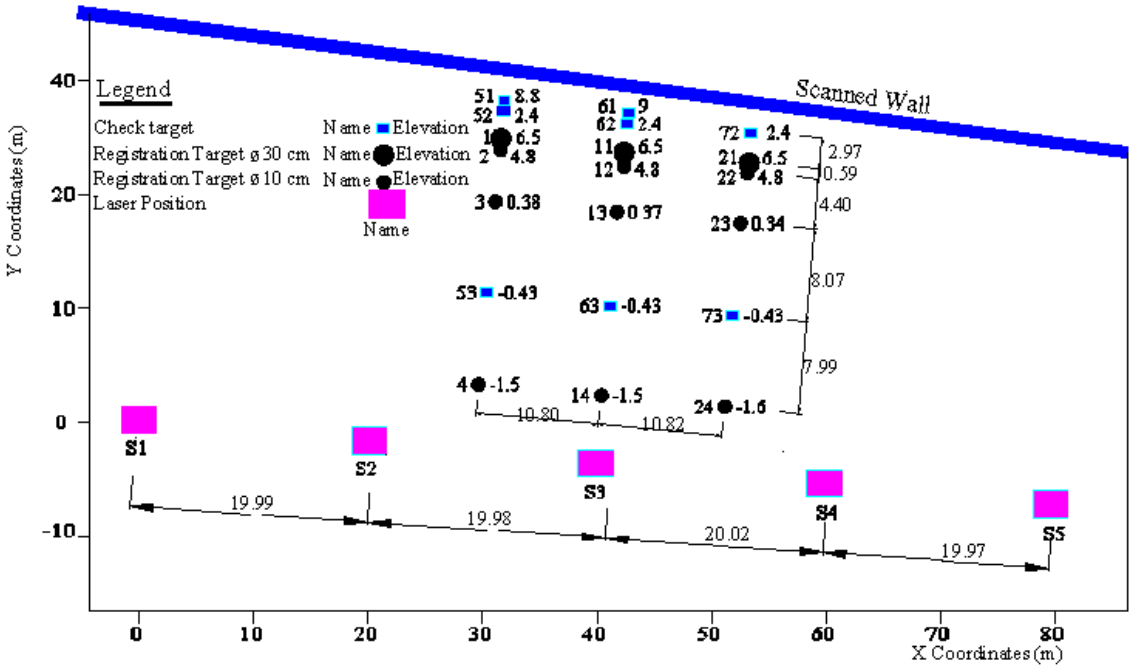

Figure 5.2: Configuration of the experimental scan test.

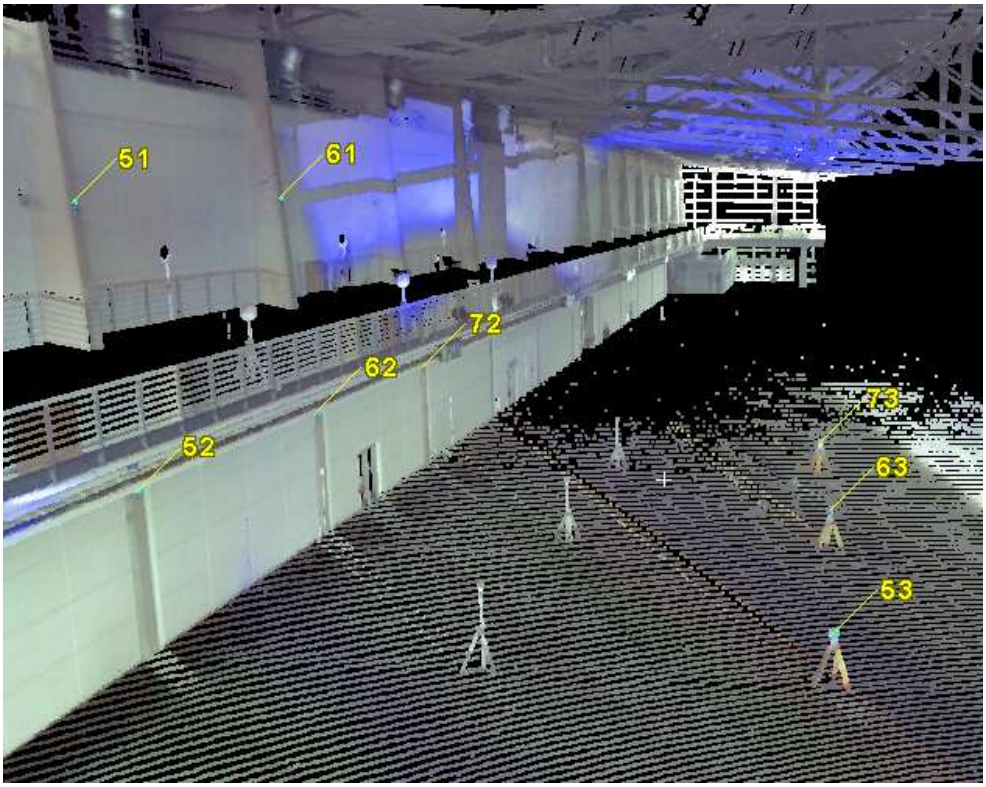

Figure 5.3: An RGB image for a scan test. The cyra targets are used to control the registration results.

position. Also targets reduction accuracy is dependent on the range between scanner and sphere target. Figures 5.5 and 5.6 show the standard deviation on modeled sphere centers for the last and the first scan. (As expected), if the sampling resolution of sphere surface coordinates is dense, then an accurate estimation of the target center will be made and the target reduction error will decrease. However, if

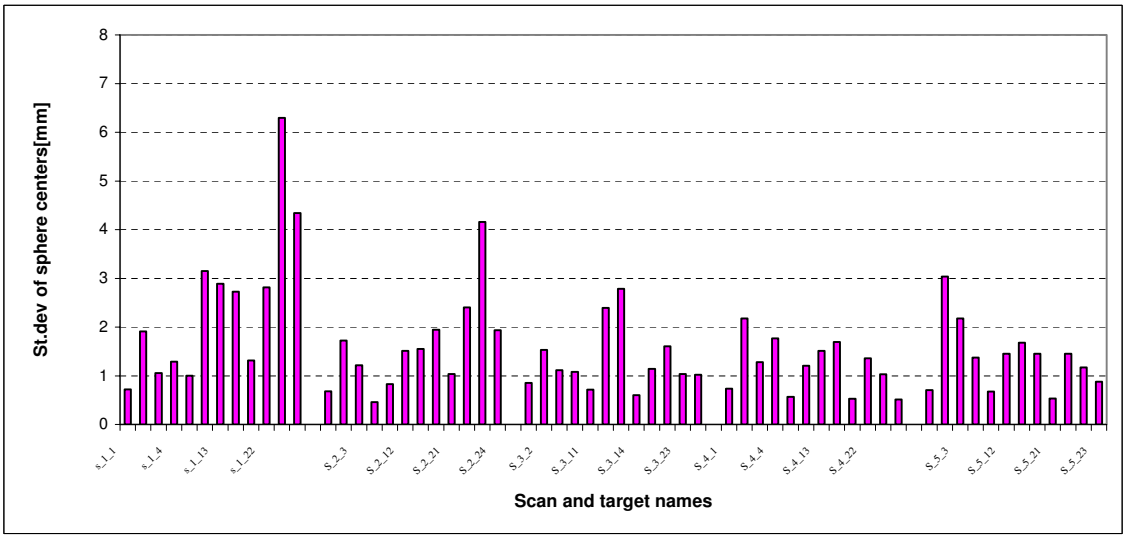

Figure 5.4: Standard deviations of spheres center for all scans.

the surface of the target is scarcely populated with point samples, then a larger target reduction error will occur. The latter may occur when the targets are situated far from the scanner. Figures 5.5 and

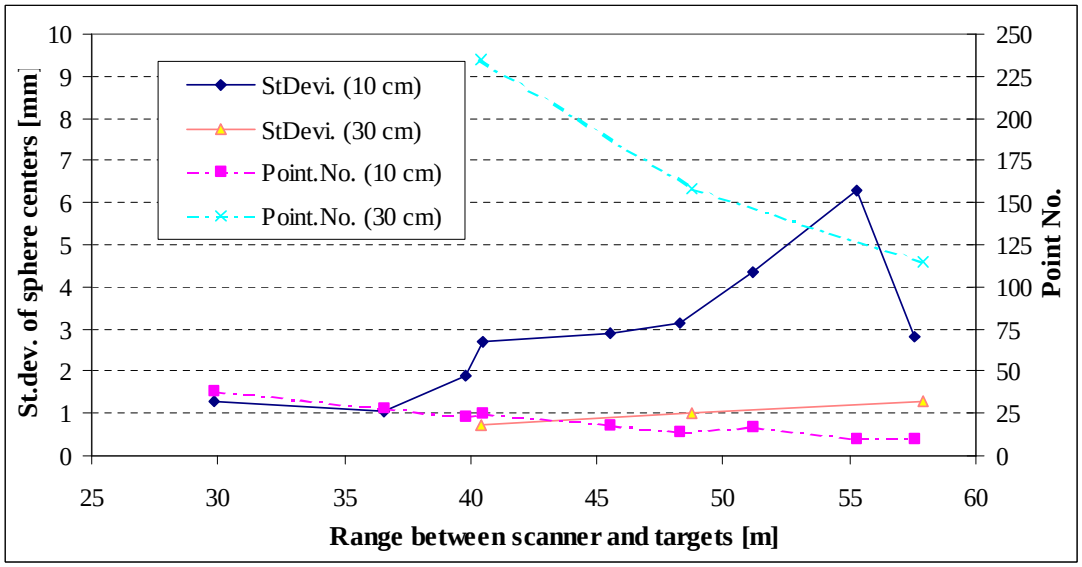

Figure 5.5: Standard deviations of sphere centers from scan number 1.

5.6 also that fitting accuracy of $30cm$ diameter spheres is less than $1.5mm$ with ranges between $40m$ and $68m$ from the scanner. Results from figure 5.5 also describe center coordinates at a range of $57.57m$ (sphere number 22) that is more accurate than the sphere at a range of 55.31 m (sphere number 23), the two spheres are modeled from 10 sample points. The coverage angles for sphere targets number 23 and 22 that are obtained by projecting surface point cloud in horizontal plane contains sphere center. The diagram of maximum coverage angle is schematically shown in figure 5.7. The coverage angle of surface point clouds is an important factor for the sphere fitting quality of, the bigger the angle, the more accurate the sphere parameters.

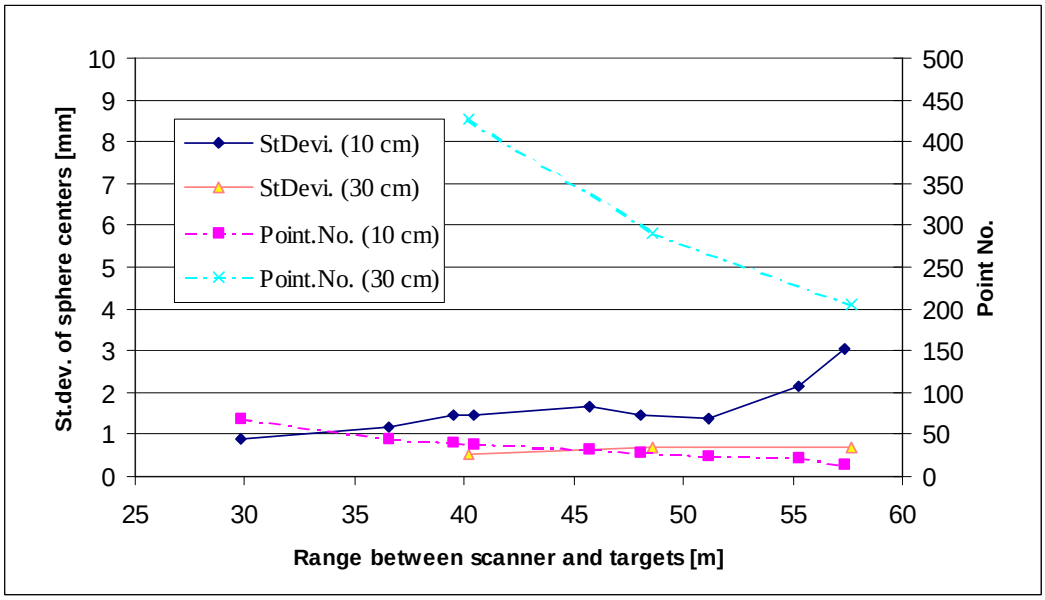

Figure 5.6: Standard deviations of sphere centers from scan number 5.

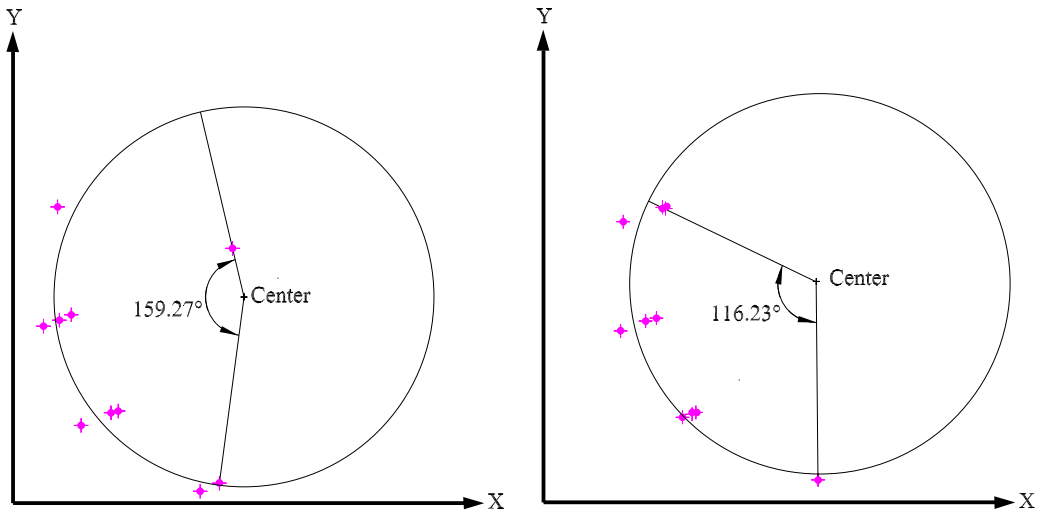

(a) Sphere number 23 (b) Sphere number 22

Figure 5.7: Coverage angles on different surface spheres with diameter = 10 cm.

5.3 Impact of Target Geometry on Data Registration Accuracy

5.3.1 Problems and Objectives

Methods for data registration have been widely investigated, but practical rules for capturing the data have not been examined yet. An example is the distribution of the registration targets which are used in the registration and their position according to the laser scanner position in each of the two adjacent scans. In order to evaluate the accuracy of the complete model obtained by the scanning process, a lot of measurements in different positions for distance and orientation of the laser scanner have been performed. In this section the results of the precision achieved are described using the registration of

two adjacent scans. Also some practical rules to manage the geometrical distribution of registration targets for improving the precision of the final 3D model are examined. The data from the last test field is used to test the registration algorithm and to get the results. See section 5.2.2 for more details on scan tests. The reflecting targets have been used to check and evaluate the registration results.

5.3.2 Computation of Transformation Parameters

Transformation parameters between the first scanworld coordinate system and adjacent scans will be calculated in two steps. The first one is calculating approximate parameters, the second one is to refine the approximate parameters by using the least squares solution. The first step is based on the approach proposed by [Sanso, 1973]. For the second step, the combined least squares adjustment model is used, see chapter 4 for details on data registration algorithm based on the target method.

5.3.3 Registration Results with Different Target Configurations

The first scan coordinate system has been considered as a global or a reference coordinate system, then the other 4 scans have been registered onto the first scan using only coordinates of three targets. Three different target configurations have been studied to evaluate the accuracy as follows:

1. Targets in a collinear fashion parallel to the line, which connects laser scanner set-up locations, configuration codes 1, 2, 3 and 4 (four trails).
2. Targets in a collinear fashion perpendicular to the line, which connects laser scanner set-up locations, configuration codes 5, 6, and 7 (three trails).
3. Targets in a zigzag fashion between Laser scanner set-up locations, configuration codes 8, 9, 10, 11, 12, 13 and 14 (seven trails).

Using the known coordinates of the reflecting targets (Cyra targets), estimated from a very high resolution scanning, the differences (distances between the known points and the calculated positions after registration) expressed in meters have been calculated. Tables from 5.1 to 5.3 show the maximum, minimum and mean of the differences on check points after the registration process in case of registration targets in a collinear parallel, collinear perpendicular and Zigzag configuration. Figure

Table 5.1: Differences on check points: Collinear parallel configurations.

Configuration code	Used targets	Max.Diff. (m)	Min.Diff. (m)	Mean Diff. (m)
1	1-11-21	0.2789	0.0820	0.1742
2	2-12-22	15.6190	8.9992	12.3870
3	3-13-23	0.4898	0.2828	0.3401
4	4-14-24	0.1090	0.0152	0.0485

5.8 shows the standard deviations of the orientation and translation parameters between scan 1 and

Table 5.2: Differences on check points: Collinear perpendicular configurations.

Configuration code	Used targets	Max.Diff. (m)	Min.Diff. (m)	Mean Diff. (m)
5	1-3-4	0.0851	0.0102	0.0305
6	11-13-14	0.0879	0.0139	0.0332
7	21-23-24	0.0791	0.0121	0.0302

Table 5.3: Differences on check points: Zigzag configurations.

Configuration code	Used targets	Max.Diff. (m)	Min.Diff. (m)	Mean Diff. (m)
8	11-4-24	0.0762	0.0124	0.0296
9	11-3-23	0.0786	0.0088	0.0290
10	11-2-22	0.0810	0.0143	0.0310
11	3-24-21	0.0801	0.0106	0.0301
12	3-11-14	0.0793	0.0115	0.0302
13	3-23-22	0.0834	0.0106	0.0322
14	3-13-12	0.0787	0.0126	0.0295

scan 5 with three different target configurations: **Collinear parallel**, **collinear perpendicular** and **zigzag configuration**. As expected, it has been shown that the configurations of registration targets in a collinear or neared collinear made the registration solution fail, or to contain inflated levels of accuracies. Figure 5.9 shows more zooming in the results only for perpendicular and zigzag configurations. The distribution of the targets in a zigzag form gives the best registration results. As the three

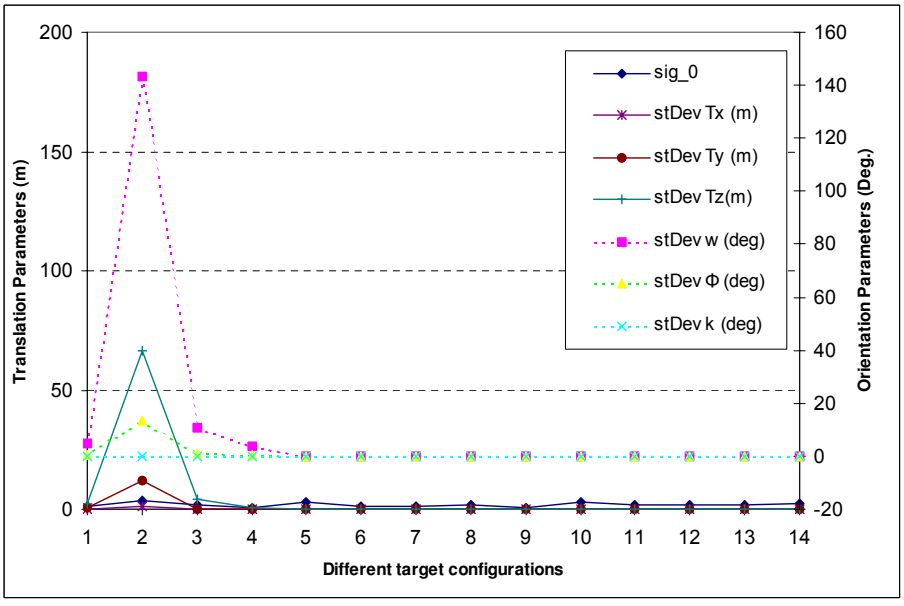

Figure 5.8: Standard deviations of registration parameters between scan numbers S1 and S5, (Collinear parallel, collinear perpendicular and zigzag configurations).

registration targets in a zigzag form but near from collinear form, the results were very bad (see figure 5.8 case configuration number 10). Rotation angle κ parameters were independent of these configurations. The standard deviations of all parameters were lower and homogeneous in configuration 9 and 11. Figures 5.10 and 5.11 show the standard deviations of the orientation and translation parameters

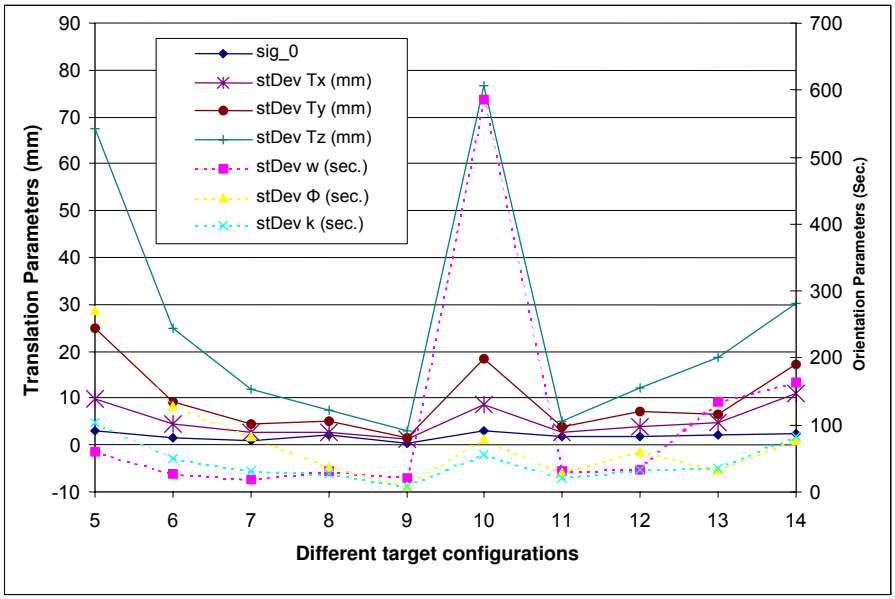

Figure 5.9: Standard deviations of registration parameters between scan numbers S1 and S5, (collinear perpendicular and zigzag configurations).

between scan 1 and all the scans only for target configuration numbers 9 and 11. The results indicated that configuration number 9 is the most accurate one.

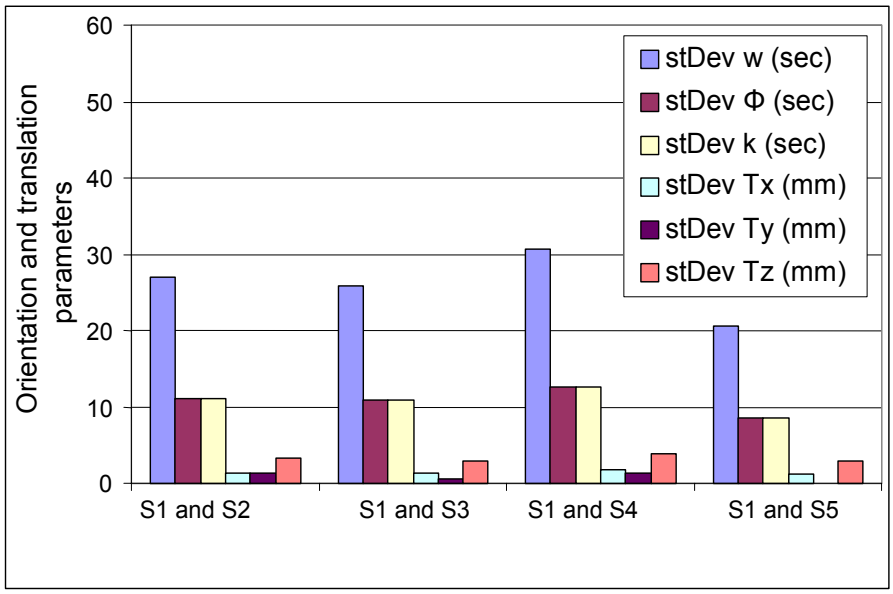

Figure 5.10: Standard deviations of registration parameters between scan number S1 and the available other scans for configuration number 9.

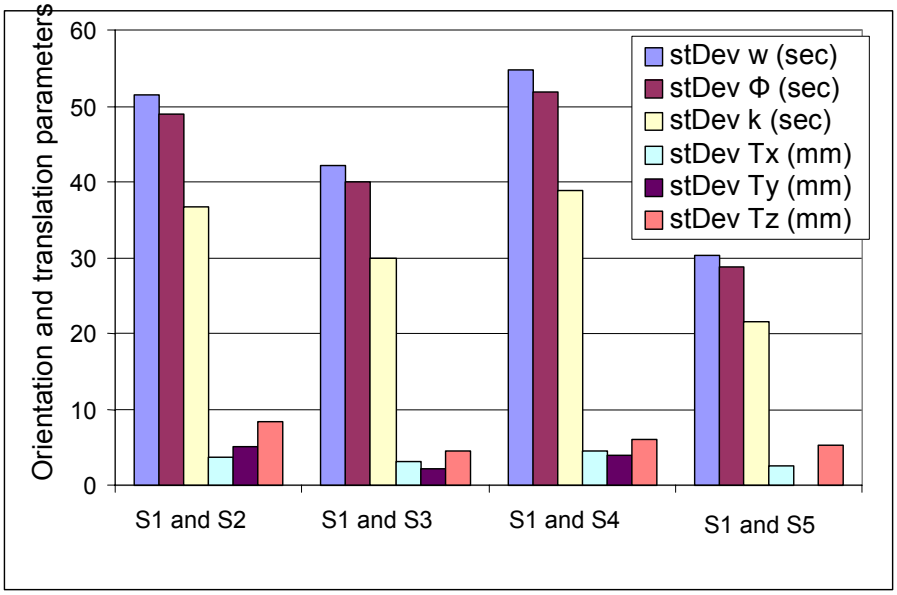

Figure 5.11: Standard deviations of registration parameters between scan number S1 and the available other scans for configuration number 11.

5.4 Stochastic Assessment to Improve Data Registration Accuracy

5.4.1 Problems and Objectives

The mixed least square solution was used to calculate the transformation parameters. Using this model, the coordinates of registration targets in left and right scans are considered as observations. The advantage of this approach is giving the same registration target different weights in every two adjacent scans. A stochastic assessment procedure has been developed to take into account the range between the scanner and the registration targets in the left and right scan. A comparison between current study results and other commercial available software (Cyclone 5.1, Australis and Panda) indicated that the reliability of the estimated transformation parameters between the adjacent scans is improved.

5.4.2 Data Registration Models

In chapter 4 the least square adjustment for the corresponding tie points between adjacent scans is considered as a model for terrestrial laser scanner data registration. If the coordinates of the corresponding tie points (or ground control points like photogrammetry methods) are known in one global coordinate system (for example measured by a total station). Also the coordinates of the corresponding tie points from the laser scanner is considered the observation in least square solution while the coordinates from total station (in global system) are error less. In this case the parametric least squares adjustment model could be used to solve the transformation problem. the parametric least squares adjustment model is shown in equation 5.1:

$$\hat{\boldsymbol{l}} = f(\hat{\boldsymbol{x}}) \tag{5.1}$$

The stochastic model or the variance-covariance matrix $\boldsymbol{C}_{ll}$ considers only the observations from the right scan. The weight matrix of the observations will take the following form.

$$\boldsymbol{P} = \boldsymbol{Q}_{ll}^{-1} \tag{5.2}$$

So, the residual of the solution will go only to the coordinates from laser scanner observations. To safe money and time, most of the surveyors do not prefer this data registration method. They simply use the laser scanner to capture 3D information of the scan object containing registration targets from many laser stand point. They consider the coordinate system of the first scan or any scan is the reference scan and register the rest into it (see figure 5.12). In case of considering only two scans for the

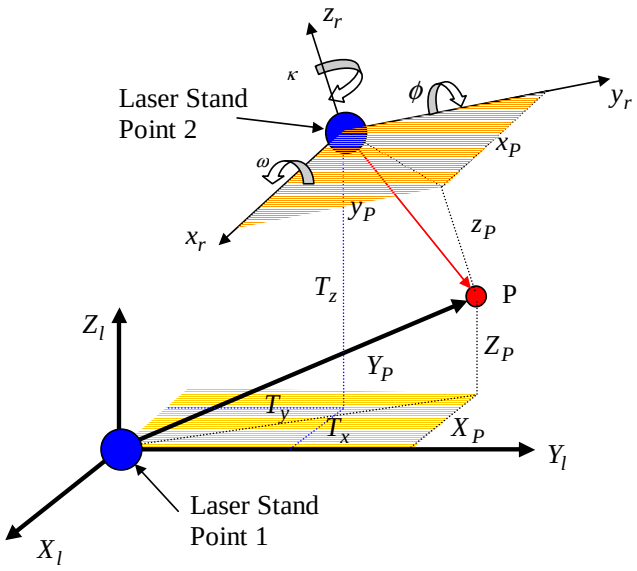

Figure 5.12: Data registered to a local coordinate system, for example by considering first scan coordinate system is the reference.

registration process, this means the coordinates of the first scan and second scan are observations and the residuals should be distributed to all of them. In this case, the combined least squares adjustment model is utilized based on assuming a set of targets coordinates in two adjacent reference systems are observations. With the combined least squares adjustment solution the stochastic model or the variance-covariance matrix $\boldsymbol{C}_{ll}$ will take the following form:

$$\underset{n,n}{\boldsymbol{C}_{ll}} = \underset{n,n}{\boldsymbol{Q}_{ll}}\, \sigma_0^2 = \begin{bmatrix} \boldsymbol{\sigma}_{x_r}^{\mathbf{2}} & \mathbf{0} \\ \mathbf{0} & \boldsymbol{\sigma}_{X_l}^{\mathbf{2}} \end{bmatrix} \tag{5.3}$$

where:

$$\begin{aligned} \boldsymbol{\sigma}_{x_r}^{\mathbf{2}} &= \text{covariance matrix of observations 1} \\ \boldsymbol{\sigma}_{X_l}^{\mathbf{2}} &= \text{covariance matrix of observations 2} \end{aligned}$$

Equation 5.3 indicates that all covariances are zero. The weight matrix of the observations will take the following form:

$$\boldsymbol{P} = \boldsymbol{Q}_{ll}^{-1} = \begin{bmatrix} \boldsymbol{Q}_{x_r}^{-1} & \mathbf{0} \\ \mathbf{0} & \boldsymbol{Q}_{X_l}^{-1} \end{bmatrix} \tag{5.4}$$

The accuracy of the final complete scan object depends on the accuracy of the transformation parameters between all the scans. The accuracy of acquiring the coordinates of registration targets depends on the range between the scanner and the targets and also the distribution of these targets according to the field of view of the scanner. Figure 5.13 shows that the geometrical representation of the overlapped sphere target between adjacent scans is not identical while the target is scanned from two different positions. A stochastic assessment procedure has been developed taking into account the

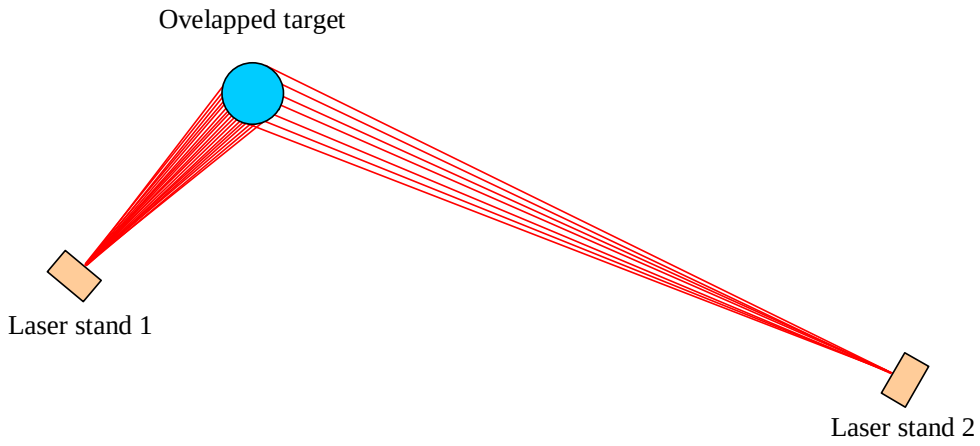

Figure 5.13: Acquiring the same sphere target from two overlapped scans.

range between the scanner and the registration target for the adjacent scans. Results of transformation parameters from the used registration targets have been compared. Different stochastic models were employed with the least squares solution.

5.4.3 Test Field

In order to test the registration algorithm and to get the results, the laser system Imager 5003 from the Zoller+Froehlich company has been used to scan the cross section Wenden (about 15 kilo meter away from the Braunschweig city center). The scanned area is approximately $50m$ wide and $40m$ long. Table 2.3 in chapter 2 describes the technical specifications of Imager 5003 scanner system. From two different standpoints, two scans have been made. Figure 5.15 is a plane for the scan test. It describes the different standpoints for the scanner position.

For registration purposes, 10 black and white plane (printed with size DIN A4) targets have been placed. Also non calibrated 4 polystyrene spheres with diameter $\approx 30cm$ are used see figure 5.15. By using the commercial available software Z+F Laser control, two scans have been made. Each one has extension *.zfs with the size 160 and 157MB respectively. Figure 5.16 and 5.17 are intensity images for the left and the right scan.

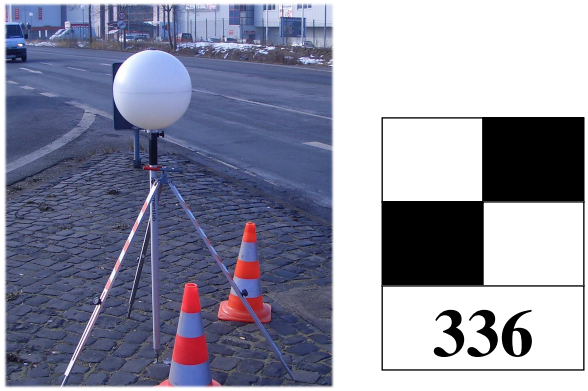

(a) Sphere target $\Phi \approx 30$ cm (polyester) (b) Black and white plane target

Figure 5.14: Used targets.

Figure 5.15: Distribution of sphere targets and two scan positions.

5.4.4 Extracting Registration Targets Coordinates

The scanning program Z+F Laser control has a special function to find only the black-white registration targets. To do this, the user should manually find and adjust the mouse as close as possible to the cross which separate the black-white color for every target. All acquired targets have been labeled. Their coordinates are exported into ASCII files with 4 columns (point number x, y and z).

Table 5.4 shows the registration parameters and their fitting quality by using the best 5 black-white registration targets. Also, the registration parameters are calculated using available software products, these software products are:

- Leica Geosystems HDS Cyclone 5.1 [Geosystems, 2005] a 3D point cloud processing software for laser scanner observation.

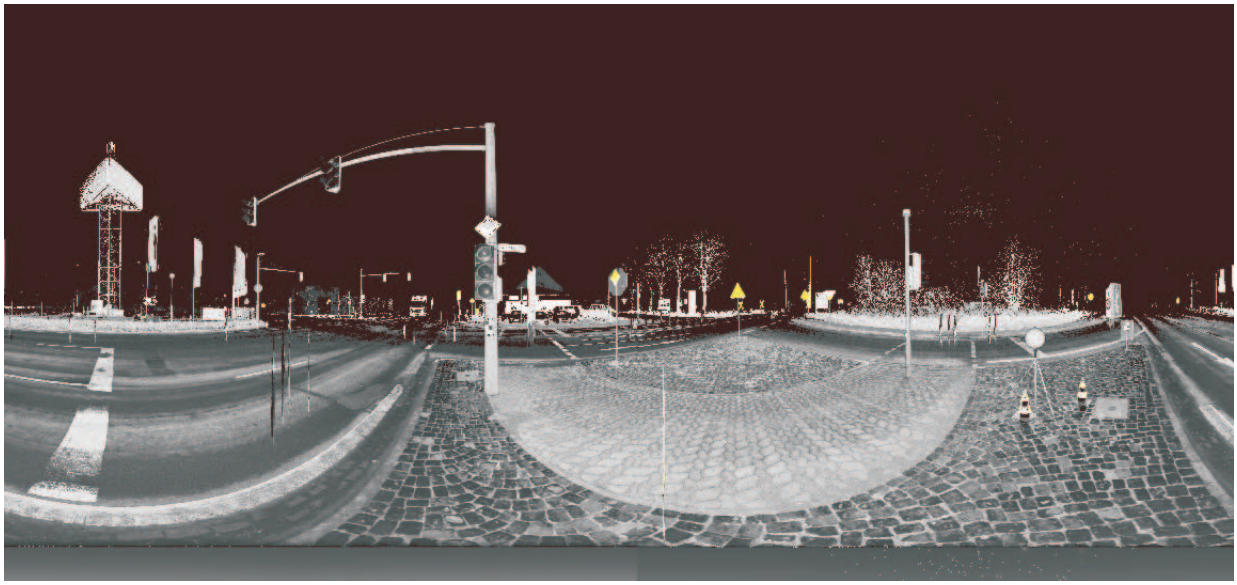

Figure 5.16: Left scan.

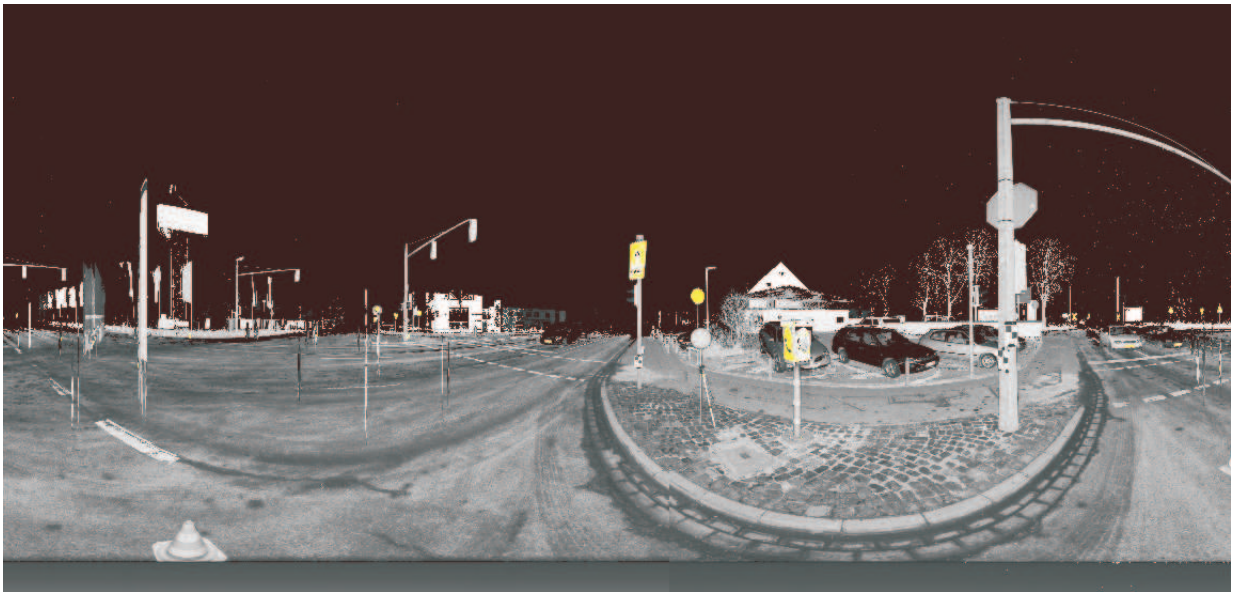

Figure 5.17: Right scan.

- Australis [Photometrix, 2005] software system for automated off-line digital close range photogrammetric image measurement, orientation triangulation and sensor calibration.
- Panda [Niemeier and Tengen, 1990] is a program for the adjustment of the networks and deformation analysis.

No quality fitting to describe the goodness of the parameters by using Cyclone software. The differences in the rotation angles ω, ϕ and κ were $06'57''$, $09'55''$ and $008''$, respectively. Also the differences in the translation vectors T_x, T_y and T_z were 18.4, 6.8 and 3.0 mm respectively.

[1]Not available with Cyclone software

Table 5.4: Transformation parameters and their fitting quality by using black-white targets.

Parameters	Registration results			Fitting quality of the parameters		
	Improved solution	Cyclone	Australis and Panda	Improved solution	Cyclone	Australis and Panda
ω	-00°26′24″	-00°33′21″	-00°26′24″	359″	na[1]	321″
ϕ	00°01′26″	-00°11′21″	00°01′26″	177″	na[1]	158″
κ	-44°02′39″	-44°02′47″	-44°02′39″	159″	na[1]	142″
T_x m	14.4597	14.4413	14.4597	13.9 mm	na[1]	16.0 mm
T_y m	-7.5088	-7.5156	-7.5088	17.5 mm	na[1]	16.1 mm
T_z m	0.080	0.0797	0.080	20.7 mm	na[1]	18.5 mm

5.4.5 Extraction of Sphere Targets from Point Clouds

Cyclone 5.1 has the advantage of using a 3D window selection to cut and edit point clouds. The two data scans which are represented in figure 5.17 and figure 5.16 are imported from *.zfs data to *.imp data by using Cyclone 5.1. With this program it is possible to select and export the point clouds manually for each sphere into *ASCII* files formate 4 columns x, y, z and intensity. Sphere targets in two scans are used as three-dimensional targets. The main advantage of the spherical targets are their viewing from any laser standpoint. In our test, 4 polystyrene spheres with non calibrated radius $\approx$ 15 cm are used.

Algorithms for fitting a sphere to 3D point clouds is discussed in section 3.3.2. Figure 5.18 and 5.19 represent the relation between the accuracy of the center coordinates of modeled 4 spheres from two scans. The results show inversely relation between the range from the scanner and the accuracy of sphere parameters, for example the accuracy in between 1 to 8 mm for 10 to 28 m range between sphere target and laser scanner stand point.

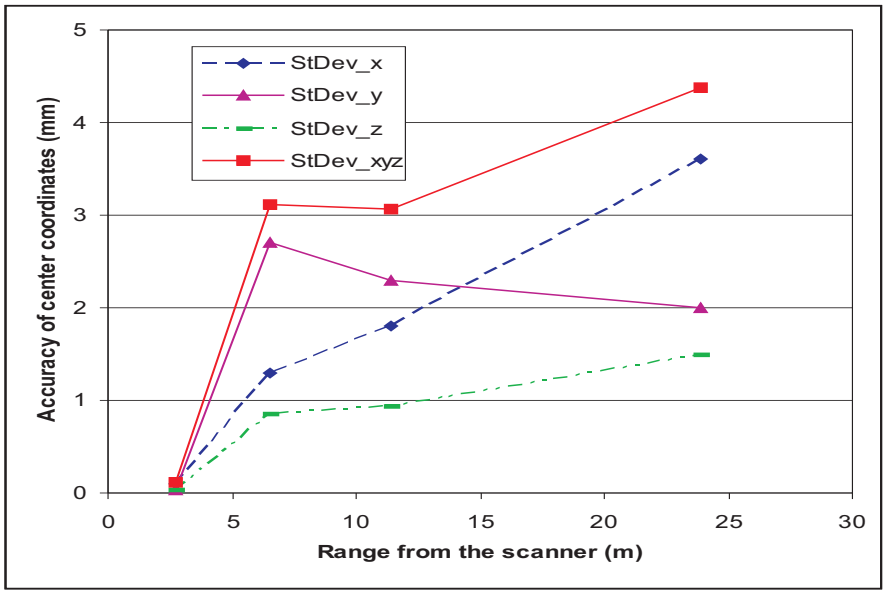

Figure 5.18: Accuracy of center coordinates of modeled spheres from scan 1.

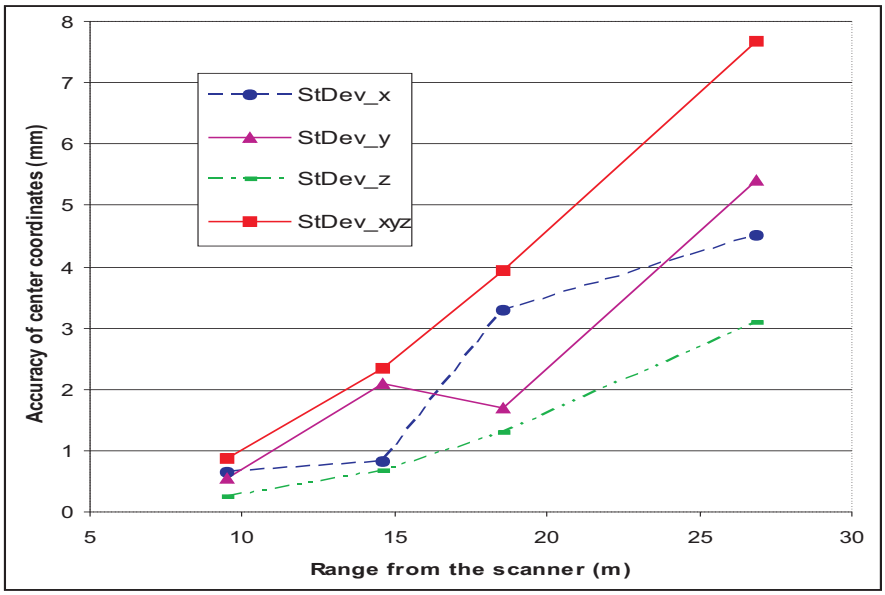

Figure 5.19: Accuracy of center coordinates of modeled spheres from scan 2.

5.4.6 Stochastic Assessment of Registration Target Coordinates

Laser scanner observations are contaminated by several kinds of errors and biases, namely, the surface properties (e.g. material, roughness and color), the angle of incidence and the distance between the scanner and the target. Also for long range applications the present atmosphere (temperature and air pressure) influences the distance accuracy. Due to the complex nature of these errors, rigorous modeling, in general, cannot be achieved. The remaining error components must be modeled stochastically through the least square stochastic model (the observation covariance matrix). The variances (diagonal elements of the covariance matrix) describe their statistical quality while the covariance (off-diagonal elements) describes their correlation between the observations. Accuracy of tie points which are used in the data registration is accounted by weighting the more precise one. Equation 5.5 represents a model of the relative weight matrix for one tie point which has 3D coordinates from two adjacent scan.

$$\boldsymbol{P} = \begin{bmatrix} \frac{1}{p_r} & \mathbf{0} & \mathbf{0} & & & \\ \mathbf{0} & \frac{1}{p_r} & \mathbf{0} & & \mathbf{0} & \\ \mathbf{0} & \mathbf{0} & \frac{1}{p_r} & & & \\ & & & \frac{1}{p_l} & \mathbf{0} & \mathbf{0} \\ & \mathbf{0} & & \mathbf{0} & \frac{1}{p_l} & \mathbf{0} \\ & & & \mathbf{0} & \mathbf{0} & \frac{1}{p_l} \end{bmatrix} \tag{5.5}$$

where:

p_r = range between scanner stand point and registration target in right scan
p_l = range between scanner stand point and registration target in left scan

According to the results from figures 5.18 and 5.19 which mean that the variance of center coordinates of the sphere tie target is inversely proportional to the range between the sphere center and the scanner

Table 5.5: Transformation parameters and their fitting quality by using spheres targets.

Parameters	Registration results			Fitting quality of the parameters		
	Equal weighted	Weighted $\frac{1}{range}$	Weighted $\frac{1}{range^2}$	Equal weighted	Weighted $\frac{1}{range}$	Weighted $\frac{1}{range^2}$
ω	-0°26′04″	-0°26′04″	-0°26′04″	253″	207″	186″
ϕ	-00°00′45″	-00°00′46″	-00°00′46″	139″	130″	126″
κ	-44°04′57″	-44°04′54″	-44°04′47″	122″	109″	103″
T_x m	14.4383	14.4411	14.4423	9.1 mm	7.7 mm	7.0 mm
T_y m	-7.5236	-7.5236	-7.5233	10.7 mm	9.5 mm	8.8 mm
T_z m	0.0955	0.0955	0.0955	12.0 mm	10.4 mm	9.8 mm

stand point. Three candidates or models for the relative weight are used with the least square solution to calculate transformation parameters and their impact on the quality of the unknowns that were discussed:

1. An identity weight matrix (Equal weights) $P = 1$.
2. The range between scanner stand point and target position dependent (i.e. $\sigma_i^2 = \sigma_{x_c}^2 = \sigma_{y_c}^2 = \sigma_{z_c}^2 = range_i$).
3. The range square between scanner stand point and target position dependent(i.e. $\sigma_i^2 = \sigma_{x_c}^2 = \sigma_{y_c}^2 = \sigma_{z_c}^2 = range_i^2$).

Table 5.5 shows registration parameters and their fitting quality by using 4 modeled sphere registration targets for three candidates of relative weight matrix. With the last two relative weight models, the influence of the less precise registration target is reduced and the more precise is increased. That means better results for the data registration is accomplished.

5.5 Summary

The least square solution gives a set of quality parameters for the unknown which measures the goodness of the fitting solution. In the stochastic model the distance from the targets to the laser scanner was used as parameter. Considering the coordinates from the left and right scan as observations, has the possibility to give different weights for the same registration targets. Using the spheres as targets for the registration gave us the best result. Modifying the mathematical model for the least square solution gives the possibility to weight the registration target different weight from two adjacent scans. The study indicated that by weighting the coordinates of registration targets with the square range between the scanner and registration targets, the residuals of the unknowns are smaller and thus the accuracy of the final complete 3D model of the scanned object is improved.

Chapter 6

Correspondence Features Identification Between Point Clouds

6.1 Introduction

There are two concepts for Laser scanner data registration as mentioned before in chapter 3, one is based on the targets method and the other is based on overlapping point clouds. For the following reasons, the point clouds data registration method is preferable. Firstly, reducing effort and time on-site during the scanning process as no targets are used. Secondly, due to the complexity of the scanned object or space restrictions, the targets registration method could not be employed, like in high facades or tall buildings. Finding correspondence features between adjacent scans in the overlapping zone is an important task for the point clouds data registration method. Figure 6.1 is an overview of different methods for identifying correspondence features between overlapping scans. In this chapter the surface curvature is used to identify correspondence features between the overlapped scans. Because both color and intensity values of point clouds depend on laser incidence angle and surface condition. Furthermore, most of the laser scanners are not able to provide color information. The method is tested through simulated and real data.

6.2 Correspondence Features Search Method

Correspondence between overlapped scans can be established by calculating distinct features of one scan and then finding the same on the other. Based on geometrical properties of the scan object, the correspondence could be identified. Surface curvature feature is invariant under any rigid transformation. The advantage of using curvature to find correspondence can be summarized as follows:

1. Easy to be calculated.
2. Instated of 3D Surface coordinates (xyz), we have 2D (u, v) coordinates.
3. Representing the curvature as gray scale, enables to use image processing concepts.

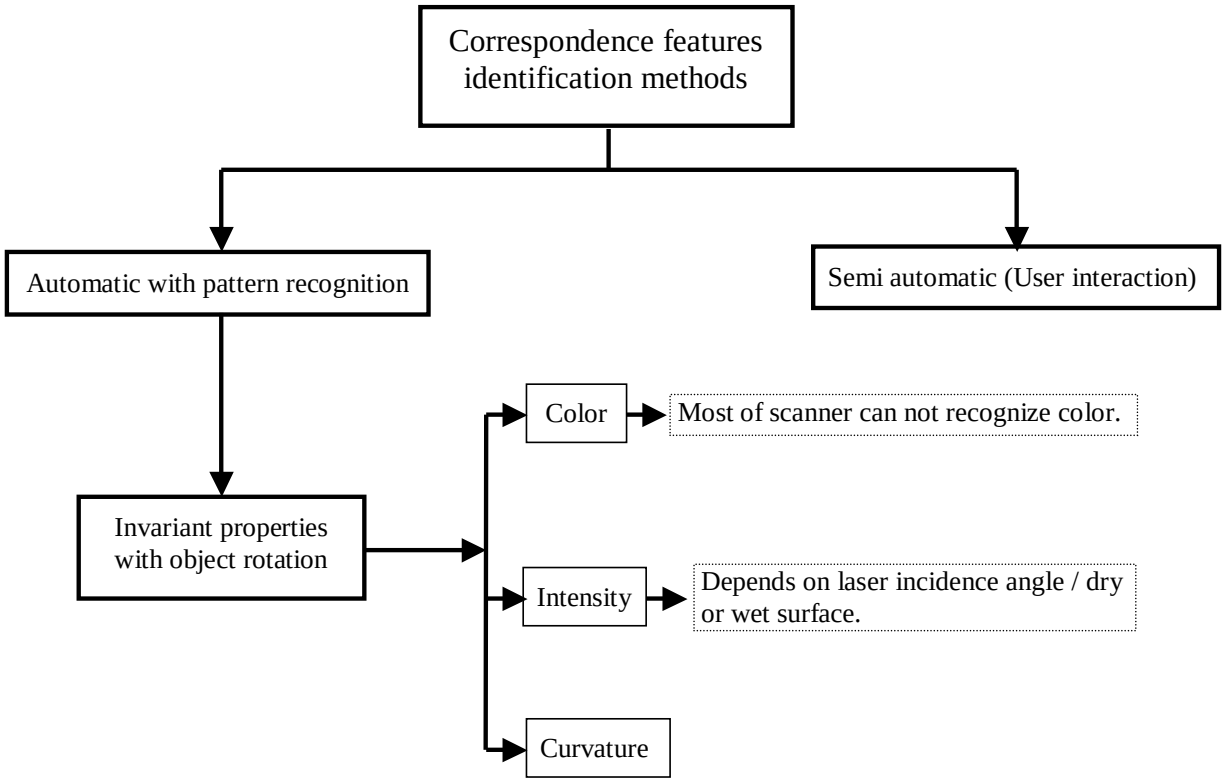

Figure 6.1: Identifying correspondence features methods.

After getting correspondence between overlapped point clouds, the ICP registration method is applied. The surface curvature could be calculated after getting surface interpolation from point clouds. The surface could be fitted by using NURBS fitting algorithm or by Delaunay triangulation procedures as shown in figure 6.2. In this work the NURBS surface fitting algorithm is used to get surface information and differential property calculation [Piegl and Tiller, 1995, p. 361].

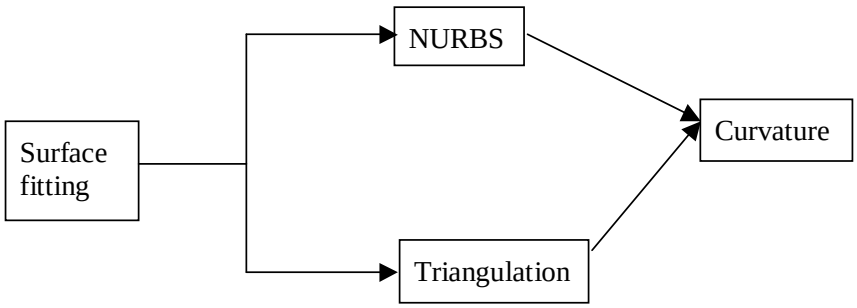

Figure 6.2: Curvature calculation methods.

6.2.1 NURBS Surfaces Construction

NURBS, Non-Uniform Rational B-Splines, are mathematical representations of a 3-D geometry that can accurately describe any shape from a simple 2-D line, circle, arc, or curve to the most complex 3-D

organic free-form surface or solid. Development of NURBS began in the 1950s by engineers who were in need of a mathematically precise representation of free form surfaces like those used for car bodies and ship hulls, which could be exactly reproduced whenever technically needed. Detailed mathematical descriptions can be found in [Piegl and Tiller, 1995], [Rogers, 2001] and [K.Agoston, 2005]. In this work the NURBS algorithm from [Lavoie, 2002] is used to construct the surface from point clouds. The construction of NURBS surface could be summarized as follows:
A surface is a vector-valued function of two parameters, u and v. It has the form $S(u,v) = (x(u,v), y(u,v), z(u,v))$. The curve $C(u)$ is a vector-valued function of one parameter u. An nth-degree Bezier curve is defined by:

$$C(u) = \sum_{i=0}^{n} B_{i,n}(u) P_i \qquad 0 \leq u \leq 1 \tag{6.1}$$

The basis functions $B_{i,n}$ are the nth-degree Bernstein polynomials given by:

$$B_{i,n}(u) = \frac{n!}{i!(n-i)!} u^i (1-u)^{n-i} \tag{6.2}$$

The geometric coefficients of P_i are called control points.
Example 1:
$n = 1$. From equation 6.2 $B_{0,1}(u) = 1 - u$ and $B_{1,1}(u) = u$ and equation 6.1 takes the form $C(u) = (1-u)P_0 + uP_1$ [Piegl and Tiller, 1995, p. 10]. This is a straight line segment from point P_0 to P_1.
Example 2:
$n = 2$. From equation 6.2 and and equation 6.1 we have $C(u) = (1-u)^2 P_0 + 2u(1-u)P_1 + u^2 P_2$. This is a parabolic arc form P_0 to P_2.

A NURBS surface or cubic equation are said to be "piecewise" and "parametric," which means the curve or surface is a sequence of connected segments that use parametric u and v values ranging from 0 to 1 to calculate points along the curve or surface, see figure 6.3. The surface is obtained geometrically

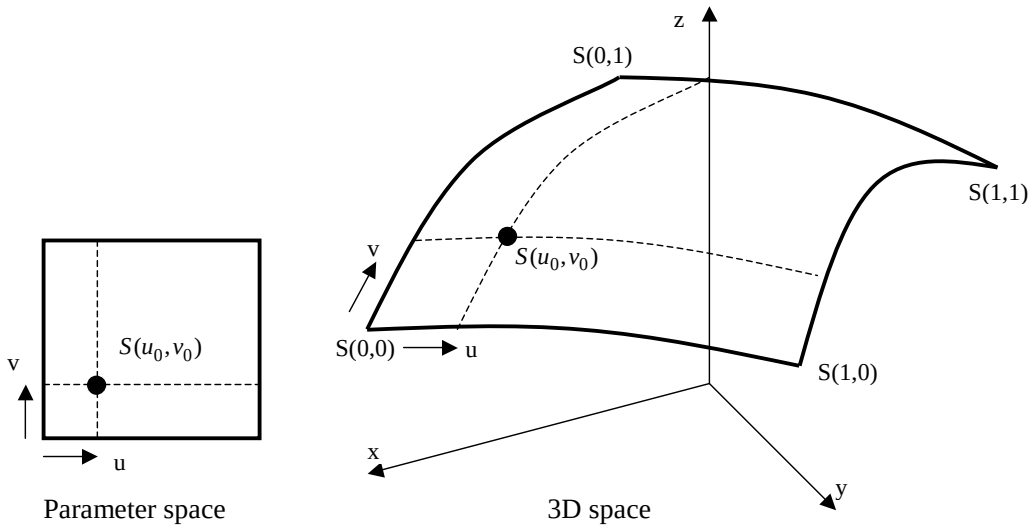

Figure 6.3: From Euclidean $3D$ (x, y, z) space to parameters space $(S(u, v))$.

by taking a bidirectional net of control points and products of the univariate Bernstein polynomials (see equation 6.3).

$$S(u,v) = \sum_{i=0}^{n}\sum_{j=0}^{m} B_{i,n}(u)B_{j,m}(v)P_{i,j} \qquad 0 \leq u,v \leq 1 \tag{6.3}$$

Bernstein polynomials take the following forms:

$$B_{i,n}(u) = \frac{n!}{i!(n-i)!}u^i(1-u)^{n-i} \tag{6.4}$$

$$B_{j,m}(v) = \frac{m!}{j!(m-j)!}v^j(1-v)^{m-j} \tag{6.5}$$

The control net on a NURBS surface is a rectangular grid of connected straight-line elements which define the tangency of the surface at positions along the control net see figure 6.4. Weights in the

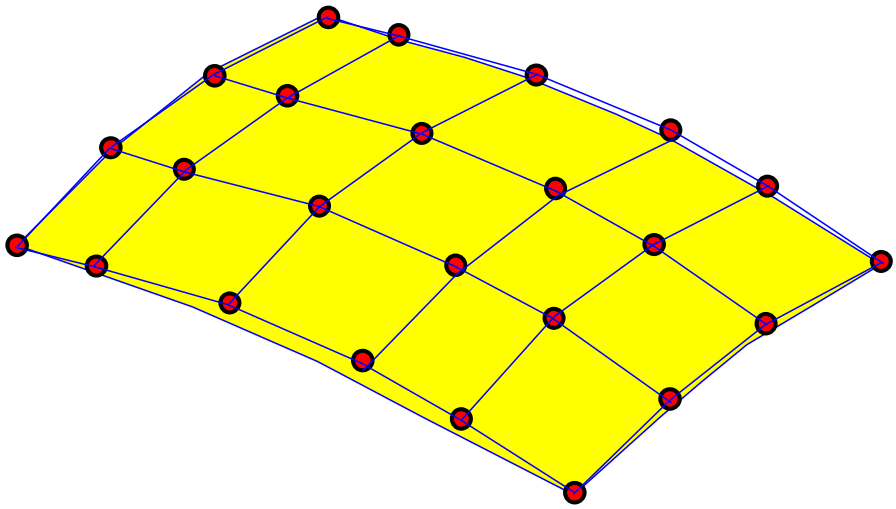

Figure 6.4: A NURBS surface interpolated from 4x6 control points.

NURBS data structure determine the amount of surface deflection toward or away from its control point. The weights are associated with each control point. Because of their flexibility and accuracy, NURBS models can be used in any process from illustration and animation to manufacturing.

6.2.2 Computation of Surface Curvatures

Curvature is the amount by which a geometric object deviates from being flat. Curvature is a differential geometry term that is popular in computer vision because of its invariance to transformation. The curvature of a planar curve at a point P is defined as the reciprocal of the radius r of the best fit circle that touches the curve at P and whose center intersects the line that is normal to the tangent of the curve at P (see Figure 6.5). Note that the curvature of a straight line is 0 everywhere since the best fit circle at any point has infinite radius. Consider a surface S with a surface normal at point P Figure 6.6, despite the orientation of the surface, the curve of intersection of a plane containing the normal to the surface at P and the surface has a curvature k. As the plane is rotated around the normal, the curvature changes. *Euler* proved that unique directions for which the curvature is a

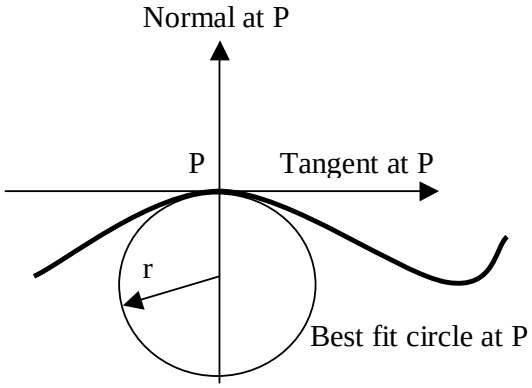

Figure 6.5: Curvature of curve at point P.

maximum and a minimum exist [Rogers, 2001, p. 197]. The curvatures in these direction are called the principal curvatures k_{max} and k_{min}. There are many textbooks available for theoretical treatment

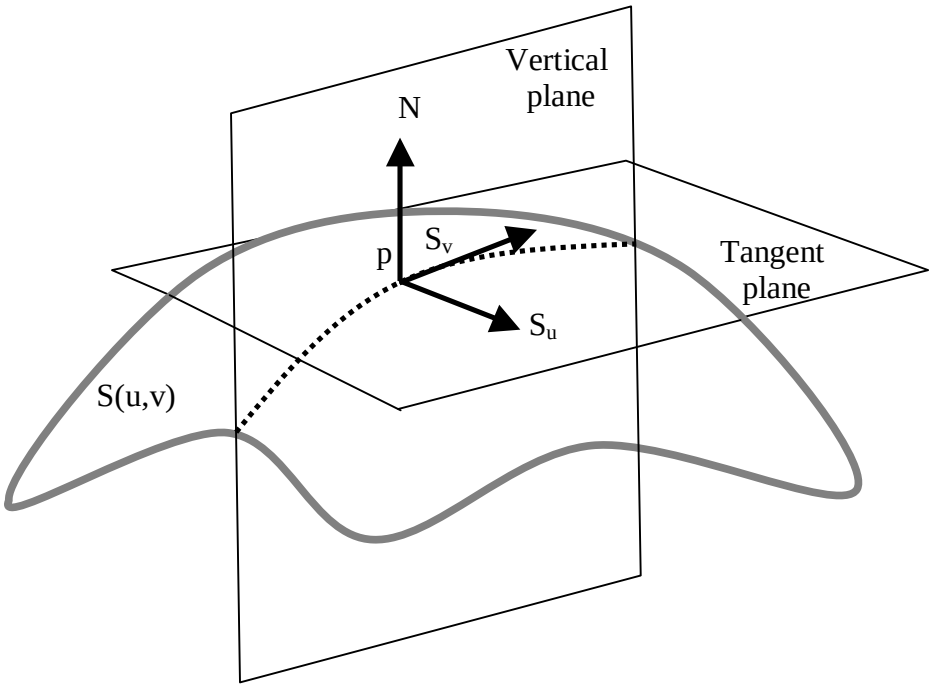

Figure 6.6: Derivation of surface curvature at point P.

of the differential geometry of surfaces such as [Carmo, 1976], and what follows is a summary of the relevant definitions and derivations used in this work. The values K and H are computed in terms of the first and the second fundamental form. The surface normal at point P is the cross-product of the first partial derivatives as follows:

$$N = \frac{S_u \times S_v}{||S_u \times S_v||} \tag{6.6}$$

where:

$$\begin{aligned} N &= \text{surface normal at the surface point } P. \\ S_u &= \text{derivative in the } u \text{ direction.} \\ S_v &= \text{derivative in the } v \text{ direction.} \end{aligned}$$

For any surface point, two other terms defined as the two fundamental forms:

$$I(u,v) = \begin{pmatrix} S_u \cdot S_u & S_u \cdot S_v \\ S_v \cdot S_u & S_v \cdot S_v \end{pmatrix} = \begin{pmatrix} E & F \\ F & G \end{pmatrix} \tag{6.7}$$

$$II(u,v) = \begin{pmatrix} S_{uu} \cdot N & S_{uv} \cdot N \\ S_{uv} \cdot N & S_{vv} \cdot N \end{pmatrix} = \begin{pmatrix} l & m \\ m & n \end{pmatrix} \tag{6.8}$$

where:

$$\begin{aligned} \text{I(u,v)} &= \text{First fundamental form.} \\ E, F, G &= \text{coefficients of the first fundamental form.} \\ \text{II(u,v)} &= \text{Second fundamental form.} \\ l, m, n &= \text{coefficients of the second fundamental form.} \end{aligned}$$

The *Gaussian curvature* K and the *mean curvature* H are given by the following equations [Pressley, 2001, p. 148]:

$$K = \frac{ln - m^2}{EG - F^2} \tag{6.9}$$

$$H = \frac{En + Gl - 2Fm}{2(EG - F^2)} \tag{6.10}$$

The principal curvatures k_{min} and k_{max} at any surface point are the eigenvalues of the following *Weingarten curvature matrix* [Pressley, 2001, p. 140]:.

$$W = -1 \cdot \begin{pmatrix} E & F \\ F & G \end{pmatrix}^{-1} \begin{pmatrix} l & m \\ m & n \end{pmatrix} = \frac{1}{EG - F^2} \begin{pmatrix} Fm - Gl & Fn - Gm \\ Fl - Em & Fm - En \end{pmatrix} \tag{6.11}$$

where:

$$\text{W} = \text{Weingarten curvature matrix.}$$

Many combinations of the principal curvatures k_{max}, k_{min} such as mean, root mean square (RMS) and absolute curvatures are of particular interest in this study. *Gaussian curvature* K:

$$K = k_{min} \cdot k_{max} \tag{6.12}$$

Mean curvature H:

$$H = \frac{k_{min} + k_{max}}{2} \tag{6.13}$$

Absolute curvature:

$$k_{abs} = |k_{min}| + |k_{max}| \tag{6.14}$$

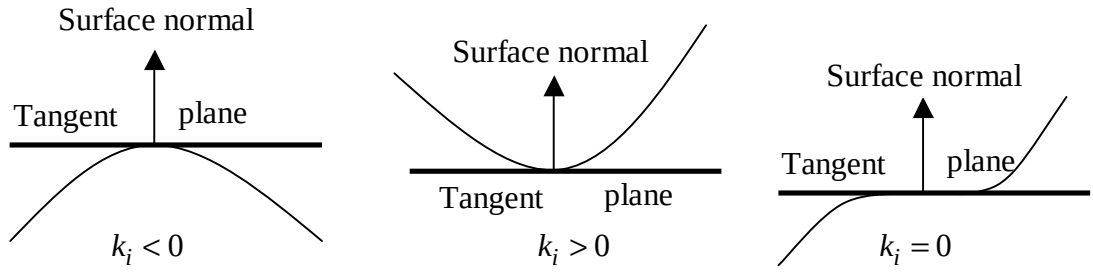

Figure 6.7: Shape and sign of the Gaussian curvature.

Root mean square curvature is a good measure for the surface flatness and is given by:

$$k_{rms} = \sqrt{\frac{k_{min}^2 + k_{max}^2}{2}} \tag{6.15}$$

Figure 6.7 explain the meaning of the curvature sign. The local surface shape could be classified based on Gaussian curvature as follows (see figure 6.8):

1. $curvature = 0$. At least one principal curvature is zero. At such a point the surface is neither convex/concave nor saddle-shaped.

2. $curvature < 0$. The normal curvature becomes zero twice during the half rotation of the normal plane around the normal. The tangent plane intersects with the surface in these directions of zero curvature. The surface is locally saddle-shaped.

3. $curvature > 0$. The normal curvatures have the same sign in all directions, so the tangent plane touches the surface at one point. The usual convex or concave regions corresponding to this.

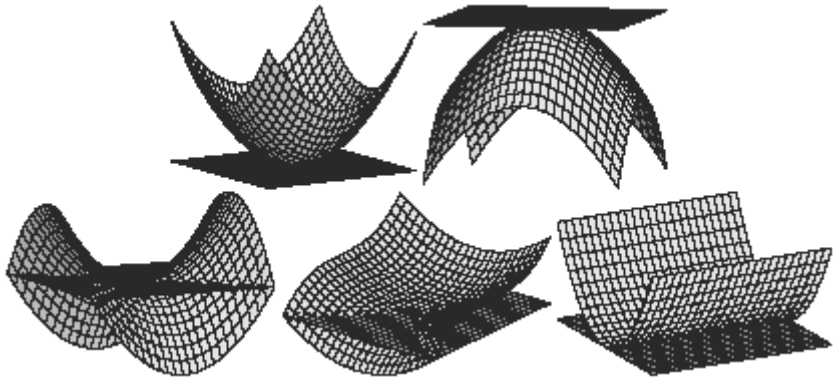

Figure 6.8: With the gaussian curvature the local shape of the surface can be classified. Top: convex and concave regions (Curvature > 0). Bottom left: saddle-shaped region (Curvature < 0). Bottom middle and right: parabolic regions (Curvature $= 0$).

Curvature computation procedures can be summarized as follows:

1. Least squares NURBS surface approximation to point clouds (degree 3).

2. Compute surface points and partial derivatives of arbitrary order on a NURBS surface

3. Compute the surface normal at every surface point (equation 6.6).

4. Compute curvature from on a NURBS surface (through equations from 6.9 to 6.15).

6.2.3 Testing the NURBS Interpolation Algorithm with Simulated Data

The tests that will be conducted in this section are briefly summarized as follows. The NURBS interpolation algorithm will be first tested with a set of the simulated data of which the true curvature and shape are known. Two tests with two different simulated data are used as follows:

First test

Figure 6.9 shows simulated point clouds. The number of points in is u direction is 102 and in v direction is 102 (the total number is 10404 points). It contains a half sphere (radius 0.2 m), a cylinder and a cube and the rest of point clouds are lay in the horizontal plane. The algorithm [Lavoie, 2002]

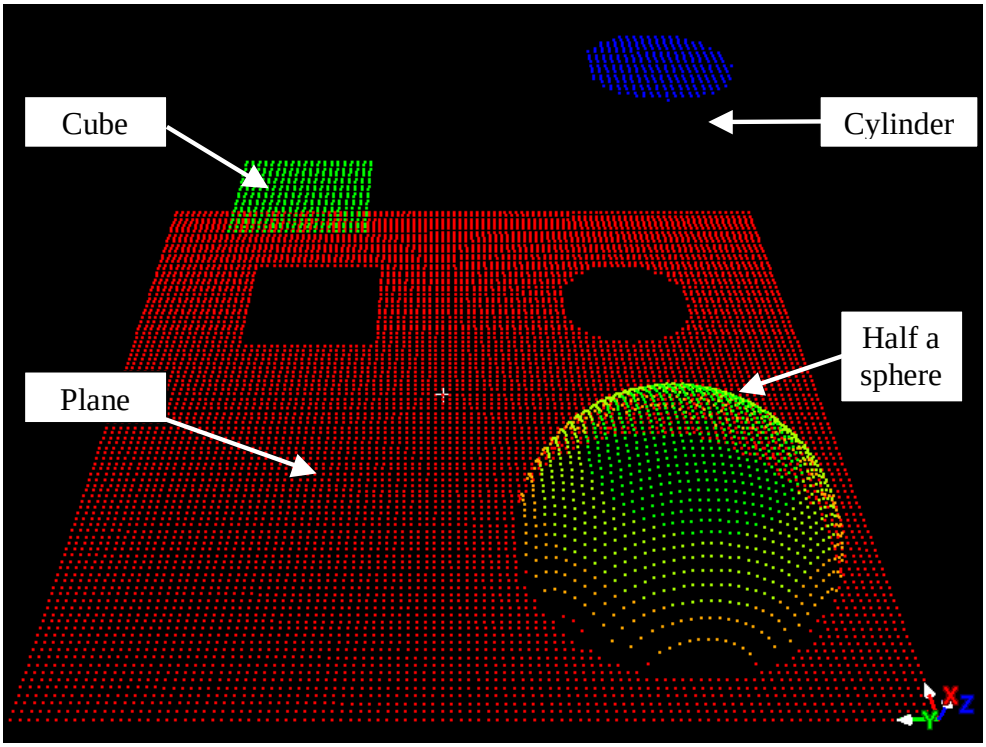

Figure 6.9: Simulated point clouds.

for NURBS fitting surface is used with degree 3 in u and v direction. The surface after fitting is presented in figure 6.10. By using NURBS algorithm, it is possible to calculate the first and second fundamental forms S_u, S_{uu}, S_v, S_{vv}). By using the fundamental forms and the equations from 6.7 to 6.11, the curvature could be calculated. The mean curvature (H) and gauss curvature (K) is calculated for the simulated point clouds. Figure 6.11 shows both mean and gauss curvatures for the simulated point clouds. The point clouds which are in the plane have the values 0 curvature. Near the cylinder coordinates, the point clouds are not dense, so the curvature values not in a clear circle around the cylinder as expected.

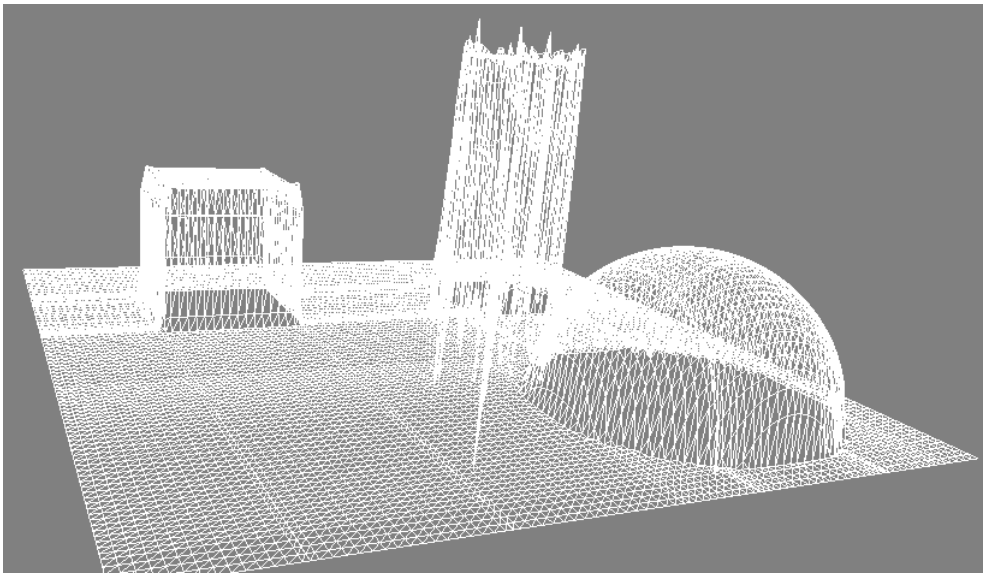

Figure 6.10: Fitted simulated point clouds.

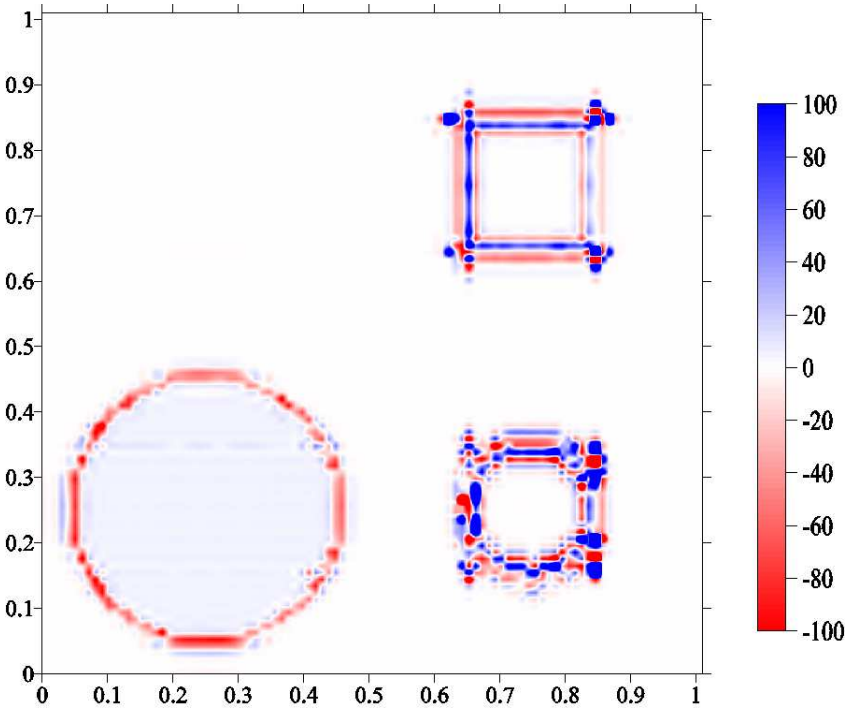

Figure 6.11: Mean curvature for simulated point clouds.

Second test

The NURBS algorithm has a special function *makeSphere* to construct a sphere. The function is used to construct a sphere with radius 0.20 m. The curvature for the sphere equals $\frac{1}{r}$, where r is the sphere radius. Table 6.1 shows results of the fundamental forms and curvatures values. The results for only four surface point are presented. The curvatures values (mean and gauss) are exactly as expected $\frac{1}{0.2} = 5$.

Table 6.1: The fundamental forms and curvatures of a sphere with radius 0.2 m

u, v	S_u	S_{uu}	S_v	S_{vv}	K	H
0.0, 0.01	0.0, 0.03,0.00	-0.18,0.07,0.00	0.57,0.00,-0.016	0.60,0.00,-1.65	25	5
0.00, 0.02	-0.0, 0.06,0.00	-0.36, 0.15, 0.00	0.58, 0.0,-0.03	0.54, 0.00,-1.70	25	5
0.43,0.88	-0.18, -0.41, 0.0	2.86,-0.71, 0.0	0.53,-0.24,-0.22	0.27,-0.12,2.02	25	5
0.43, 0.89	-0.17, -0.37, 0.0	2.62, -0.65, 0.0	0.54, -0.2, -0.20	0.18, -0.08,2.02	25	5

6.2.4 Edge Detection Based on Curvature Segmentation

The goal of edge detection is to produce a line drawing of a surface. The algorithm will look for regions in the surface where geometry feature, such as curvature, changes quickly. These edge points provide initial information for many applications using point clouds from TLS, e.g. automatic features extraction or automatic data registration. Surface curvatures are used as a geometric feature to determine surface edges for adjacent scans. Unfortunately, curvature values for the scan object from different scan position are not similar due to the principle of laser scanning. Therefore the curvature edge information that we extract from surfaces will not always indicate a correct object boundary. A threshold related to curvature values is used to classify edge points.

Segmentation is a very important task in digital image processing and computer vision. The algorithm depends on computing a curvature value at each surface point. A threshold related to the curvature values is used to classify edge points. Curvature segmentation goals could be listed as follows:

1. Curvature within a region is relatively consistent.

2. Curvature at boundary between two regions is high.

After the segmentation step based on curvature values has been done, the edge points are available. Extract the different lines and define them mathematically is the next step. The popular Hough transform method [Duda and Hart, 1972] and [Russ, 2006] is used to detect lines for every scan part. This method is used to detect 2D lines. Hough transform is applied in order to detect lines by using only a uv coordinate system. A brief description of Hough transform is presented as follows.

To use the Hough transform, a way to characterize a line is required. One representation of a line is the slope-intercept form

$$y = mx + b \tag{6.16}$$

where m is the slope of the line and b is the y-intercept (that is, the y component of the coordinate where the line intersects the y-axis). With this characterization of a line, then iterate through any number of lines that pass through any given point (x, y). , To solve for b, iterate through fixed values of m by:

$$b = y - mx \tag{6.17}$$

However, this method is not very stable. As lines get more and more vertical, the magnitudes of m and b grow toward infinity value. A more useful representation of a line is its normal form see figure 6.12.

$$x\cos\theta + y\sin\theta = \rho \tag{6.18}$$

This equation specifies a line passing through (x, y) that is perpendicular to the line drawn from the

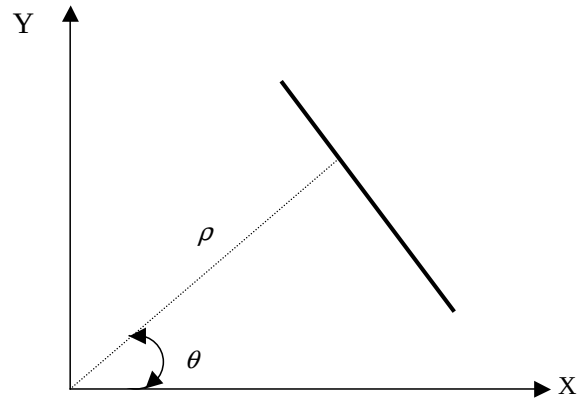

Figure 6.12: Parametric description of a straight line.

origin to (ρ, θ) in polar space (i.e., $(\rho\cos\theta, \rho\sin\theta)$ in rectangular space). For each point (x, y) on a line, θ and ρ are constant. Now, for any given point (x, y), lines passing through that point could be obtained by solving for ρ and θ. A line in the (x, y) plane is a point in the (ρ, θ) plane. Each point in the (x, y) plane is a line in the (ρ, θ) plane. The points in the (ρ, θ) plane where many lines intersects corresponds to a line in the (x, y) plane. By iterating through possible angles for θ, ρ could be solved by equation 6.18 directly. This method proves to be more effective than equation 6.17, as it is numerically stable for matching lines of any angle. The proposed algorithm has been implemented in $C++$ program in order to calculate the parameters of the edge lines for the two scans. After defining all the lines parameters, for each line parameters, the points which are near from that line parameter are segmented by a threshold value $1cm$. After that, the points are fitted to perform a 3D lines for each detected edge.

Fitting a 3-Dimensional Line to Data Points:
Fitting a straight line to a set of data points or simply linear regression is the process of minimizing the sum of the squared deviations between the points and the line. After getting line parameters in 3D, we can get the natural registration targets by calculating the intersection points between these edge lines for every scan part. The rest steps could be summarized as

The shortest line between two lines in 3D:
Two lines in 3 dimensions generally do not intersect at a point, they may be parallel (no intersections) or they may be coincident (infinite intersections) but most often only their projection onto a plane intersect. When they do not exactly intersect at a point they can be connected by a line segment, the shortest line segment is unique and is often considered to be their intersection in 3D. The method to calculate the shortest line between two segments is to define the line segment joining the two lines

and then find the minimum distance. The intersection values for all the edge lines are provided by an algorithm [Eberly, 1999]. The proposed algorithm has been implemented in $C++$ program in order to calculate natural registration targets.

Matching overlapping zone:
Using intersection points between different segmented edges as a boundary to determine overlapping zone. By calculating the distances and the angles between different intersection points we can match the correspondence registration targets between adjacent scans

Using the ICP data registration method:
The ICP data registration method need at first a very good correspondences. Now we can use the point clouds which are obtained by edge intersections.

6.3 Summary of the Overall Procedure

The method of finding correspondence feature points between adjacent scans is based on the edge detection and calculating edge point intersections. Surface curvature is used for edge detection procedures. Point clouds which are inside the correspondence feature points are detected. After that, the ICP is used to obtain the final registration results. The procedure consists of three main steps:

1. Point clouds fitting to calculate curvature.
2. Edge detection based on curvature value.
3. Calculation of edge intersections.
4. Using intersection points to determine overlapped point clouds to calculate an approximation values for transformation matrix.
5. Iterate the ICP algorithm until convergence to get the final registration results.

The different steps, which are summarized in figure 6.13, will be presented with a real scan test for Richmond Palace in Braunschweig.

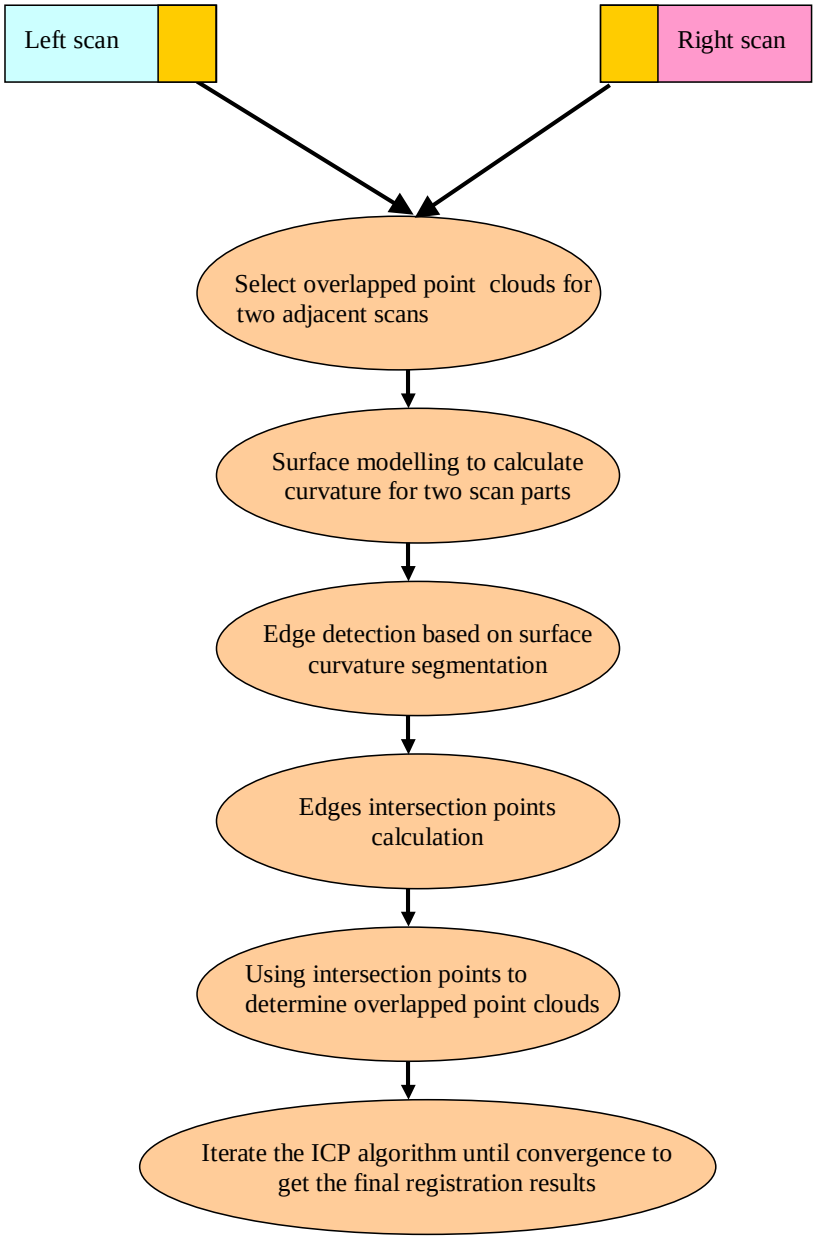

Figure 6.13: Data registration procedures.

Chapter 7

Experimental Test

7.1 Overview of the Experiment

A real scan object was scanned by the Cyrax 2500 laser scanner to test the method. Figure 7.1 shows the scan object. Two scans have been made with about 2 cm point cloud resolution in both horizontal and vertical direction. Figure 7.2 shows point cloud of two scans which have been captured from the

Figure 7.1: Richmond Palace in Braunschweig.

terrestrial laser scanner. A small part from the left scan (175*81 point clouds) and from the right scan (167*76 point clouds) have been selected to calculate surface properties (see Figures 7.3).

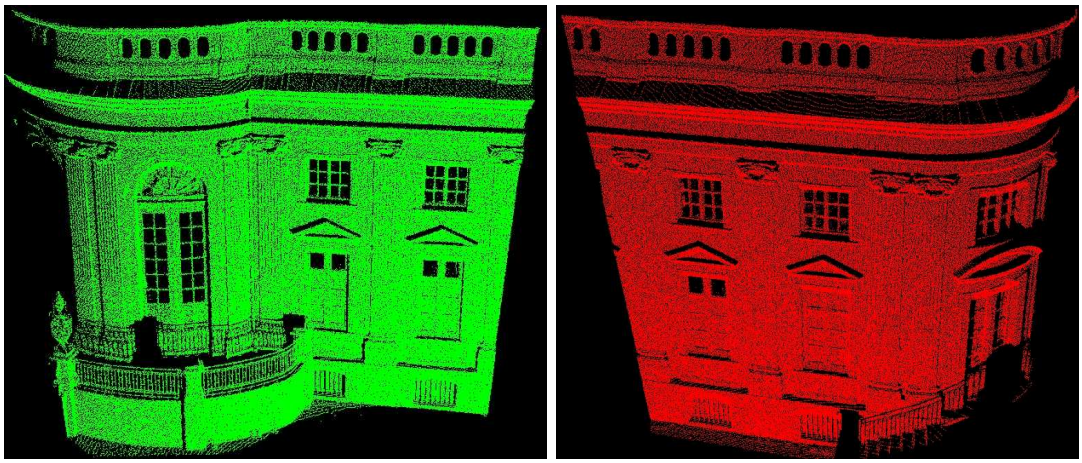

(a) Left scan (b) Right scan

Figure 7.2: Point clouds visualization before registration.

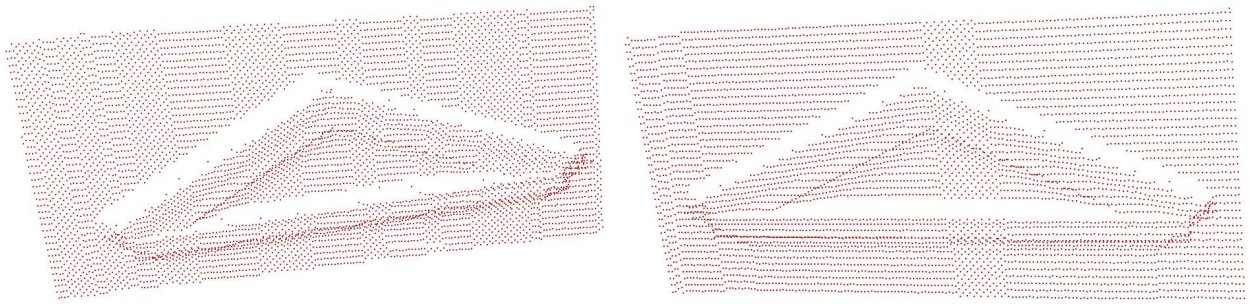

(a) Left scan (b) Right scan

Figure 7.3: Visualization of a selected part before modeling.

7.2 Curvature Results and Analysis

With degrees $m = 3$ and $n = 3$ the point clouds have been interpolated by using the NURBS algorithm. Figure 7.4 shows the modeled surface points for the left and the right scan.

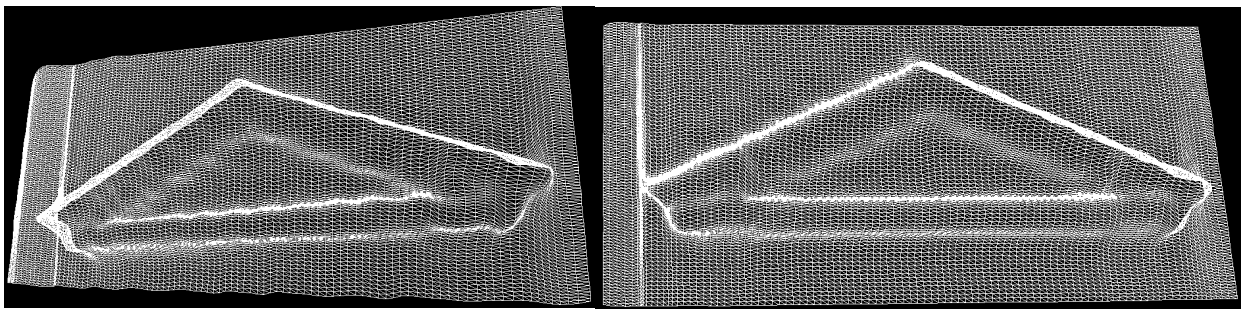

(a) Left scan (b) Right scan

Figure 7.4: Visualization of a selected part after modeling.

Figure 7.4 represents the interpolation of point cloud for two scan parts. The modeled surface points appear without the occlusion problem. Graphical display of gauss, mean and root mean square

Figure 7.5: An image for the selected part.

curvatures are represented in figures 7.6, 7.7 and 7.8 respectively. From the representations of all curvature types, the gauss curvature is the worst and mean curvature is the most useful to recognize and detect the edges.

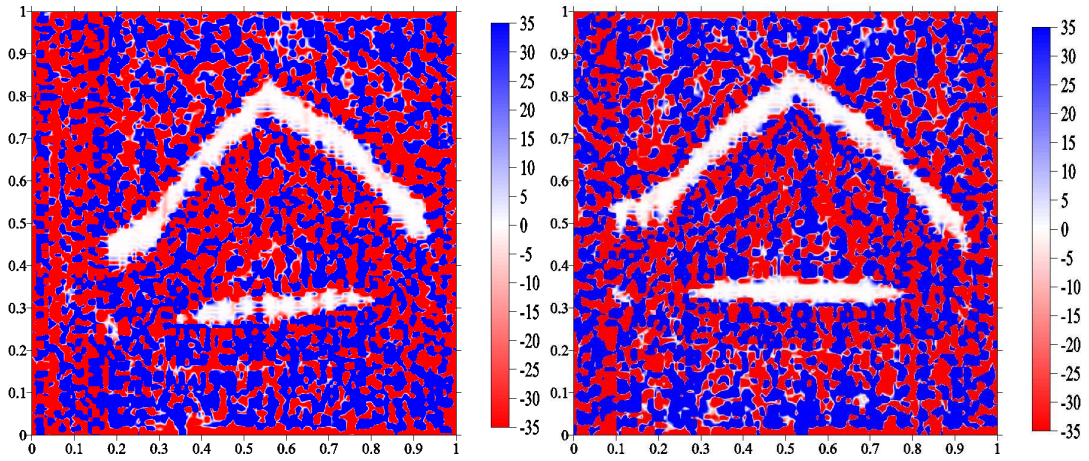

(a) Left scan (b) Right scan

Figure 7.6: Gauss curvature.

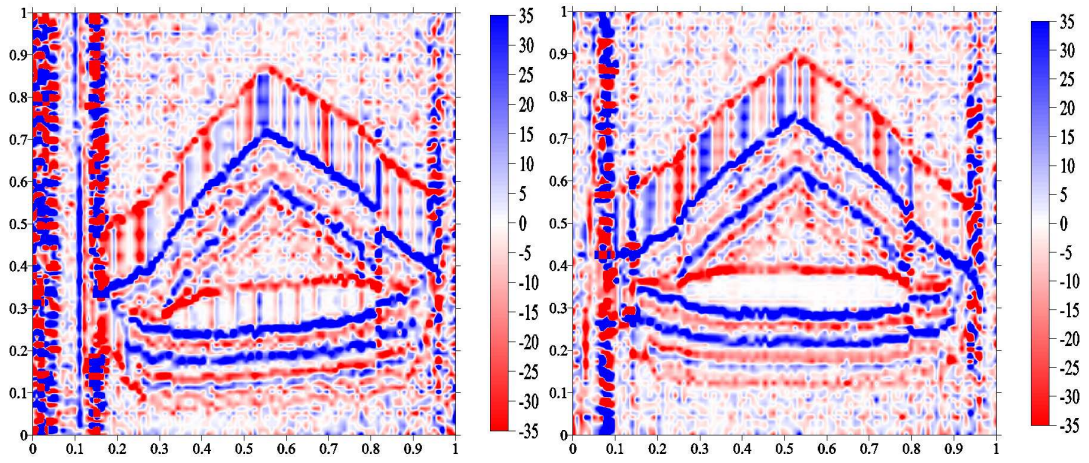

(a) Left scan (b) Right scan

Figure 7.7: Mean curvature.

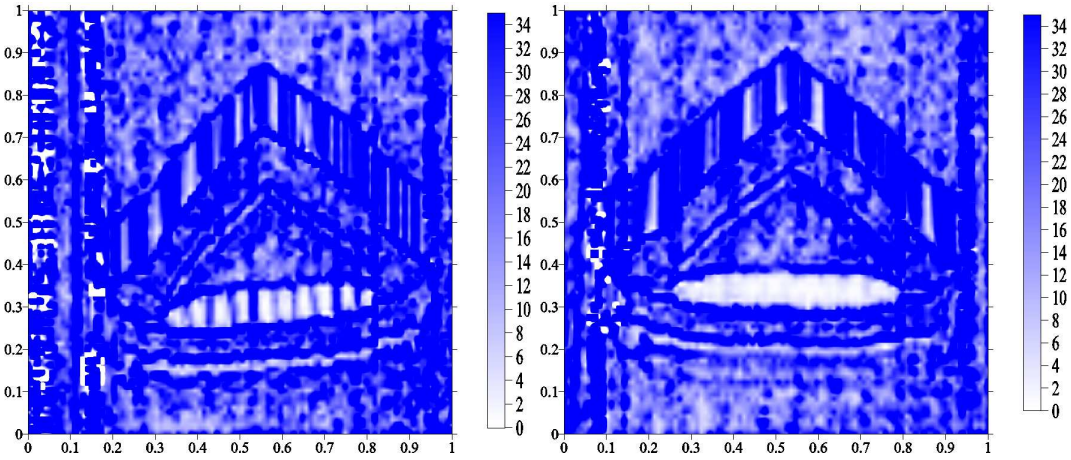

(a) Left scan (b) Right scan

Figure 7.8: Root mean square curvature.

The NURBS algorithm has the advantage to define the number of control points to be used to construct the surface. For the same test data, by using 25% of the point cloud, a new surface and a new curvature value is calculated . Figures 7.9, 7.10 and 7.11 show the new curvature values. The curvature values are improved and the shape edges are very clear to observe. Figures 7.12 and 7.13 show the

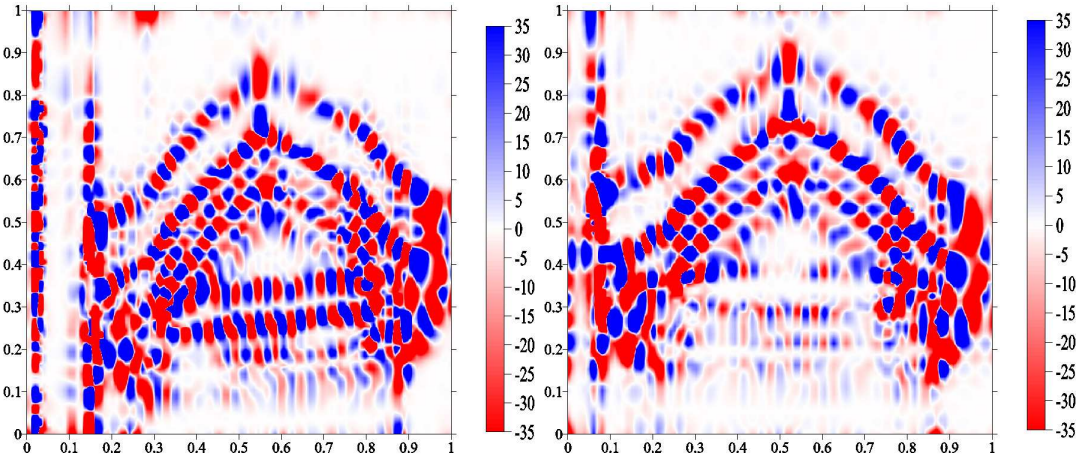

(a) Left scan (b) Right scan

Figure 7.9: Gauss curvature after using only 25% from the control points.

distribution profile of the mean curvature values at $u = 0.5$ for using the total point cloud first and only 25% from them second for data fitting with the NURBS algorithm. The points coordinates of all edges are available in each scan. The surface points which has $-10 \geq$ mean curvature $\geq +10$ is presented in figure 7.14.

7.3 Edge Detection Results

Each edge needs to be described mathematically. The image in figure 7.15 is the result of performing the Hough transformation algorithm as an edge-detection technique on the segmented edges. It represents

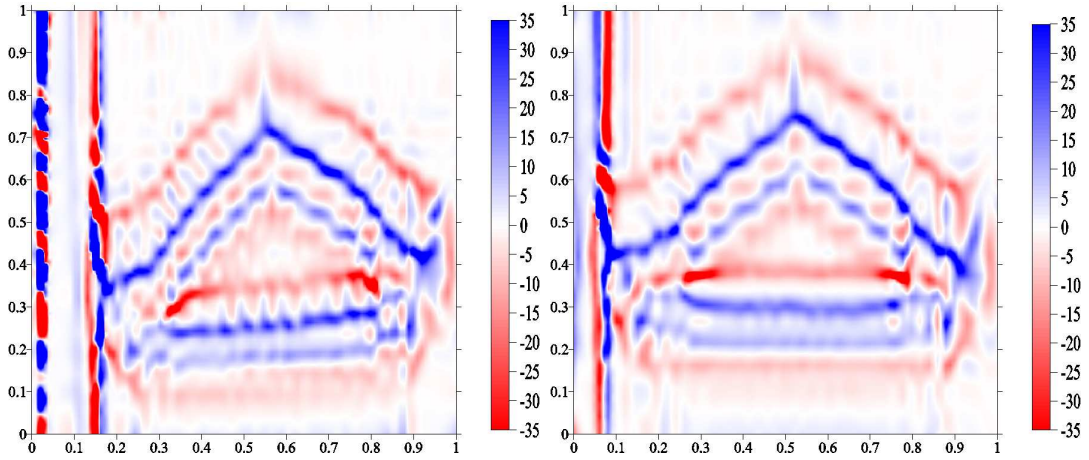

(a) Left scan (b) Right scan

Figure 7.10: Mean curvature after using only 25% from the control points.

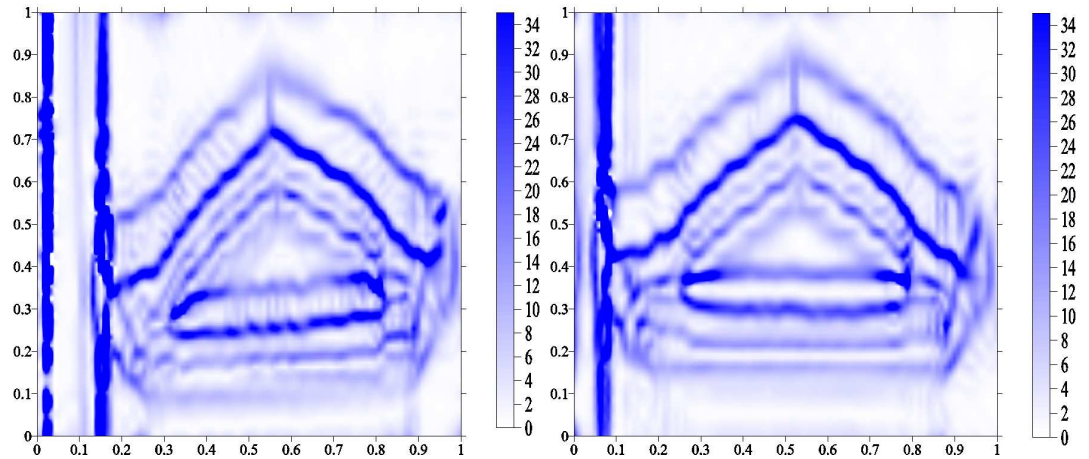

(a) Left scan (b) Right scan

Figure 7.11: Root mean square curvature after using only 25% from the control points.

all the edge parameters which are detected in the point clouds. Figure 7.16 shows the edge lines. Figure 7.17 shows edge intersection points which are detected in each point cloud.

7.4 Registration Results

These intersection points which are extracted based on edge information from two adjacent scans are used as natural features in order to define an overlapping zone between adjacent scans. The overlapped zone is used by the ICP algorithm to register data. Figure 7.18 shows the final 3D model after registration between two scans. Cyra registration targets are distributed before the scanning process Figure 7.19. The least square data registration solution is performed to evaluate the method. A comparison between the method and the least square method is presented in table 7.1. The differences between two solutions are improved compared with first improvement for ICP solution in section 4.3.3. Table 7.2 shows the coordinates of the Cyra targets after registration based on the least square

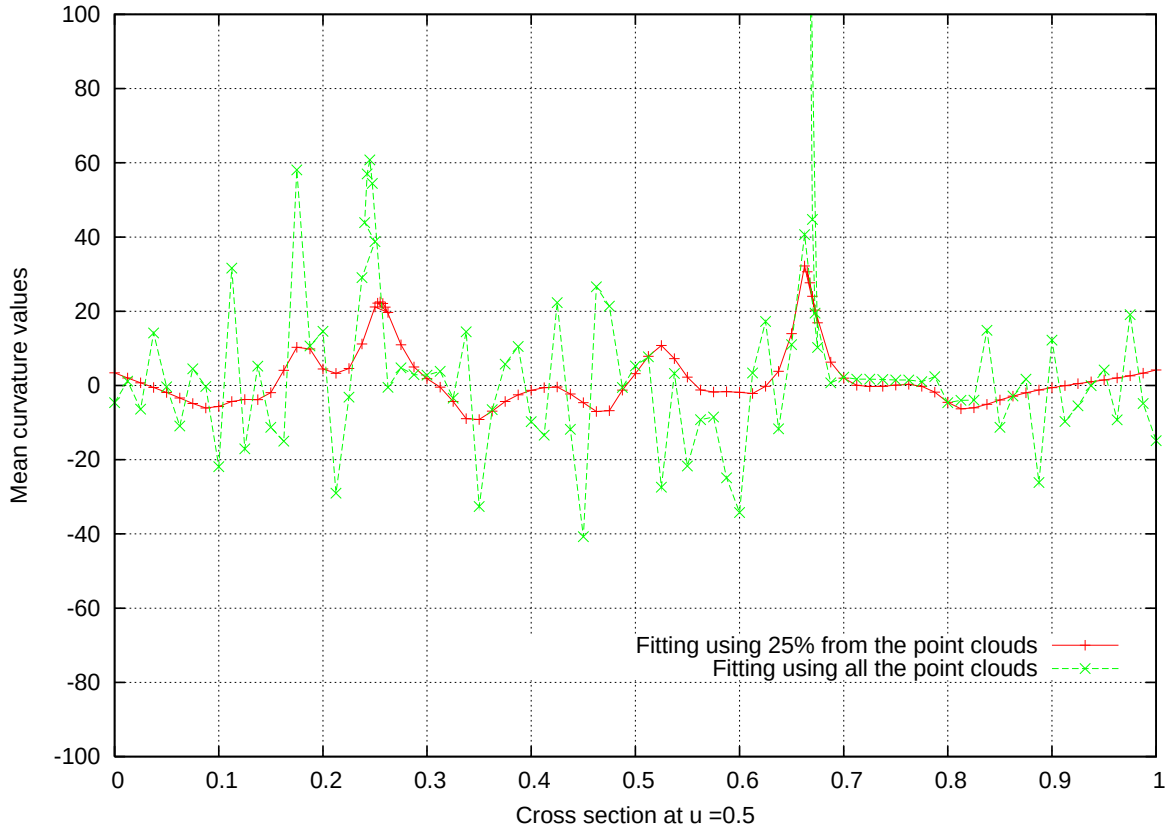

Figure 7.12: Distribution of the mean curvature values for the cross section at u =0.5 in the right scan. Look at Figure 7.7a and 7.10a to compare the curvature values. With using 25% from the point cloud to fit the surface and to calculate the curvature, the curvature values are more reable to describe the surface.

Table 7.1: Comparison between transformation parameters form different solutions.

Registration method	**Transformation Parameters**					
	ω °	ϕ °	κ °	T_x (m)	T_y (m)	T_z (m)
Cyra targets	1.8351	-28.3743	6.5352	-0.0156	0.0130	0.0011
Improved solution	1.8710	-27.9633	7.6925	0.0436	0.0617	0.0200
Differences	0.0359	-0.4110	-1.1573	-0.0592	-0.0487	-0.0189

solution and their relative distances. Table 7.3 shows the coordinates of the check registration targets

Table 7.2: Discrepancies on Cyra registration targets after registration based on least square solution.

Target	**Target coordinates** (m)						**Discrepancies**
	After transformation			**Scan 2(target)**			
	X	Y	Z	X	Y	Z	(m)
1	2.6860	-4.1454	-15.8015	2.6851	-4.1457	-15.8026	0.0014
2	3.5358	-2.8337	-15.8955	3.5358	-2.8318	-15.8958	0.0019
3	5.4666	-3.0999	-14.3003	5.4694	-3.1000	-14.2980	0,0037
4	4.2162	2.0214	-16.7428	4.2174	2.0353	-16.7441	0.0140
5	4.7474	2.0989	-16.4166	4.7458	2.0912	-16.4164	0.0078

after registration and their discrepancies. Table 7.3 shows that the minimum discrepancies on the

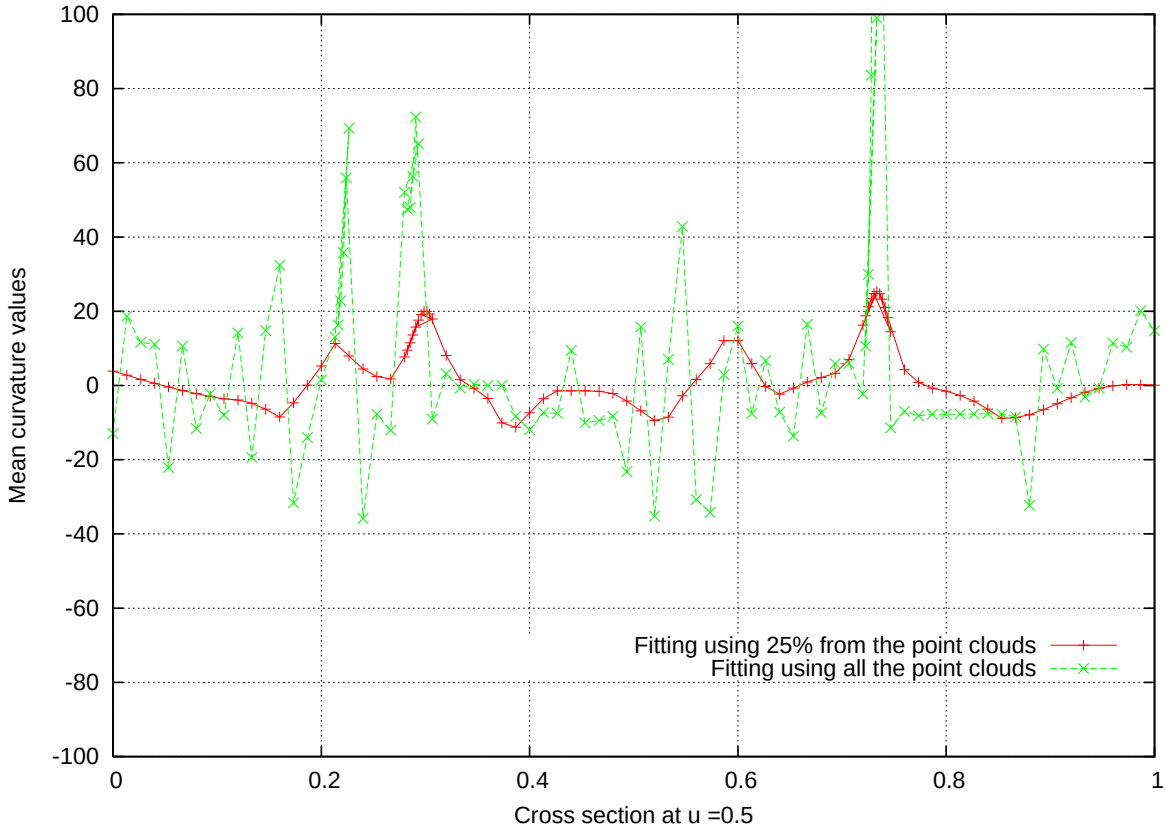

Figure 7.13: Distribution of the mean curvature values for the cross section at u =0.5 in the right scan. Look at Figure 7.7b and 7.10b to compare the curvature values. With using 25% from the point cloud to fit the surface and to calculate the curvature, the curvature values are more reable to describe the surface.

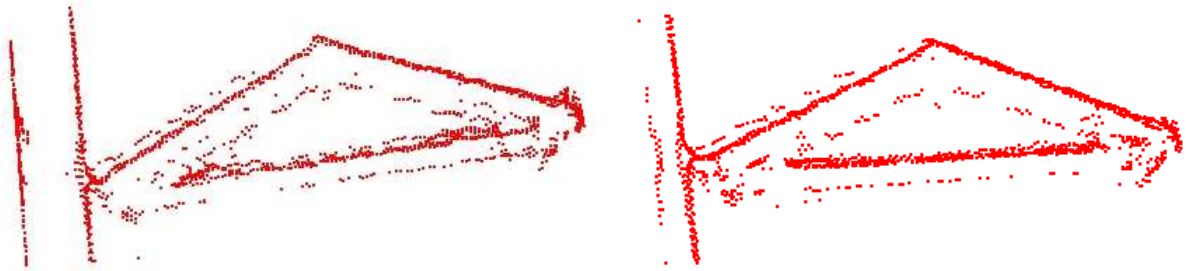

(a) Left scan (b) Right scan

Figure 7.14: Point clouds which exhibit $-10 \geq$ mean curvature $\geq +10$.

check points was 2.5 cm and the maximum was 11.2 cm with 6.7 cm mean value.

7.5 Summary

With real scan data the devolved algorithms are tested. Using the change of surface curvature, a group of high curvature edge points is detected for each point cloud. These edge points provide an initial correspondence features between overlapped point clouds. These correspondences are used as

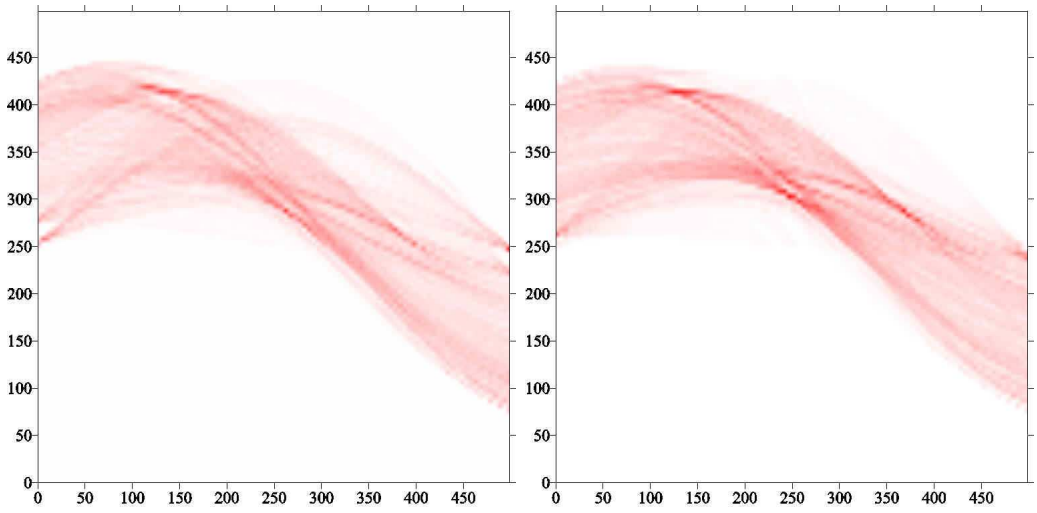

(a) Left scan (b) Right scan

Figure 7.15: Visualization of th

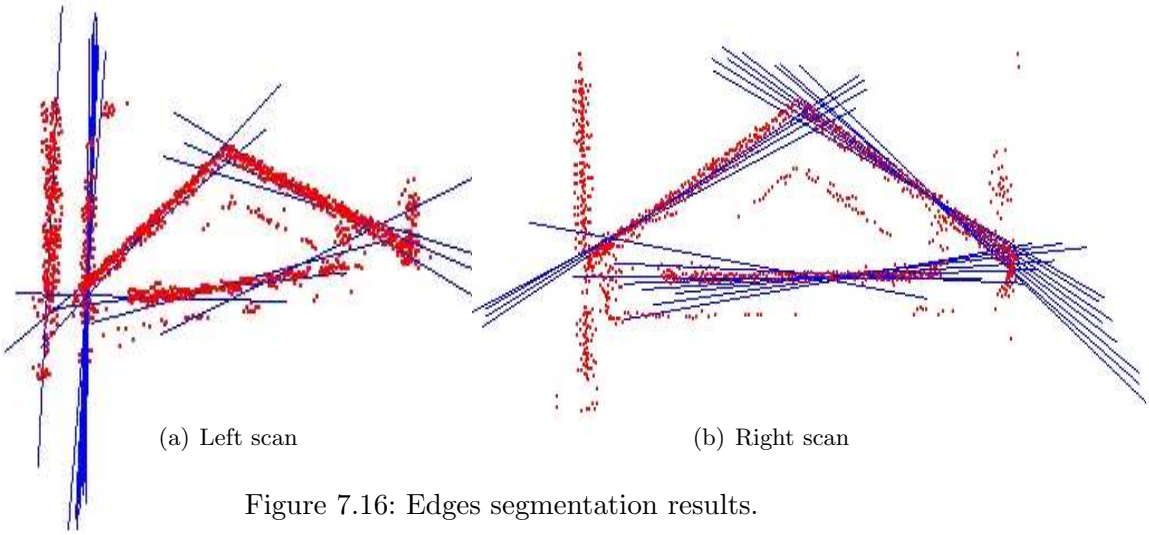

(a) Left scan (b) Right scan

Figure 7.16: Edges segmentation results.

initial information to be used by the ICP solution method. The precision of the registration results is compared with the target registration method. The mean discrepancies for the check targets was

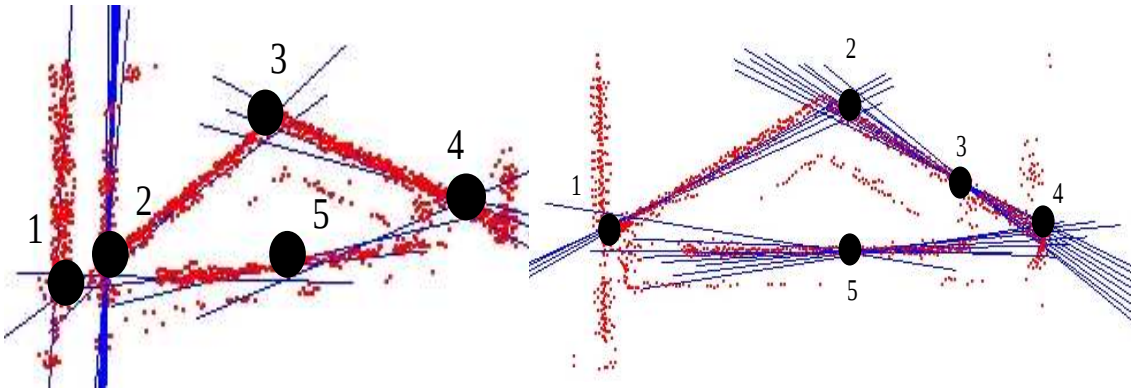

(a) Left scan (b) Right scan

Figure 7.17: Acquired natural registration targets.

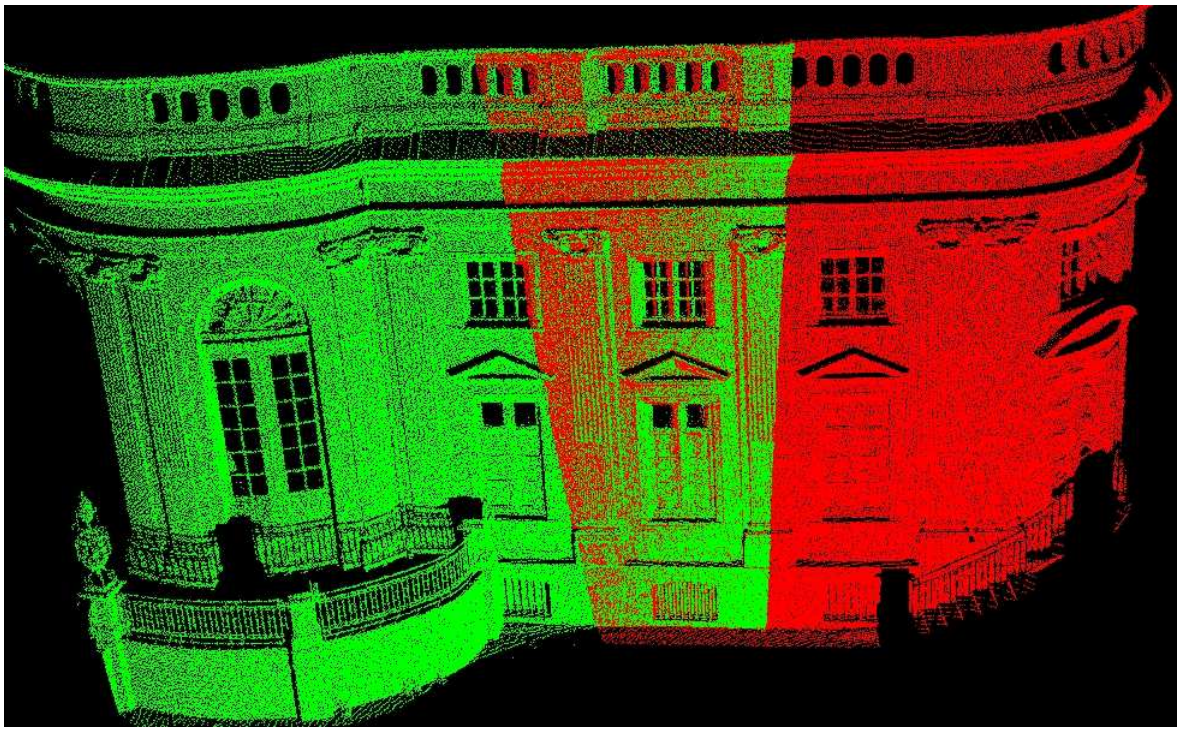

Figure 7.18: Visualization of point clouds after the registration step.

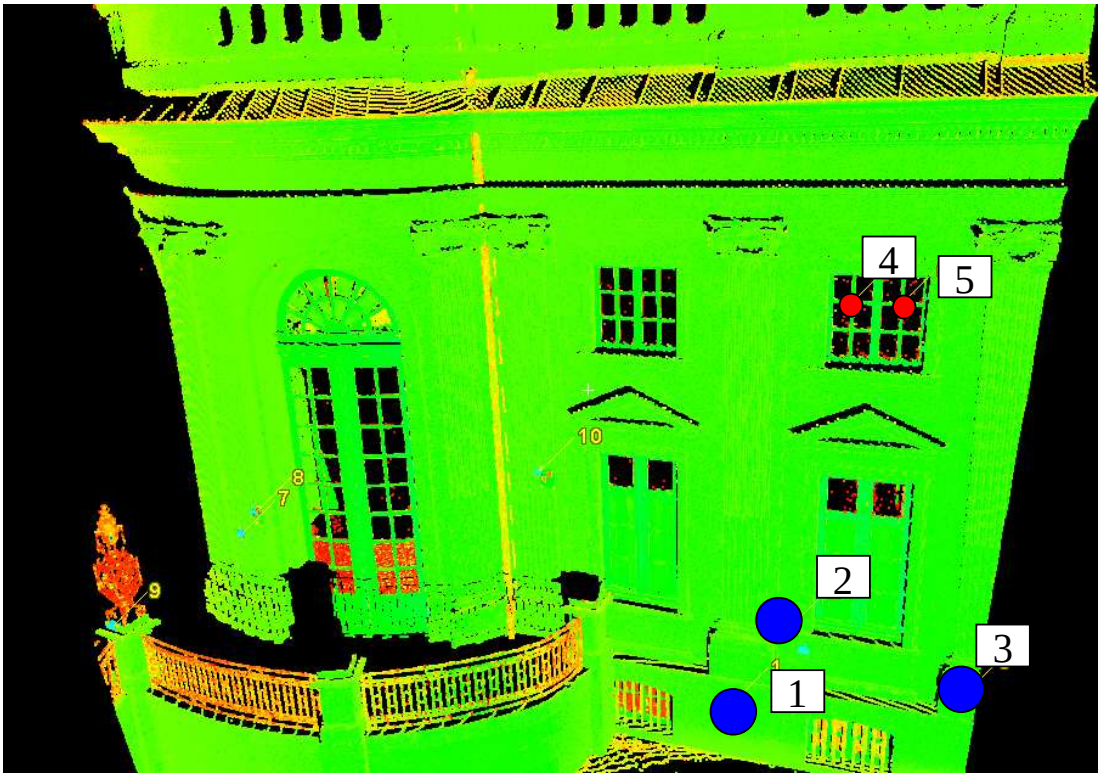

Figure 7.19: Three cyra targets and two intersection points are used as check targets.

found 0.0667 m.

Table 7.3: Discrepancies on check points (Cyra registration targets) after registration based on the improvement for the ICP solution.

Target	**Target coordinates** (m)						**Discrepancies** (m)
	After transformation			**Scan 2(target)**			
	X	Y	Z	X	Y	Z	
1	2.7101	-4.1940	-15.7828	2.6851	-4.1457	-15.8026	0.0579
2	3.5364	-2.8664	-15.8948	3.5358	-2.8318	-15.8958	0.0347
3	5.4852	-3.0838	-14.3096	5.4694	-3.1000	-14.2980	0.0255
4	4.1235	1.9979	-16.7909	4.2174	2.0353	-16.7441	0.1114
5	4.6561	2.0879	-16.4689	4.7458	2.0912	-16.4164	0.1040

Table 7.4: A statistical analysis between discrepancies on control points for tow solution methods.

Registration method	Max.Diff. (m)	Min.Diff. (m)	Mean Diff. (m)
Improved solution	0.1114	0.0255	0.0667
Cyra targets	0.0140	0.0014	0.0063

Chapter 8

Conclusions and Future Directions

8.1 Conclusion

Within the thesis the potential of data registration for terrestrial laser scanning is discussed. More than one scan by using the terrestrial laser scanning system is required to describe complete scan objects. The terrestrial laser scanning data registration aims to determine the rigid body transformation, which make two or more scans match as closely as possible. Data registration methods can be categorized into two cases:

Case 1: Data registration by using targets: With this case, special targets attached onto the object like reflective target, black-white targets are used as correspondence points. Chapter 4 dealt with a background about the algorithms and some techniques for terrestrial laser scanner data registration based on known correspondence information between adjacent scans.

Data registration results from real tests could be summarized as follows:

- Spherical targets are omni directional, the main advantage of using spherical targets for data registration is their viewing from any laser standpoint.
- By using the black and white registration targets, the standard deviation of rotation parameters σ_ω, σ_ϕ and σ_κ were $359''$, $177''$ and $159''$ respectively. The standard deviation of translation vector σ_{T_x}, σ_{T_y} and σ_{T_z} were 13.9 mm, 17.5mm and 20.7 mm (table 5.4. By using the sphere targets, the standard deviation of rotation parameters were $253''$, $139''$ and $122''$ respectively. The standard deviation of the translation vectors were 9.1 mm, 10.7 mm and 12.0 mm (table 5.5).
- Accuracy of extracting the sphere target parameters is range dependent. By using range with the relative weight matrix which is used in the combined model to calculate transformation parameters between adjacent scan. The standard deviation of rotation parameters were $186''$, $126''$ and $103''$. The standard deviation of the translation vectors were 7.0 mm, 8.8 mm, and 9.8mm.

- Accuracy of data registration depends on the geometric distribution of registration targets. Many configurations of registration targets have been studied. It has been shown that the poor target distribution, the low quality of the transformation parameters.

Case 2: Data registration using the point clouds:
Iterative closest point (ICP) technique is introduced as data registration method based on unknown correspondences. The ICP solution technique needs an initial estimation for the corresponding features between overlapping point clouds. Two methods are presented to get an initial transformation.

First, depending on the nature of point clouds from Cyrax 2500, bounds of each scan point clouds are calculated to take into consideration the overlapped point clouds. The accuracy of that method was 20.15 cm, see table 4.4.

Second, surface curvature as a geometrical feature to search for correspondence features are used. The curvature algorithms are tested by using simulated data. With real data, mean curvature is calculated for the two selected point clouds in each scan. Edges which are detected based on threshold curvature values are detected. The intersections of edge points are fitted and calculated. Edges Intersection points are matched between adjacent point clouds. The ICP algorithm is used to complete the registration process. The results of data registration are compared with the target registration method. The mean discrepancies on control targets were 6.67 cm, see table 7.4.

8.2 Future Directions

The missed or noise point clouds led to not accurate surface curvature. Therefore, developing of such an algorithm to delete noise or dense surface point clouds is an important further research area. The method which is used during the last two chapters is a semi automatic point cloud registration method. The full automatic registration procedure could be done by calculating the curvature of the hole adjacent point clouds and developing algorithms to match the correspondence features directly with a full automatic procedure. The ICP data registration method is not able to give an evaluation of the precision of transformation parameters. The precision of the estimated parameters is a very important information in the surveying engineering field. Therefore, developing of such an algorithm is also an important further research area.

Bibliography

[Abdelhafiz and Niemeier, 2006] Abdelhafiz, A. and Niemeier, W. (2006). Developed technique for automatic point cloud texturing using multi images applied to a complex site. In *IAPRS Volume XXXVI, Part 5, Dresden 25-27 September*.

[Akca, 2004] Akca, D. (2004). Full automatic registration of laser scanner point clouds. In XX^{th} *ISPRS Congress*.

[Akca and Grün, 2005] Akca, D. and Grün, A. (2005). Recent advances in least squares 3d surface matching. In *Optical 3-D Measurement Techniques*, pages 197–206.

[Angelopoulou and Wright, 1999] Angelopoulou, E. and Wright, J. R. J. (1999). Laser scanner technology. Technical report MS-CIS-99-16, University of pensylvania.

[Atkinson, 2003] Atkinson, K. (2003). *Close Range Photogrammetry and Machine Vision*. Whittles Publishing.

[Bahndorf, 2005] Bahndorf, J. (2005). Verknüpfung von Laserscans. In Schrader, B., editor, *65 DVW-Seminar Terrestrisches Laser-Scanning*, pages 67–80.

[Baumann, 1995] Baumann, E. (1995). *Vermessungskunde, Lehr und Übungsbuch für Ingenieure: Band 2 Punktbestimmung nach Höhe und Lage*. Fred.Dümmler Verlag, Kaiserstraße 31-37, 53113 Bonn.

[Beinat and Crosilla, 2001] Beinat, A. and Crosilla, F. (2001). Generalised procrustes analysis for size and shape 3-d object reconstructions. *Optical 3-D Measurement Techniques*, V:345–535.

[Beraldin et al., 1999] Beraldin, J., Blais, F., Cournoyer, L., G. Godin, G., and Rioux, M. (1999). Active 3d sensing. In *tutorial 3D Digital Imaging and Modeling conference, Ottawa, October*.

[Beraldin, 2004] Beraldin, J.-A. (2004). Integration of laser scanning and close-range photogrammetry - the last decade and beyond. In XX^{th} *Congress. International Society for Photogrammetry and Remote Sensing. Istanbul, Turkey*, pages 972–983.

[Bergevin et al., 1996] Bergevin, R., Soucy, M., Gagnon, H., and Laurendeau, D. (1996). Towards a general multi-view registration technique. *IEEE Trans. Pattern Anal. Mach. Intell.*, 18(5):540–547.

[Besl and Meckay, 1992] Besl, P. and Meckay, N. (1992). A method for registration of 3-d shapes. *IEEE Transaction on Pattern Analysis and Machine Intelligence*, 14 No.2:239–256.

[Bill and Fritsch, 1991] Bill, R. and Fritsch, D. (1991). *Grundlagen der Geo-Informationssysteme*. Wichmann, Karlsruhe, Germany.

[Blais and Levine, 1995] Blais, G. and Levine, M. (1995). Registering multiview range data to create 3d computer objects. *IEEE Trans. Pattern Anal. Mach. Intell.*, 17:820–824.

[Boehler et al., 2003] Boehler, W., Bordas, M., and Marbs, A. (2003). Investigating laser scanner accuracy. In *XIX. th. CIPA symposium at Antalya, Turkey, 2003.*

[Boehler and Marabs, 2002] Boehler, W. and Marabs, A. (2002). 3d scanning instruments. In *CIPA - ISPRS Workshop, Corfu, Greece.*

[Bolsakov et al., 1985] Bolsakov, V., Deumlich, D., Golubev, A., and Vasilev, V. (1985). *Elektronische Streckenmessung.* VEB Verlage für Bauwesen, Berlin.

[Bornaz et al., 2003] Bornaz, L., Lingua, A., and Rinaudo, F. (2003). Multiple scan registration in lidar close range applications. *The international Archives of the Photogrammetry. Remote Sensing and Spatial Information Sciences*, XXXIV:Part 5/W12.

[Breach, 1994] Breach, M. C. (1994). Three-dimensional resection. *Surveying and Land Information Systems*, 54(4):21–25.

[Carmo, 1976] Carmo, M. P. D. (1976). *Differential Geometry of Curves and Surfaces.* Prentice-Hall, Englewood Cliffs, NJ.

[Chen and Medioni, 1991] Chen, Y. and Medioni, G. (1991). Object modeling by registration of multiple range images. pages 2724–2729 vol.3.

[Clark and Robson, 2004] Clark, J. and Robson, S. (2004). Accuracy of measurements made with a cyrax 2500 laser scanner against surfaces of known colour. In *XX^{th} ISPRS Congress, Istanbul, Turkey.*

[Deumlich and Saiger, 2002] Deumlich, F. and Saiger, R. (2002). *Instrumentenkunde der Vermessungstechnik.* Herbert Wichmann Verlag, Heidelberg, Germany.

[Dewitt, 1996] Dewitt, B. (1996). Initial approximation for the three-dimensional conformal coordinate transformation. *Photogrammetric Engineering and Remote Sensing*, 62:79–83.

[Dijkman and van den Heuvel, 2002] Dijkman, S. and van den Heuvel, F. (2002). Semi automatic registration of laser scanner data. *International Archives of Photogrammetry, Remote Sensing and Spatial Information Sciences*, 34 (5):12–17.

[Dold and Brenner, 2006] Dold, C. and Brenner, C. (2006). Registration of terrestrial laser scanning data using planar patches and image data. *IAPRS*, XXXVI, 5, Dresden, Germany.

[Duda and Hart, 1972] Duda, R. O. and Hart, P. E. (1972). Use of the Hough transformation to detect lines and curves in pictures. *Comm. ACM.*

[Dutescu, 2006] Dutescu, E. (2006). *Digital Documentation of Cultural Heritage Sites Based on Terrestrial Laser Scanning.* PhD thesis, Universität der Bundeswehr, München.

[Eberly, 1999] Eberly, D. (1999). Least squares fitting of data. *In: www.magic-software.com isfit.pdf*, accessed march 2003.

[Edelsbrunner, 2001] Edelsbrunner, H. (2001). *Geometry and Topology for Mesh Generation*. Cambridge University Press, The Edinburgh Building, Cambridge CB2 2RU, UK.

[Elkhrachy and Niemeier, 2006a] Elkhrachy, I. and Niemeier, W. (2006a). Fitting sphere targets and their impact on data registration accuracy for terrestrial laser scanner. In *Fifth International symposium (Turkish-German Joint Geodetic Days). March 29-31, Berlin, Germany*.

[Elkhrachy and Niemeier, 2006b] Elkhrachy, I. and Niemeier, W. (2006b). Optimization and strength aspects for the georeferencing data with terrestrial laser scanner. In 3^{rd} *IAG symposium on Geodesy for Geotechnical Structural Engineering and the* 12^{th} *FIG Deformation Measurement Symposium. May 22-24, Baden, Austrian*.

[Elkhrachy and Niemeier, 2006c] Elkhrachy, I. and Niemeier, W. (2006c). Stochastic assessment of terrestrial laser scanner measurements to improve data registration. In *ASPRS Annual Conference. May 1-5, Reno, Nevada, USA*.

[Fabio, 2003] Fabio, R. (2003). From point cloud to surface the modeling and visualization problem. *International Archives of Photogrammetry, Remote Sensing and Spatial Information Sciences*, XXXIV-5/W10.

[Fangi et al., 2001] Fangi, G., Fiori, F., Gagliardini, G., and Malinverni, E. (2001). Fast and accurate close range 3d modelling laser scanning system. In *CIPA International Symposium, Proceedings - Potsdam*.

[Farin et al., 1996] Farin, G., Bieri, H., Brunnett, G., and DeRose, T. (1996). *Geometric Modelling*. Springer, New York.

[Foley et al., 1997] Foley, J. D., Dam, A. V., j. F. Hughes, and Feiner, S. K. (1997). *Computer Graphics Principles and Practice*. Addison-Wesley Publishing Company, Inc., New York.

[Fröhlich et al., 2000] Fröhlich, C., Mettenleiter, M., Härtl, F., Dalton, G., and Hines, D. (2000). Imaging laser radar for 3-d modelling of real world environments. *Sensor Review*, pages 273–283.

[Geosystems, 2005] Geosystems, L. (2005). Cyclone 5.2: 3d point cloud processing software for surveyors and engineers. Web site. Available online at http://www.leica.loyola.com/products/hds/cyclone.html.

[Gordon and Lichti, 2004] Gordon, S. J. and Lichti, D. D. (2004). Terrestrial laser scanners with a narrow field of view: the effect on 3d resection solution. *Survey Review*, 37(292):448–468.

[Heinz and Marabs, 2001] Heinz, W. B. G. and Marabs, A. (2001). The potential of non-contact close range laser scanners for cultural heritage recording. In *Surveying and documentation of historic buildings-monuments-site: Traditinal and modern methods,Postdam, Germany*, page 8.

[Hinsken, 1987] Hinsken, L. (1987). *Algorithmen zur Beschaffung von Näherungswerten für Orientierung von beliebig im Raum angeordneten Strahlenbündeln*. PhD thesis, München: Verl. d. Bayer. Akad. d. Wiss.

[Höpcke, 1980] Höpcke, W. (1980). *Fehlerlehre und Ausgleichsrechnung*. Walter de Gryter, Berlin, New York.

[Hu, 1962] Hu, M. K. (1962). Visual pattern recognition by moment invariants. *Information Theory, IEEE Transactions on*, 8:179– 187.

[Huber, 2002] Huber, D. (2002). *Automatic Three-dimensional Modeling from Reality*. PhD thesis, Carnegie Mellon University, The Robotics Institute.

[Huber and Hebert, 2003] Huber, D. and Hebert, M. (2003). 3d modelling using a statistical sensor model and stochastic search. In *IEEE conference on computer vision and pattern Recognition (CVPR)*, volume 1, pages 858–865.

[Jaselskis, 2003] Jaselskis, E. J. (2003). Pilot study on improving the efficiency of transportation projects using laser scanning. Final project Report, Center for Transportation Research and Education, Iowa State University, Available online at www.ncgia.ucsb.edu/ncrst/research/groundlaser/LaserScan.pdf.

[Jähne, 1997] Jähne, B. (1997). *Digital Bildverarbeitung*. Springer-Verlag London Limited 2005, Springer-Verlag Berlin Heidelberg 1997, Germany.

[Johansson, 2004] Johansson, M. (2004). Exploration into the behaviour of three different high-resolution ground-based laser scanners in the built environment. *International Archives of Photogrammetry, Remote Sensing and Spatial Information Sciences*, XXXV. Commission IV, Part B4:1031–1037.

[K.Agoston, 2005] K.Agoston, M. (2005). *Computer Graphics and Geometric Modeling*. Springer-Verlag London Limited 2005, USA.

[Kern, 2001] Kern, F. (2001). Supplementing laser scanner geometric data with photogrammetric images for modeling. In *XVIII International CIPA Symposium Surveying and Documentation of Historic Buildings-Monuments - Sites Traditional and Modern Methods, CIPA*.

[Kern, 2003] Kern, F. (2003). *Automatisierte Modellierung von Bauwerksgeometrien aus 3D-Laserscanner-Daten*. PhD thesis, TU Braunschweig, Institut für Geodäsie und Photogrammetrie.

[Konecny and Lehmann, 1984] Konecny, G. and Lehmann, G. (1984). *Photogrammetrie*. Berlin; New York: de Gruyter.

[Lange et al., 1999] Lange, R., Seitz, P., Biber, A., and Schwarte, R. (1999). Time-of-flight range imaging with a custom solid-state image sensor. *Laser Metrology and Inspection, Proc. SPIE Munich*, 3823:858–865.

[Lavoie, 2002] Lavoie, P. (2002). Nurbs++ 3.0.11 library. http://libnurbs.sourceforge.net/.

[Lichti et al., 2000a] Lichti, D., Stewart, M., Tsakiri, M., and Snow, A. (2000a). Calibration and testing of a terrestrial laser scanner. In *International Archives of Photogrammetry and Remote Sensing*, volume XXXIII, Part B5, Amsterdam, The Netherlands, July, pages 485–492.

[Lichti and Harvey, 2002] Lichti, D. D. and Harvey, B. R. (2002). An investigation into the effects of reflecting surface material properties on terrestrial laser scanner measurements. *GEOMATICS RESEARCH AUSTRALASIA*, ISSU 76:1–22.

[Lichti et al., 2000b] Lichti, D. D., Stewart, M. P., Tsakiri, M., and Snow, A. J. (2000b). Benchmark tests on a three-dimensional laser scanning system. *Geomatics Research Australasia*, 72:1–24.

[Lingua and Rinaudo, 2002] Lingua, A. and Rinaudo, F. (2002). The statue of ramsete ii - integration of digital photogrammetry and laser scanning technique for 3d modelling. *International Archives of Photogrammetry, Remote Sensing and Spatial Information Sciences*, 34; PART 5/C7:206–211.

[Marbs, 2002] Marbs, A. (2002). Experiences with laser scanning at i3mainz. In *CIPA, Heritage Documentation - International Workshop on Scanning for Cultural Heritage Recording.*

[March, 1999] March, D. (1999). *Applied Geometry for Computer Graphics and CAD.* Springer, Verlag London Berlin Heidelberg.

[Masuda et al., 1996] Masuda, T., Sakaue, K., and Yokoya, N. (1996). Registration and integration of multiple range images for 3-d model construction. In *ICPR '96: Proceedings of the 1996 International Conference on Pattern Recognition (ICPR '96) Volume I*, page 879, Washington, DC, USA. IEEE Computer Society.

[Masuda and Yokoya, 1995] Masuda, T. and Yokoya, N. (1995). A robust method for registration and segmentation of multiple range images. *Comput. Vis. Image Underst.*, 61(3):295–307.

[Mathsoft, 2005] Mathsoft (2005). Mathcad version 6.0 plus.

[McGlone et al., 2004] McGlone, J., Mikhail, E., and Bethel, J. (2004). *Manual of photogrammetry.* Fifth edition. American Society for Photogrammetry and Remote Sensing.

[Microsoft, 2005] Microsoft (2005). *Microsoft Visual C++: Programmer's Guide.*

[Monti et al., 2001] Monti, C., Fregonese, L., and Achille, C. (2001). Laser scanner application on complex shapes of architecture. profiles extraction processing and 3d modelling. *International Archives of Photogrammetry, Remote Sensing and Spatial Information Sciences*, XXXIV-5/W10.

[Nave, 2006] Nave, R. (2006). Hyperphysics. http://hyperphysics.phy-astr.gsu.edu/hbase/ems1.html Last Viewed Mar. 30, 2006.

[Niemeier, 2002] Niemeier, W. (2002). *Ausgleichungsrechnung.* Walter de Gruyter, Berlin.

[Niemeier and Tengen, 1990] Niemeier, W. and Tengen, D. (1990). Panda - the software package for precise engineering networks. In *Proc. 2nd Accelerat Workshop, DESY.*

[Niemeier et al., 2006] Niemeier, W., Tengen, D., and Elkhrachy, I. (2006). Automatische Extraktion von Geometrieinformationen aus Punktwolken. In *72. DVW-Seminar "Terrestrisches Laserscanning (TLS 2006)". November 9-10, Fulda, Germany.*

[Niemeier et al., 2002] Niemeier, W., Thomsen, S., and Schäfer, M. (2002). 3-D Geometrieerfassung mit Terrestrischen Laserscannern. In Luhmann, T., editor, *Photogrammetrie und Laserscanning Anwendung für As-Built-Dokumentation und Facility-Mangaement*, pages 15–26, Heidelberg. Herbert Wichmann.

[Niemeier and Wild, 1995] Niemeier, W. and Wild, P. (1995). Einsatz von Laserscannern für die Erfassung von Gebäudegeometrien. In Schrader, B., editor, *Gebäudeinformationssysteme*, pages 155–168, Stuttgart. Konrad Wittwer. Schriftenreihe DVW 19/1995.

[Novotni and Klein, 2001] Novotni, M. and Klein, R. (2001). A geometric approach to 3d object comparison. In *International Conference on Shape Modeling and Applications*, pages 167–175.

[O'Rourke, 2000] O'Rourke, J. (2000). *Computational Geometry in C.* Cambridge University Press, The Edinburg Building, Cambrige CB2 2RU,UK.

[Pfeifer et al., 2007] Pfeifer, N., Haring, A., and Briese, C. (2007). Automatische auswertung im terrestrischen laserscanning. In *74. DVW-Seminar "Terrestrisches Laserscanning (TLS 2007)". Dezember 5-6, Fulda, Germany.*

[Photometrix, 2004] Photometrix (2004). *Australis Demo version.* Available online at http://doi.acm.org/10.1145/166117.166151, downloaded on april 2005.

[Photometrix, 2005] Photometrix (2005). *Australis user s manual.* Available online at http://www.photometrix.com.au/downloads/australis/AustralisGuide.pdf, downloaded on april 2005.

[Piegl, 1991] Piegl, L. (1991). *On NURBS: A survey.* EEE Computer Graphics. and Applications.

[Piegl and Tiller, 1995] Piegl, L. and Tiller, W. (1995). *The NURBS book.* Springer-Verlag, London, UK.

[Pressley, 2001] Pressley, A. (2001). *Elementary Differential Geometry.* Springer-Verlage, London Berlin Heidberg.

[Prokop and Reeves, 1992] Prokop, R. J. and Reeves, A. P. (1992). A survey of moment-based techniques for unoccluded object representation and recognition. *CVGIP: Graph. Models Image Process.*, 54(5):438–460.

[Rüeger, 1996] Rüeger, J. (1996). *Electronic distance measurement.* Springer, Berlin Heidelberg.

[Riegl, 2006] Riegl (2006). Reflectivity of various surfaces / materials. Web site. http://www.riegl.com/distancemeters-/distancemeter-applications-/notes-/e-gi004.htm.

[Rietdorf, 2004] Rietdorf, A. (2004). *Automatisierte Auswertung und Kalibrierung von scannenden Messsystemen mit tachymetrischem Messprinzip.* PhD thesis, Institut für Geodäsie und Geoinformationstechnik der Technischen Universität Berlin.

[Rogers, 2001] Rogers, D. F. (2001). *An Introduction to NURBS With Historical Perspective.* Academic Press, 525 B Street, Suite 1900, San Diego, CA 92101-4495, USA.

[Rottensteiner, 2001] Rottensteiner, F. (2001). *Semi-automatic extraction of buildings based on hybrid adjustment using 3D surface models and management of building data in a TIS*. PhD thesis, Vienna University of Technology Faculty of Science and Informatics.

[Runne et al., 2001] Runne, H., Niemeier, W., and Kern, F. (2001). Application of laser scanners to determine the geometry of buildings. In *Optical 3-D Measurement Techniques*, pages 41–48.

[Rusinkiewicz, 2001] Rusinkiewicz, S. (2001). *Real-Time acquisition and rendering*. PhD thesis, Department of computer science, Stanford University.

[Russ, 2006] Russ, J. C. (2006). *Image Processing Handbook, Fifth Edition*. CRC Press, Inc., Boca Raton, FL, USA.

[Sakeek, 2007] Sakeek, H. (2007). Physics education center. Web site. Available online at http://hazemsakeek.com/.

[Samet, 1990] Samet, H. (1990). *The Design and Analysis of Spatial Data Structures*. Addison-Wesley Publishing Company, Inc., The Edinburgh Building, Cambridge CB2 2RU, UK.

[Sanso, 1973] Sanso, F. (1973). An exact solution of the roto-translation problem. *Photogrammetria*, 29:203–216.

[Scaioni and Forlani, 2003] Scaioni, M. and Forlani, G. (2003). Independent model triangulation of terrestrial laser scanner data. *The international Archives of the Photogrammetry. Remote Sensing and Spatial Information Sciences*, XXXIV:Part 5/W12.

[Schlemmer, 1996] Schlemmer, H. (1996). *Grundlagen der Sensorik*. Wichmann, Heidelberg, Germany.

[Schroeder et al., 2002] Schroeder, W., Matin, K., and Lorensen, B. (2002). *The Visualization Toolkit, An Object-Oriented Approach To 3D Graphics, 3rd edition*. Pearson Education, Inc, formerly known as Prentice-Hall, Inc.

[Schulz, 2007] Schulz, T. (2007). *Calibration of a Terrestrial Laser Scanner for Engineering Geodesy*. PhD thesis, Eidgenössische Technische Hochschule ETH Zurich.

[Schulz and Ingensand, 2004] Schulz, T. and Ingensand, H. (2004). Terrestrial laser scanning: Investigations and applications for high precision scanning. In *FIG Working Week, Athens, Greece, May 22-27*.

[Seul et al., 2000] Seul, M., O'Gorman, L., and Sammon, M. J. (2000). *Practical Algorithms for Image Analysis: Descriptions, Examples, and Code*. Cambridge University Press, The Edinburgh Building, Cambridge CB2 2RU, UK.

[Staiger, 2003] Staiger, R. (2003). Terrestrial laser scanning technology, systems and applications. In 2^{nd} *FIG Regional Conference Marrakech, Morocco, December 2-5, 2003*, volume 1.

[Staiger and Weber, 2007] Staiger, R. and Weber, M. (2007). Die passpunktlose Verknüpfung von Punktwolken - ein Erfahrungsbericht. In *74. DVW-Seminar "Terrestrisches Laserscanning (TLS 2007)". Dezember 5-6, Fulda, Germany*.

[Svelto, 1998] Svelto, O. (1998). *Principles of Lasers.* A Division of Plenum Publishing Cooporation, 233 Spring Street, New York, N.Y. 10013.

[Turk and Levoy, 1994] Turk, G. and Levoy, M. (1994). Zippered polygon meshes from range images. In *SIGGRAPH*, pages 311–318, New York, NY, USA. ACM.

[Weik, 1997] Weik, S. (1997). Registration of 3-d partial surface models using luminance and depth information. In *First International Conference on Recent Advances in 3-D Digital Imaging and Modeling*, page 93.

[Willms, 1996] Willms, A. (1996). *C-Programmierung.* Addison Wesly Longman. Inc., Bonn.

[Wolf, 1974] Wolf, P. R. (1974). *Elements of Photogrammetry.* McGraw-Hill, United State of America.

[Zhang, 1994] Zhang, Z. (1994). Iterative point matching for registration of free-form curves and surfaces. *Int. J. Comput. Vision*, 13(2):119–152.

[Zoller+Fröhlich, 2005] Zoller+Fröhlich (2005). Z+f lasercontrol software. Web site. Available online at www.zf-laser.com/e_z_f_viewer.html, downloaded on april 2005.

PERSONAL RESUME

Personal Data

Name:	Ismail Elkhrachy
Birth Date :	19. Sep. 1968
Birth Place :	Egypt
Marital State:	Married
Nationality:	Egyptian
E-Mail:	I.Elkhrachy@yahoo.com
	I.Elkhrachy@tu-bs.de

ACADEMIC QULIFICATION

Master of science	Civil Engineering, Al-Azhar University Cairo Egypt in Jun 1999
Title of thesis	Study of Some Recent Aspect in Geodetic Astronomy
Bachelor of science	Civil Engineering, Al-Azhar University Cairo Egypt in Jun 1992
Secondary school	Alexandria secondary school, Alexandria, Egypt in Jun 1987
Primary school	Alexandria secondary school, Alexandria, Egypt in Jun 1983

PROFESSIONAL EXPERIENCE

1994 – 2003	Assistance lecturer in Civil Engineering, Al-Azhar University Cairo Egypt, Teaching the following undergraduate courses 1- Plane surveying (first year, civil engineer student) 2- Geodesy surveying (third year, civil engineer student) 3- Photogrammetry (second year, civil engineer student) 4- Descriptive geometry (preparatory year, engineer student)
2003 –Now	Ph. D. Student at Institut für Geodäsie und Photogrammetrie, Technische Universität Braunschweig, Germany

PC and Computer Skills

Operating system:	Windows and DOS
Programming:	C, C++, VTK, and LaTeX.
Commercial :	Open Office, MS Word, MS Excel, MS Power Point, AutoCad, GNU-plot and Cyclone

Languages

German :	Good
English:	Good
Arabic:	Mother language

Publications

Elkhrachy, I. and Niemeier, W. (2006): Fitting sphere targets and their impact on data registration accuracy for Terrestrial laser scanner. Fifth International symposium "Turkish-German Joint Geodetic Days". March 29-31, Berlin, Germany.

Elkhrachy, I. and Niemeier, W. (2006): Stochastic Assessment of Terrestrial laser scanner measurements to Improve Data Registration. ASPRS Annual Conference Reno, Nevada, USA, May 1-5, 2006

Elkhrachy, I. and Niemeier, W. (2006): Optimization and Strength Aspects for the Georeferencing Data with Terrestrial laser scanner. 3^{rd} IAG Symposium on Geodesy for Geotechnical Structural Engineering and the 12^{th} FIG Deformation Measurement Symposium.

Niemeier, W., Tengen, D. und Elkhrachy, I. (2006): Automatische Extraktion von Geometrieinformationen aus Punktwolken, 72. DVW-Seminar "Terrestrisches Laserscanning (TLS2006)".